Temperature, lipid charge and septin dependence of lateral lipid diffusion in biomimetic membrane systems

Master Thesis Biomedical Engineering
Specialization: Tissue biomechanics and implants
Faculty 3mE, TU Delft

AMOLF Institute
Systems Biophysics Department
Biological Soft Matter Group

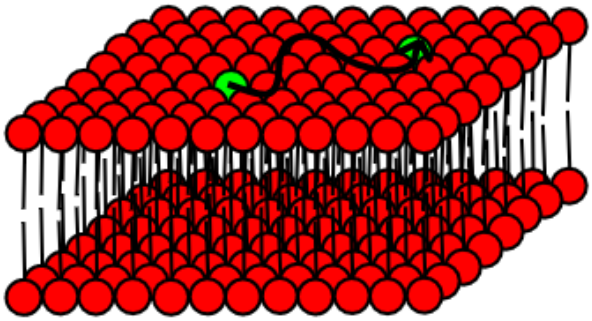

Philippine Doekes
Student number: 4507967
AMOLF supervisors: Prof. dr. Gijsje Koenderink and Yuval Mulla
TU Delft supervisors: Dr. Ir. Lidy Fratila-Apachitei and Prof. Amir Zadpoor

February 1, 2017 - November 17, 2017

TU Delft

AMOLF

Abstract

Plasma membrane dynamics have become increasingly of interest due to recent discoveries on anomalous lipid diffusion in live cells. A specific characteristic has been found in the exponential relation between lateral lipid diffusion and temperature. The finding was reported to be surprising as a linear dependence was theoretically predicted.
In this study, the gap between simple theoretical models and experimental in vivo results on lipid diffusion is investigated by studying model membrane systems experimentally. Specifically, lateral lipid diffusion is further characterized as function of temperature, lipid charge and asymmetry. To induce anomalous diffusion, a peripheral protein known to act as a diffusion barrier, fly-septin, was associated to the lipid bilayer to explore its effect on lipid slow-down.

Lateral lipid diffusion was measured by fluorescence recovery after photobleaching (FRAP) on a bare, or with associated septin, model phospholipid membrane system. The supported lipid bilayer (SLB) model membrane systems were formed by vesicle fusion (VF) or Langmuir-Blodgett/vesicle fusion (LBVF), specifically for asymmetric SLBs. Temperature variations were induced by using an in-house built sample heater. The quality of the lipid bilayers was defined by investigating influencing variables; lipid batches, substrate surface treatment, SLB formation methods and lipid tracers.

Results show that membrane viscosity exhibits linear scaling to lipid diffusion. Furthermore, lateral lipid diffusion appears to be charge dependent and influenced by lipid composition of both leaflets. Considering the influence of septin, lateral lipid diffusion is reproducibly increased as compared to a bare membrane, in contrast to the reported septin induced lipid slow-down due to a diffusion barrier mechanism. These findings have brought the gap between theoretical models and membrane dynamics one step closer together.

List of abbreviations

SUVs	Small unilamellar vesicles
DOPC	1.2-dioleoyl-sn-glycero-3-phophocholine
DOPS	1.2-dioleoyl-sn-glycero-3-phospho-L-serine
SLB	Supported lipid bilayer
VF	Vesicle fusion
LBVF	Langmuir-Blodgett/vesicle fusion
FRAP	Fluorescence recovery after photobleaching
D_{LL}	Lateral lipid diffusion coefficient

Keywords

Plasma membrane

Lateral lipid diffusion

Septin

Lipid charge

Supported lipid bilayer

Asymmetric supported lipid bilayer

Temperature dependence

Membrane fluidity

Vesicle fusion

Langmuir - Blodgett

Fluorescence Recovery After Photobleaching

Contents

1 Introduction

1.1 Motivation

The great challenge in the development of implant materials is to improve the degree of bio-compatibility for implants, specifically osseointegration for bone and dental implants [1, 2]. Osseointegration is direct in-growth of cells into a surface topography, which restricts progressive moment between implant and bone tissue, enhancing implant stability [1]. Tissue response is to a great extent dependent on the surface of the implant [3]. Better tissue-to-implant adhesion has largely been achieved by research on surface coating and topography [3]. Comparatively, few have considered diving into the interesting area of fundamental cell dynamics to enhance cellular implant integration.

Cells are triggered by mechanical stimuli in their surrounding environment to differentiate, proliferate and migrate, which are parts of the self-renewal abilities of cells [4]. These self-renewal characteristics of cells allow for osseointegration occur. Nowadays it is known that cells are able to sense and respond to mechanical stimuli via focal adhesions, facilitated by integrins, and the cell cortex, which are both linked to the plasma membrane [4, 5]. Mechanical properties of the cytoskeleton have been defined, however how forces are sensed via molecular mechanisms of the local microstructures of the actomyosin cortex are largely unknown [4]. Mechanical stimuli that the cell reacts upon are directly projected onto the plasma membrane [4]. To better realize optimal mechanical stimuli that mimic physiological circumstances, in surface topography of implants, it is essential to understand what and how these stimuli are interpreted by the cell.

The plasma membrane of the cell is in immediate contact with the extracellular environment. The plasma membrane perceives information from the extracellular environment and communicates this across to the cytoplasm [6]. Understanding plasma membrane dynamics can therefore give interesting insight how to improve enhancing cell adhesion onto an implant.

The plasma membrane is essentially composed of lipids and proteins [6]. Within the plasma membrane numerous types of lipids are combined, resulting in a unique lipid composition for each cell type [7]. Lipids are amphiphatic molecules [8] that are made up of a hydrophilic head group with a hydrophobic tail [6]. Due to the hydrophilic head group lipids can suspend in aqueous environments by self-assembling into a stable structure [9]. The plasma membrane is self-assembled into a bilayer, consisting of two lipid leaflets that each contain a hydrophilic shell, which faces the inner or outer aqueous environment and a hydrophobic core [9].

Initially, both proteins and lipids were known to have clearly defined roles; proteins execute membrane functions [7], whereas the lipids ensure a stable environment for the embedded and associating proteins [7].
It is increasingly recognized that the spatiotemporal behavior of lipids is important for membrane functioning. Therefore it is important to understand the physics governing lipid dynamics [10].
Lateral lipid diffusion (D_{LL}) can either be continuous free movement without hindrance except for continuous drag [11], better known as normal diffusion, or otherwise anomalous diffusion.
Normal diffusion exhibits no net direction nor displacement, with the distribution of displacements following a Gaussian distribution [11]. The general model describing the diffusion coefficient is the Stokes-Einstein model for 3D systems [12]:

$$D = \frac{kT}{f} \tag{1}$$

, where k is the Boltzmann constant, T is temperature in Kelvin and f is the friction coefficient; a constant that depends on the viscosity and the shape and size of the diffusing species.
Unfortunately, this model cannot be converted to 2D membrane system, as not all boundary conditions can be satisfied when deriving an expression for the friction coefficient f in 2D [12, 13]. Therefore, Saffman and Delbrück developed a well-known model that considers an infinite 2D lipid bilayer, where the lipids are assumed as a viscous medium that mediates protein diffusion [14, 15]. The Saffman-Delbrück model is, however, limited to modelling only diffusion behaviour of proteins, as the lipid bilayer is modelled as a general viscous medium, not as separate particles [13], therefore only correctly describing diffusion coefficients for components with a radius of 10 nm or larger. Lipids are typically smaller in size. Furthermore, their diffusion is predominantly independent of their tail length [12], whereas Saffman and Delbrück assumes that the whole length of the molecule affects diffusion [12, 13].

For these reasons, a specific lipid diffusion model was developed, to come to a closer agreement to experimentally obtained lipid diffusion. The free area model uses the semi-quantitative 3D free volume model for gas diffusion, to

estimate lateral lipid diffusion [12]:

$$D_{LL} = D_0 exp(-\gamma a^*/a_f) \tag{2}$$

, where D_0 is the diffusion constant inside the critical free area (areas below this value are too small to model the diffusion of a system), γ is a geometric factor correcting for free-area overlap (between 0.5 and 1), a^* is the critical free area (usually the van der Waals area [16]) and a_f is $a_f = a_t - a^*$, where a_t is the total average area per molecule, which is a function of temperature and therefore a_f is also a function of temperature [12].
The expression D_0 is the pre-exponential factor of unhindered diffusion, which can be expressed by the Stokes-Einstein-Sutherland relation [12]:

$$D_0 = \frac{k_B T}{4\pi\eta R_H} \tag{3}$$

, where k_B is the Boltzmann constant, T is the temperature, η is the viscosity of the solvent/medium/bilayer, R_H is the diffusing molecules' hydrodynamic radius and D_0 is the unhindered diffusion coefficient.

Combining the Stokes-Einstein-Sutherland equation with the free area model suggests that a linear relationship exists between D_{LL} and temperature in the plasma membrane and therefore implies normal diffusion of membrane molecules. Research in live cells has been performed to characterize D_{LL}. However, these studies have reported a clear exponential relationship between D_{LL} and temperature [13, 17, 18], and implied an anomalous diffusion mechanism by plotting D_{LL} against time [18, 19].

The disagreement between this relationship, of equations 2 and 3, and the diffusion behavior found in live cell experiments, can be explained by energy barriers. The plasma membrane is composed of numerous types of lipids that have widely varying properties, which can cause internal energy barriers such as gel or fluid state domains or lipid phase separated domains [13, 20]. Furthermore, other molecules than lipids also habitate the plasma membrane, such as interacting peripheral proteins, also causing energy barriers [6]. These energy barriers hinder lateral lipid diffusion, resulting in hop diffusion [21]. Lipids can hop to other domains by overcoming the activation energy related to these diffusion barriers [13].
Macedo-Litovitz derived an equation that provides an expression taking the energy barriers into account [12]. This activation energy term expresses the energy lipids have to overcome to hop over diffusion barriers. When an activation energy is involved, hop diffusion is temperature dependent and therefore thermally activated process, which can be described by the Arrhenius law [13]:

$$D_{LL} = D_0 exp(-\frac{E_{Arr}}{RT}) \tag{4}$$

, where D_{LL} is the diffusion coefficient in μm^2/sec, D_0 is the pre-exponential constant in μm^2/sec, E_{Arr} is the activation energy in J/μmol, R is the molar gas constant and T is the temperature in Kelvin [13].

Although the previously noted hindrance of energy barriers could explain the exponential relation of D_{LL} to temperature, another mechanism might be in play, which has yet not been reported. Viscosity is also dependent on temperature, however it is unknown how this relationship scales. Membrane viscosity could therefore also relate exponentially to temperature and explain the exponential relations found for live cell diffusion. This hypothesis must be examined in a simple membrane model, to be able to estimate the temperature dependence of viscosity in the complex plasma membrane.

1.2 Lipid diffusion in bilayers

Research on diffusion-temperature relations has been reported for model membrane systems [13, 20]. Temperature dependent diffusion has been used to characterize properties between lipid domains in a gel or fluid state [20], or in phase separating lipid bilayers, which both have been shown to induce exponential relations of D_{LL} to temperature [13]. However, the temperature dependent diffusion coefficient far away from phase transitions has not yet been characterized. This information is essential to assess the temperature dependence of the membrane viscosity. Following, first the effect of lipid charge will be discussed, where after the influence of adhering proteins will also be considered.

To examine the relation of membrane viscosity to temperature a transition temperature is undesirable. Therefore a supported lipid bilayer (SLB) membrane model, see section 2.3 , with a fluid state lipid composition was used. Diffusion measurements were obtained by fluorescent recovery after photobleaching (FRAP), see section 2.6. These results showed a linear relation between D_{LL} and temperature. Next, the relation for a partially charged lipid bilayer

was also found to be linear, but diffusion for this charged condition was generally slower than for a neutral lipid bilayer, indicating an influence of lipid charge on diffusion.

To follow-up on this finding, influence on lipid diffusion was characterized as function of lipid charge on asymmetrically charged SLBs. Thereby addressing the influence on lipid diffusion of leaflets on each other, by varying the percentage of lipid charge per leaflet. In this manner, leaflet coupling could be determined.
We observed that increased concentrations of lipid charge decreased D_{LL}. In the plasma membrane, new lipids are transported to the non-cytosolic leaflet by flip-flop. Flip-flop is transverse lipid diffusion and is essential to maintain a properly functioning plasma membrane. In the cell, this process is catalyzed to ensure sufficient turnover of lipids. Coupling of leaflets has been investigated in asymmetric lipid bilayers mainly focused on lipid organization [22]. In this research, the coupling of leaflets was defined in terms of lipid diffusion. By using the lipid charge effect of decreasing lipid diffusion, the influence of one leaflet on the other could be determined when lipid charge compositions differ between leaflets. The findings of this research imply that such an interleaflet coupling is present.

1.3 Protein-based diffusion barriers

The findings described in this report suggest that the exponential relation between diffusion in the plasma membrane and temperature cannot be explained by a viscosity effect. Instead, the relation could be due to intramembranous diffusion barriers, as mentioned before, or by interacting proteins. Anomalous diffusion induced by cytoskeletal proteins has been reported before [21, 23, 24]. To test this concept, a peripheral protein, septin, suggested to induce a diffusion barrier [25, 26, 27, 28], was added to the lipid bilayer assay and characterized by variation in temperature. Septin is a cortical protein that connects the plasma membrane to the cytoskeleton [25, 29]. Additionally, it is suggested to be involved in facilitating the detection of cell shape change [30]. Septin interacts with charged, phosphoinositides (PS), lipids with a cluster of basic amino acid residues (at the N-terminus), which is located at the proteins' surface [31, 32].
Septin adhesion on the SLBs was poor on numerous occasions and did not induce lipid slow-down. Surprisingly, septin proved to occasionally increase the D_{LL}. To further characterize this unexpected effect of septin, the degree of influence on each leaflet was investigated.
Septin affected the D_{LL} of the distal leaflet predominantly, as could be expected due to septin interacting with this leaflet. Strikingly, however, this research shows that septin binding is dependent, not only on the lipid charge of the distal leaflet, but also on the proximal leaflets' lipid charge composition.

This study has multiple aims. First, we aim to understand the contribution of membrane viscosity on lateral lipid diffusion in bare supported lipid bilayers. Moreover, we aim to understand the characteristics of lipid bilayer charge and how lateral lipid diffusion can be affected by lipid batches, substrate surface treatment, SLB formation methods and lipid tracers. Secondly, we address leaflet coupling through the individual lateral lipid diffusion of both leaflets via asymmetric SLBs. DOPC (1.2-dioleoyl-sn-glycero-3-phophocholine) and a mixture of DOPC:DOPS (1.2-dioleoyl-sn-glycero-3-phospho-L-serine) are studied due to their absence of phase transitions. Thirdly, the influence of the cortical protein septin on lateral lipid diffusion is explored, as this protein is suggested to induce a diffusion barrier in membranes.

2 Methods

2.1 Lipid vesicle preparation

Small unilamellar vesicles (SUVs) were prepared by drying a chloroform ($CHCl_3$) solution of bulk lipid (DOPC or DOPC/DOPS mix, see section 2.1.2) and fluorescent lipid tracer (see section 2.1.2.1 in a glass vial. The glass vial was cleaned before vesicle preparation (see section 2.1.1). The $CHCl_3$ solvent was removed by drying, which was accelerated by slow flow nitrogen (N_2) gas, while rotating the vial. To completely evaporate the $CHCl_3$, the vials were held under vacuum (0.1-0.5 bar) for at least 30 minutes.
Hereafter, the thin lipid film was rehydrated in 1 ml of F-buffer (see section 2.1.3) by vortex. The suspension was transferred to a 1.5 ml plastic Eppendorf vial, resulting in a final total lipid concentration of ± 1 mM. This cloudy suspension of multi-lamellar vesicles (MLV) was sonicated for 15 minutes, in the cold room (4.5 °C), using a Branson tip sonicator, pulse on/off of 5/5 seconds, and amplitude of 10%. After sonication, a clear solution of SUVs was obtained. Vesicles were stored on ice in the cold room and discarded after a week maximum.

2.1.1 Preparation of glass vials for SUV preparation

Glass vials for solvent evaporation were used as a disposable in the optimized protocols, earlier glass vials were reused.
Before addition of the lipid-chloroform solution, the glass vials were cleaned by; first, shaking and vortexing lukewarm tap water and hand soap simultaneously in the vial. Second, rinsing with more tap water, followed by deionized water (18.2 ΩM). Further cleaning steps were rinsing with acteone and ethanol, one after the other, and lastly drying the vial with N_2 gas.

2.1.2 Lipid types

1.2-dioleoyl-sn-glycero-3-phophocholine (DOPC, net charge = 0) and 1.2-dioleoyl-sn-glycero-3-phospho-L-serine (DOPS, net charge = -1 at pH 7.4, isoelectric point at pH 4.1 [Avanti Polar Lipids]) were ordered from Avanti Polar Lipids (Birmingham, AL) and Sigma Chemicals (St. Louis, MO). Different surface charged lipid bilayer compositions were created by varying the ratio of DOPC/DOPS. Both were stocked in chloroform at -20°C, at 25 mg/ml and 10 mg/ml respectively.

2.1.2.1 Fluorescent tracers To visualize the membrane, 1 mol% of a fluorescent tracer lipid was added to the lipid - $CHCl_3$ solution. Two types of lipid tracer were used with a different excitation/emission spectrum.
Lissamine rhodamine B sulfonyl (RhoPE), which is negatively charged (net charge = -1 at pH 7.4, isoelectric point at pH <1 [Avanti Polar Lipids]) was used to illuminate as red (560/583 nm). The neutral 1-palmitoyl-2-[6-[(7-nitro-2-1,3-benzoxadia
(NBD-PC) lipid dye emits green fluorescence (460/534 nm). All are stocked in $CHCl_3$ at -20°C.

2.1.3 Buffer conditions for vesicle solution

As some experimental assays in this research involved septin, re-suspension of lipids occurred in a suitable buffer for septin polymerization. This is F buffer or actin polymerization buffer, as septin is often analyzed combined in an actin assay. F-buffer is composed of: 20 mM imidazole-HCl, 50 mM KCl, 2 mM $MgCl_2$, 0.1 mM MgATP, 1 mM DTT, 1 mM Trolox, 2 mM PCA, 0.1 μM PCD (pH entire solution 7.4) [33].

2.2 Substrate pretreatment

Cover glasses and slides were cleaned according to an optimized protocol per lipid charge condition. Menzel-Glazer microscope cover slips type #1 24x60 mm and Menzel-Glazer cover slides of 26x75 mm were used.
For the vesicle fusion method, substrate treatment was dependent on lipid charge. Base piranha cleaning (see section 2.2.1) was used for DOPC-100% and DOPS-20%, which resulting in the highest diffusion coefficients for these membrane charges (data not shown). For higher charged membranes ethanol cleaning (see section 2.2.2) was used. Base piranha cleaning leads to lipid immobility and unwanted membrane heterogeneity for these high charged lipid bilayers.
For the Langmuir-Blodgett technique, base piranha cleaning was used to clean the cover slip for each experiment. The glass flow channel device (see section 5) was cleaned by ethanol surface treatment because the glass UV glue dissolves in base piranha.

2.2.1 Base piranha protocol

Base piranha solution is obtained by the following steps:

(i) Preheat 150 ml of deionized water in 250 mL beaker by microwave (1.5 minutes).

(ii) Put beaker on hot plate. Water should not cook, reaction starts at around 75°C.

(iii) Add 30 ml of ammonium hydroxide solution.

(iv) Add 30 ml hydrogen peroxide solution.

(v) When reaction forms small bubbles, add glass.

, where after glass can be lowered into the solution. The reaction is allowed to work in on the glass for 10 minutes. This is followed by rinsing the glass five times with deionized water. The glass remains fully submerged in deionized water until use. Before use, the glass is dried by N_2 gas.

2.2.2 Ethanol protocol

Glass cover slides and slips should be taken out of their storage confinements while wearing gloves. All sides are sprayed with ethanol multiple times, after which it is dried by N2 gas and ready for use.

2.3 Formation of supported lipid bilayers

Supported lipid bilayers (SLBs) were fabricated by two techniques, vesicle fusion and Langmuir-Blodgett/vesicle fusion. Vesicle fusion was used to make symmetric bilayers and Langmuir-Blodgett/vesicle fusion for asymmetric bilayers. Differences between the two methods were analyzed in terms of diffusion and septin influence and binding. Practically, the techniques show differences in approach, materials and preparation time. Both can be used to make bilayers with surfaces containing 0 – 50 mole% charged lipids.

2.3.1 Vesicle fusion method

Vesicle fusion (VF), **Figure 2**, is a commonly used, straightforward method to form symmetric lipid bilayers on a planar substrate, resulting in a SLB.

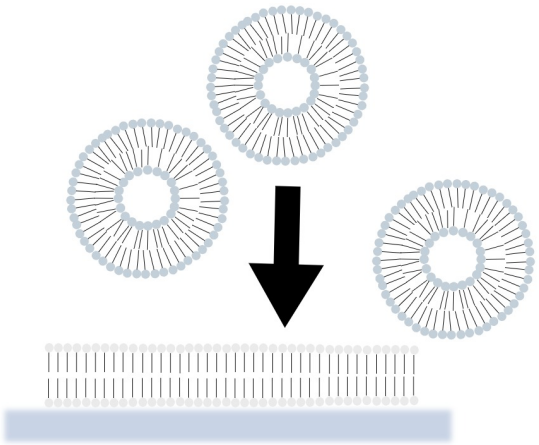

Figure 2: Vesicle fusion method. A solution of SUVs in F-buffer are flushed into a flow channel (see section 2.3.1.1), where the SUVs make contact with the glass substrate, rupture and fuse together to form a lipid bilayer that interacts with the substrate surface.

2.3.1.1 Flow channels Using cut-out parafilm strips the cleaned (see 2.2.1 or 2.2.2 depending on required lipid charge) glass cover slip and slides were assembled to form multiple flow channels per sample, see **Figure 3A**. To ensure watertight sealing of the channels, the assembly was heated on a hot plate (123°C) for 30 seconds whilst exerting downwards pressure by hand via a metal slab, see **Figure 3B**. The flow channel assembly was disposed of after measurements on the sample were completed. Channels were approximately 2x24 mm and could hold 10μl.

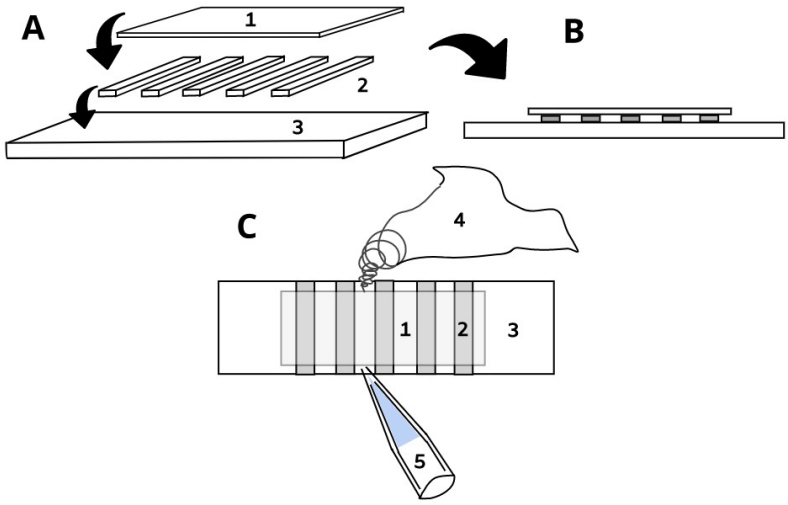

Figure 3: Flow channel and flushing technique. A) Display of the cover slip (1), parafilm channel sides (2) and cover slide (3). First the parafilm strips are pressed onto the cover slide, after which the cover slip is pressed onto the parafilm. **B)** Side view. The resulting assembly after additional heating and pressing of the layers on top of one another to ensure watertight channels. **C)** Top view. Flushing technique for vesicle solution, buffer with salt solution and buffer rinsing. On top the cover slip (1), underneath the parafilm strips (2) and below the cover slide (3). There are four channels in this sample and in one channel a pipette (5) flushes in solution, which is being sucked out, on the other side of the channel, by a rolled up piece of tissue paper (4).

2.3.1.2 Summary of optimized protocol It was extensively troubleshooted which series of flushing steps gave the most homogeneous and mobile lipid bilayers. Variations including NaCl in certain steps, pre-flushing and rinsing were played with, more information on these protocols can be found in the Supplementary information.

(i) Flow channels were assembled with cleaned glass (see 2.2.1 or 2.2.2).

(ii) 10 μl of vesicle solution (see 2.1) was flushed into each channel by pipette and incubated for 30 seconds, see **Figure 3C**.

(iii) After incubation the flow channels were rinsed with 10μl of F-buffer mixed in a 1:1 volume ratio with 1M NaCl. Suction was achieved by using tissue paper at one open side of the channel whilst adding new solution via the other opening, see **Figure 3C**. *By increasing the salt concentration vesicle fusion is accelerated. In all cases of vesicle fusion addition of salt was performed.*

(iv) Hereafter, the channels were again rinsed with a minimum of 30μl F-buffer by the aforementioned method. Sufficient rinsing with buffer is essential to remove all unbound lipid vesicles and excess salt.

(v) Depending on the experiment the flow channels are sealed off with VALAP, or septin was added to the SLB, and then sealed before imaging. Sealing is necessary to reduce the chance that the channel dries out, resulting in lipid oxidation, therefore an immobile, worthless lipid bilayer.

2.3.2 Langmuir-Blodgett technique combined with vesicle fusion process

As the vesicle fusion method was not suitable to make asymmetric lipid bilayers another method was used, namely the Langmuir-Blodgett (LB) technique, see **Figure 4**. With this method it was possible to make a monolayer with one lipid composition, **Figure 4B**. On this bottom monolayer, an upper monolayer can be formed by flushing in vesicles with a different lipid composition, **Figure 4C**. As a result an asymmetrically charged lipid bilayer is created **Figure 4D**. This combination of techniques is named the Langmuir-Blodgett/vesicle fusion (LBVF) method.
In the following section, 2.3.2.2, the optimized protocol is explained for the complete method; from Langmuir-Blodgett initial monolayer formation to secondary vesicle fusion and rinsing.

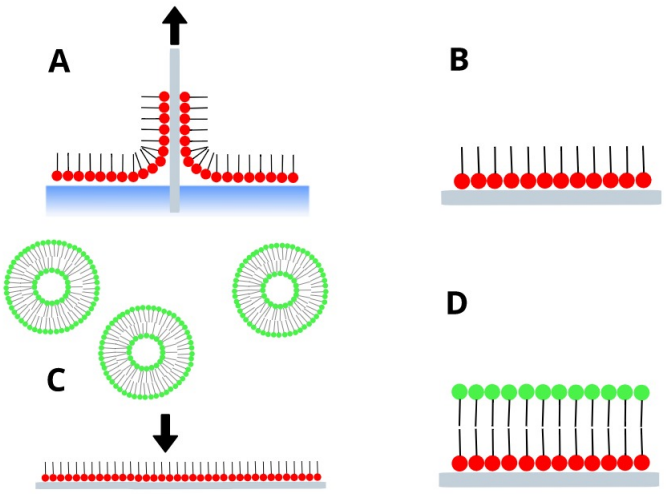

Figure 4: Langmuir-Blodgett technique combined with vesicle fusion process. A) Initial monolayer deposition by pulling hydrophilic substrate through the lipid - water interface. **B)** Substrate with single lipid monolayer, composed of one type of lipid. **C)** Substrate with monolayer are flushed over by vesicle solution, with different lipid composition. Vesicles fuse to initial monolayer. **D)** Asymmetric supported lipid bilayer.

2.3.2.1 Adapted flow channel The LBVF method required adhesion of the initial monolayer before a flow channel could be assembled. Therefore, flow channel assembly was not possible in the conventional way of melting parafilm strips; the lipid monolayer would dry out and form an immobile lipid bilayer.
To circumvent heating the cover slip, an adapted flow channel was partially pre-assembled. Glass strips (22 x 2 mm), cut from # 1 cover slips, were glued with Norland optical adhesive 68, which was cured by long wave ultra-violet (UV, exposure 320 - 400 nm), onto a cover slide. A watertight glass channel structure was thereby created, only open from the top, see **Figure 5**. This element of the adapted flow channel was reusable.
The glass strips were then covered with strips of double-sided tape, see **Figure 5 (2)**. As soon as monolayer deposition had been completed, the cover slip could be pressed onto the adapted flow channel, completing the assembly.

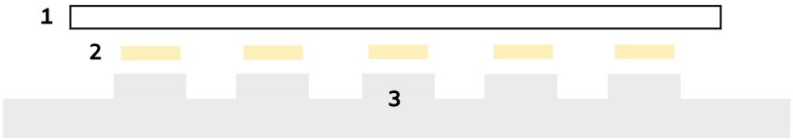

Figure 5: Adapted flow channel. (1) Cover slip **(2)** Double sided tape **(3)** Glass channel device. All components are assembled onto one another. First (3) is pre-assembled, then (2) is pressed onto the glass prominence's, where after (1) is adhered by (2) onto (3).

The LB technique requires a specilized set-up involving a Langmuir-Blodgett Kibron Microtrough X with a LB lift. The set-up includes the trough with a basin plate, sensor arm with Wilhelmy wire, barriers, LB lift above middle of the trough, attached lift controller, see **Figure 6**. More set-up details are explained in accompanying Kibron manual.

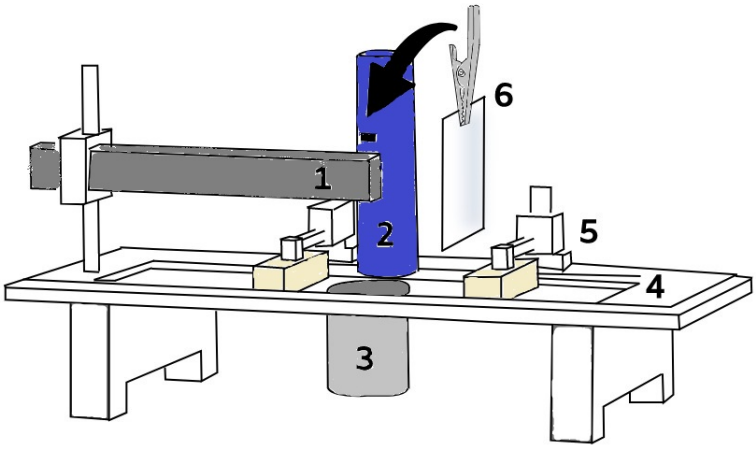

Figure 6: Langmuir-Blodgett Kibron Microtrough X trough. Sketch of the set-up, important components are coloured. **(1)** Force sensor. Wilhelmy wire hangs on the end and touched the subphase surface during measurement. **(2)** LB lift. Attaches the crocodile clamp by an extruding magnet, which can move up and down with a speed range of 1 - 10 mm/min. Velocity settings are adjustable by a turn-knob on a simple controller attached separately to the LB lift. **(3)** Trough basin. Cover slip is lowered into this basin filled with deionized water, to accomplish starting position for upwards lipid deposition. **(4)** LB trough. **(5)** Barriers. The barriers compress (or relax) the lipid surface layer to obtain optimal surface pressure. Compression and relaxation is controlled by the Firmware X software, where velocity and surface pressure can be adjusted accordingly. **(6)** Cover slip fastened by crocodile clamp. Position of the cover slip is perpendicular to the subphase surface.

2.3.2.2 Summary of optimized protocol An optimized protocol was designed for fabricating the best quality lipid bilayers, using the Kibron Microtrough X and Firmware X software. An initial monolayer was deposited on a cover slip by vertically extracting the cover slip through the subphase surface; a film of floating lipids on deionized water bulk. Vesicle fusion formed the distal leaflet on top of the initial monolayer, or proximal leaflet. Unbound vesicles were removed by rinsing, leaving a SLB for further experiments and measurements.

(i) Trough and barriers (see **Figure 6 (4) and (5)**) were cleaned with filtered millipore deionized water (18.2 ΩM), then ethanol, again with deionized water and dried with N_2 gas.

(ii) A cover slip was cleaned by base piranha (see 2.2.1). Any debris was burned off from the Wihelmy sensor wire with a lighter and suspended at one end of the force sensor of the LB, with the help of a pincer (see **Figure 6 (1)**).

(iii) 75 ml deionized water was poured in the trough, filling the basin up completely and covering the whole metal surface (see **Figure 6 (3) and (4)**).

(iv) Then the barriers were initialized, wire calibrated and subphase cleaned by aspiration using a 1 ml pipette. Aspiration resulted in a surface pressure of around 0 mN/m and in any case steady state value, fluctuations limited to ±0.3 mN/m. *It was important to ensure the wire and barriers did not touch in any conformation. Furthermore, it was essential that the wire was wetted before calibration to generate true output of surface pressure.*

(v) The required lipid for the initial monolayer was dissolved in $CHCl_3$, with a final concentration of 1 mg/ml.

(vi) 20 μl lipid solution was applied to the subphase interface, where after a waiting time of 2-3 minutes followed, until the $CHCl_3$ had completely evaporated. When adding the lipid solution the surface pressure increased to ±4 mN/m or higher. If not, more lipid solution was added in doses of 10 μl.

(vii) Lipids were compressed with a velocity of 15 cm^2/min. Hereby reaching a surface pressure of 35 mN/m. 'Constant pressure mode' was turned on to ensure continuous compression/relaxation to ensure required surface pressure, thus lipid packing.

(viii) By means of a crocodile clamp, see **Figure 6 (6)**, the cover slip was suspended from the LB lift **Figure 6 (3)** and dropped by hand quickly through the surface, as deep as possible. Then the clamp was attached to the LB lift. *It is essential to hang the cover slip in such a way that it is perpendicular to the water surface. Deviations from this angle can result in heterogeneous immobile lipid bilayers.*

(ix) The cover slip was raised through the lipid covered surface by adjusting the lift speed to 4 mm/min, until it was maximally raised. Hereafter a lipid film was adhered to the cover slip on both sides. However, only one side was used.

(x) The cover slip was secured onto the adapted flow channel device (see section 2.3.2.1) by pressing the cover slip onto the double-sided tape flow channel sides.

(xi) Immediately the vesicle solution was flushed into the channels to create the distal lipid bilayer leaflet. Incubation time was ±3 minutes, after which the flow channels were rinsed with 10μl of F-buffer mixed in a 1:1 volume ratio with 1M NaCl. Additionally, the channels were rinsed with at least 40 μl of F-buffer to remove all excess vesicles and salt.

(xii) Depending on the experiment the flow channels were sealed off with VALAP or septin was added to the SLB and then sealed before imaging. Sealing was necessary to reduce the chance of the channel drying out, resulting in lipid oxidation, therefore an immobile membrane.

2.4 Temperature dependence on lipid diffusion rate

Temperature variation in the samples was realized by in-house designed and manufactured sample heater, see **Figure 7 (1) and (3)**. Temperature regulation was achieved with home-built software called 'SuperCool' and P1000 temperature sensor, placed in the objective heater, see **Figure 7 (2)**. Temperatures between 278-333 K could be achieved. However, a temperature range of 283-318 K was chosen for these experiments due to extensive cooling and heating times.

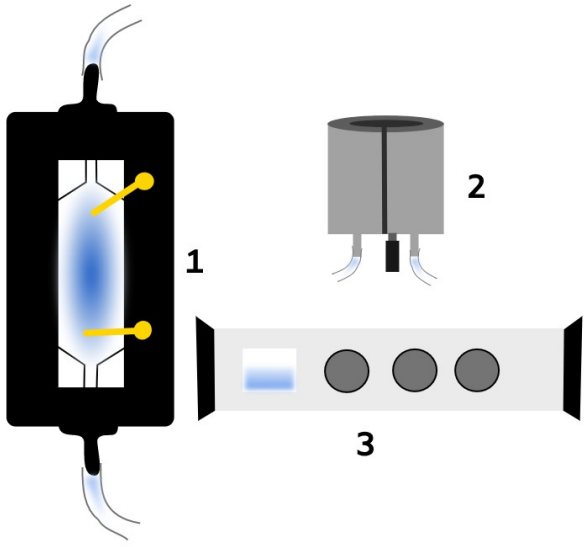

Figure 7: In-house sample heater. A sample is secured to a hollow glass cover slide by two pins **(1)**. Cooled or warmed water is pumped through the hollow glass cover slide, thereby cooling/warming the sample. Tubing runs into (1) from the sample heater **(3)** and from (1) into (2), to (3). The objective heater, **(2)**, also has an in- and outlet through which water runs. From (2) water returns to (3), completing the cycle. The objective heater has an additional inlet for the P1000 temperature sensor. The sample heater can manually be filled up with water via a fill hole above the water height display, to the left of the three fans (3).

In this research, diffusion was measured at seven different temperatures with five degrees Kelvin interval. Temperature equilibration time was 4-5 minutes. This time was determined by monitoring temperature measurements from an ultra-thin RS Pro K-type thermocouple (0.025 mm diameter) within the sample. Additionally, this thermocouple was used to calibrate the SuperCool sensor, see **Figure 8**.
Calibration of the SuperCool was determined by plotting the SuperCool measurements as function of the thermocouple measurements. The slope of the graph resulted in a linear function on which temperature calibration could be established.

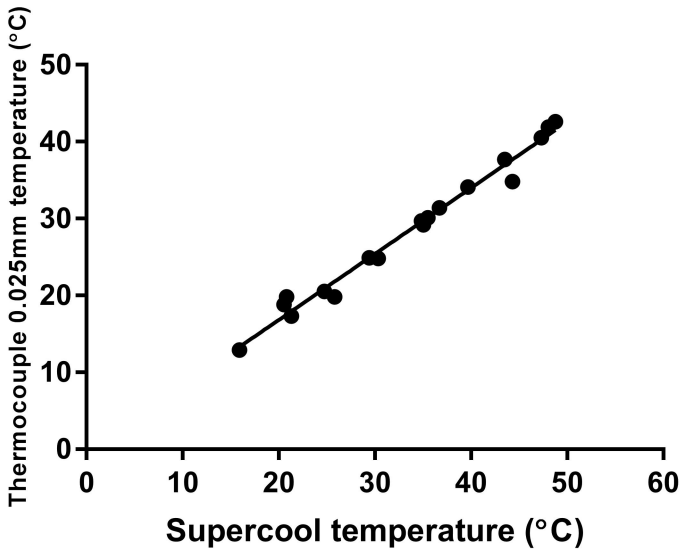

Figure 8: Calibration of the SuperCool P1000 sensor. By plotting against the reference thermocouple sensor situated in a flow channel during measurements.

The function generated by the slope of **Figure 8** was used to determined correct input values for required temperatures.

$$y_{actualtemperature} = 0.8568x_{SuperCooltemperature} - 0.3638 \quad (5)$$

For each condition, eight FRAP experiments were obtained, divided over 3 different channels and averaged. To relate results to theory, the diffusion coefficient relation to temperature was implemented into the Einstein-Stokes-Sutherland equation, see equation 3, to obtain the relation of lipid bilayer viscosity to temperature. Hydrodynamic radii for the tracer lipids RhoPE and NBD-PC with DOPC bulk lipid were 0.78 nm [34] and 0.24 nm [35].

2.4.1 Set-up

The set-up is composed of a pump with heating/cooling element, **Figure 7 (3)**, tubing, **Figure 7 (1) and (2)**, cover slide with space for water to flow through, **Figure 7 (1)**, plastic holder for cover slide and tubing inlets, **Figure 7 (1)**, temperature sensor, **Figure 7 (2)**, and a specialized microscope stage.

2.5 Septin

2.5.1 Expression, purification and labeling of WT/GFP-fly septin

All used septin batches (batches 21, 22, 23 and 24) were purified in-house, following the septin purfication protocol by Mavrakis et al. (2016)[33]. Fluorescent labeling was accomplished by genetically tagging green fluorescent protein (GFP) to wild type (WT)-septin [33].
Septin was stored and diluted in septin buffer consisting of adjusted F-buffer, containing 300 mM KCl and 5 mM $MgCl_2$ [33].

2.5.2 Working conditions

Septin was stored concentrated at ±5 mg/ml in a -80 freezer until use. Upon use, septin was mixed in WT : GFP 70:30 ratio and diluted from 300 mM to 3 μM by addition of septin buffer (see 2.5.1). Dilution continued to 0.5

μM or lower before flushing over the SLB. Concentrations of 0.05, 0.1 and 0.5 μM were used in this research. The threshold of 0.5 μM was defined by this being the critical septin concentration, after which bundles are formed and a homogeneous septin layer cannot be formed. Ratio of 6:1 septin buffer (see 2.5.1) : septin 3 μM was used to reach the critical concentration of 0.5 μM septin. More septin buffer was added for solutions with lower concentrations of septin.

2.6 Membrane and protein imaging

2.6.1 Images

All images obtained of lipid bilayers and septin were acquired by a 100-mW Argon ion laser (488 nm, 561 nm, Coherent, CA). Laser settings varied between 0.1 – 0.3% power, 30 – 60 HV, but maintained 1.2 AU and 0 offset settings for 561 nm acquired images. For 488 nm acquisition, settings varied between 0.7 – 1.77% power, 90 – 108 HV, ±2.1 AU and 0 offset.
Images and videos were analyzed and converted by ImageJ to JPEG or AVI. Overlay pictures were made and scale bars were added using this software.

2.6.2 Measurement of diffusion: Fluorescence recovery after photobleaching (FRAP)

To measure lipid diffusion in lipid bilayers, FRAP was performed on a NikonA1 confocal microscope. During FRAP experiments, a circular area of the bilayer, or region of interest (ROI, 8 μm diameter), was bleached, in one second, with a 100-mW Argon ion laser (488 nm, 561 nm, Coherent, CA). With the same laser acquisition of lipid fluorescence was acquired, however with lower intensity (100% laser power for bleach vs. 0.1 – 1.77% for acquisition). Acquisition of intensity recovery was obtained during measurement time of five minutes. Two acquisition rates were used; fast, 1 frame per second, directly after bleaching for 30 seconds and afterwards slow acquisition, 1 frame per 10 seconds, until the measurement was completed.

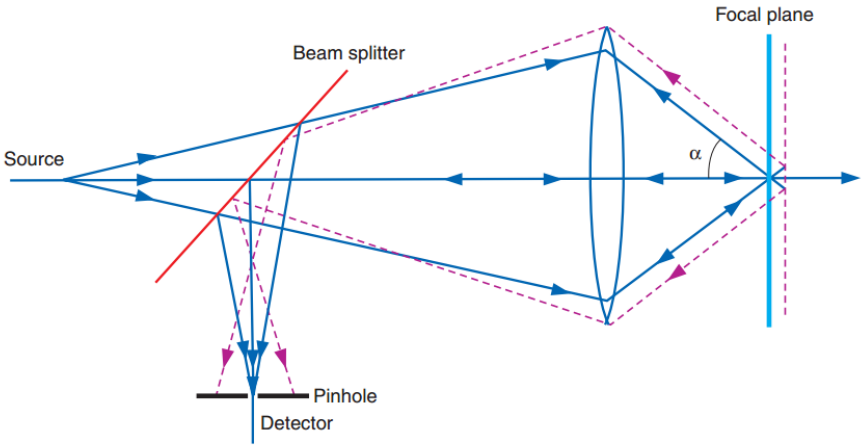

Figure 9: Sketch of the confocal principal present in NikonA1 confocal microscope used [36]. Difference between a conventional microscope, which combines all artifacts in the planes where the light can penetrate, whereas a confocal microscope images one focal plane at a time, a mechanism called optical sectioning. This is realized by adding a spatial pinhole at the confocal plane of the lens, limiting out-of-focus light.

To properly analyze the acquired FRAP data, three analyzing steps were involved. The NIS elements software generates FRAP curves by measuring the intensity in the ROI. Data points that correspond to the curve are exported as a text file. This data is then fitted by means of a Soumpasis fit in OriginsLab 2016 software. From the fitted model the recovery half time ($\tau^{1/2}$) is obtained. Subsequently, this value is implemented into the diffusion equation, see equation 7. To compare different data-sets frequency distributions or column statistics (mean, SD and N) were plotted. Confirmation of significant differences was determined by Welch's t-test or Kruskal-Wallis test. All plots and statistics were generated by GraphPad Prism 7 software.
To fit data points of FRAP curves, the Soumpasis fit was used. This fit has been proven to more accurately fit uniform circular beam profiles, used for FRAP of lipid diffusion, than a standard circular exponential fit [37, 38].

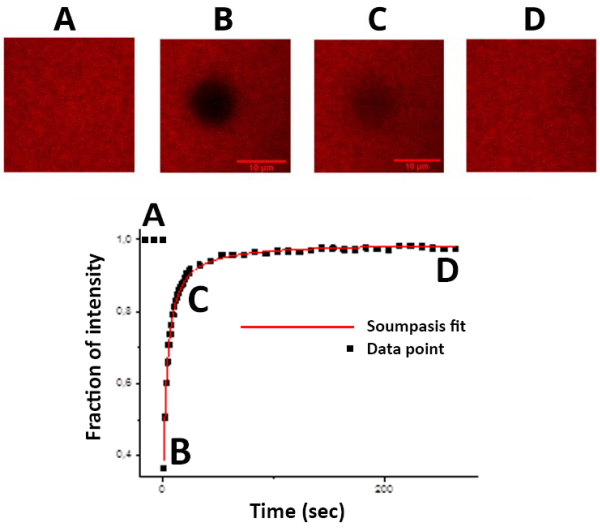

Figure 10: Principle of FRAP. A) The bilayer is uniformly labeled with RhoPE tracer **B)** Membrane area, 8 μm, is photobleached by a uniform laser beam, 561 nm **C)** The intensity within the bleached area is measured at 1 second time interval for 30 seconds and afterward 10 second interval for 4 minutes. Bleached lipid tracers diffuse out of the region of interest and new lipid tracers diffuse in **D)** Uniform intensity is restored or maximum intensity is reached.

The Soumpasis fit is based on the theoretical isotropic diffusion model to fit FRAP experiments provided by Axelrod et al. (1976) [39]. Both models involve two modified Bessel functions; for the initial intensity, I_0, and intensity after bleaching, I_1. However, problems occur in the initial model when regarding uniform circular disk profile beams, instead of Gaussian profile beams. Numerically, Axelrod's function is inconvenient at the time scale of lipid diffusion. The Soumpasis equation bypasses these problems by considering diffusion of bleached molecules out of the region of interest, instead of regarding unbleached molecules inwards [37]. The exact derivation for Soumpasis fitting of FRAP curves can be found in Soumpasis et al. (1983). Soumpasis equation:

$$f(t) = e^{-2\tau_D/t}\left(I_0(2\tau_D/t) + I_1(2\tau_D/t)\right) \tag{6}$$

To correctly fit FRAP data, fit parameters must be adjusted. There are four parameters; diffusion time, fraction of component (dependent on composition of diffusing components), recovered intensity minus initial intensity (presents immobile fraction) and intensity after bleach. Conditions for these parameters were all 1 but intensity after bleach, which was set to 0 and only fraction of component was fixed. The obtained $\tau^{1/2}$ is used to calculate the diffusion coefficient.

The diffusion coefficient of lipids is acquired by the diffusion equation for uniform circular profiles:

$$D = (r^2/4\tau^{1/2})\gamma_D \tag{7}$$

where D is diffusion coefficient in μm^2/sec, r is radius of region of interest in μm, $\tau^{1/2}$ is diffusion recovery half time and γ_D is 0.88, the bleaching parameter for laser beam with circular excitation profile [40].
To analyze the significant difference between two groups of data, the Welch's t-test was performed. Comparison of three or more groups was significantly defined by the Kruskal-Wallis test. Both do not assume equal data sets or equal variance and are therefore unpaired and non-parametric methods. Due to these properties they are suitable to analyze the acquired unequal data sets. A two-tailed P-value <0.05 must be obtained to confirm significant difference between groups.

3 Results: Lipid diffusion scales linearly with temperature in lipid bilayers

To define the temperature-dependent diffusion in a lipid bilayer, lipid compositions of 100% neutral and 20% charged SLBs were used. Using this model membrane system, the temperature was decreased from room temperature (298K) to 283 K and from there increased to 318 K with 5 degrees interval. When a steady state was reached for each temperature, FRAP was performed to obtain the corresponding diffusion coefficient (D_{LL}).
The decrease of temperature, from room temperature, to 283 and 288 K, led to non-fluorescent patches in the DOPC 100% lipid bilayers (see **Figure 11 a and b**). These dark patches disappeared when the temperature increased towards room temperature. At temperatures from 293 K onward, higher intensity patches were visible (see **Figure 11 c to h**). Specifically at 303 K movement of the lipid bilayer occurred, which could be described as oscillation around the focal plane, see **Figure 14** and **Movie 1** in **Supplementary information**. In the FRAP curve an oscillation of RhoPE intensity was shown for both the reference region of interest (ROI) as for the bleached ROI.

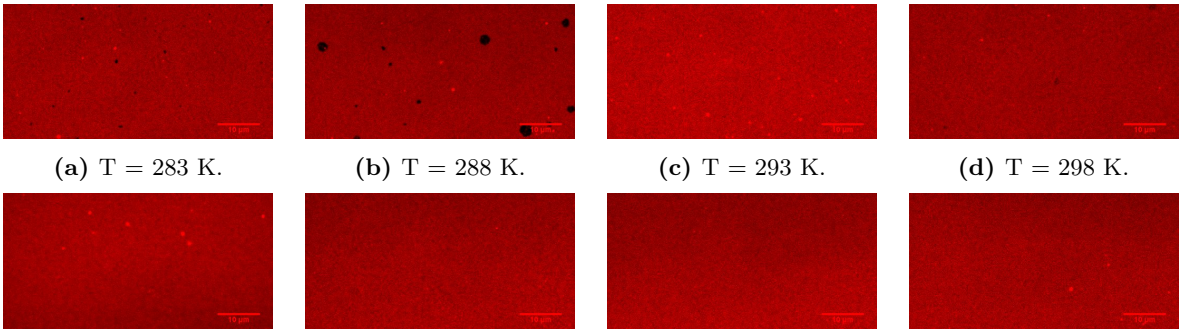

(a) T = 283 K. **(b)** T = 288 K. **(c)** T = 293 K. **(d)** T = 298 K.

(e) T = 303 K. **(f)** T = 308 K. **(g)** T = 313 K. **(h)** T = 318 K.

Figure 11: Symmetric DOPC 100% SLBs with varying temperatures. Images were acquired after temperature incubation time of 5 minutes after the sample heater reached steady state. All experiments were carried out in F-buffer at room temperature. Scale bar is 10 μm.

For this 100% neutral lipid bilayer the D_{LL} scaled linearly to the temperature range studied. The linear regression fit almost completely runs through the averages of the obtained data points (see **Figure 12**). The oscillation effect corresponded to a larger deviation of D_{LL} at this temperature compared to the other temperatures, however the results at 303 K still fit the linear regression (see **Figure 12**).

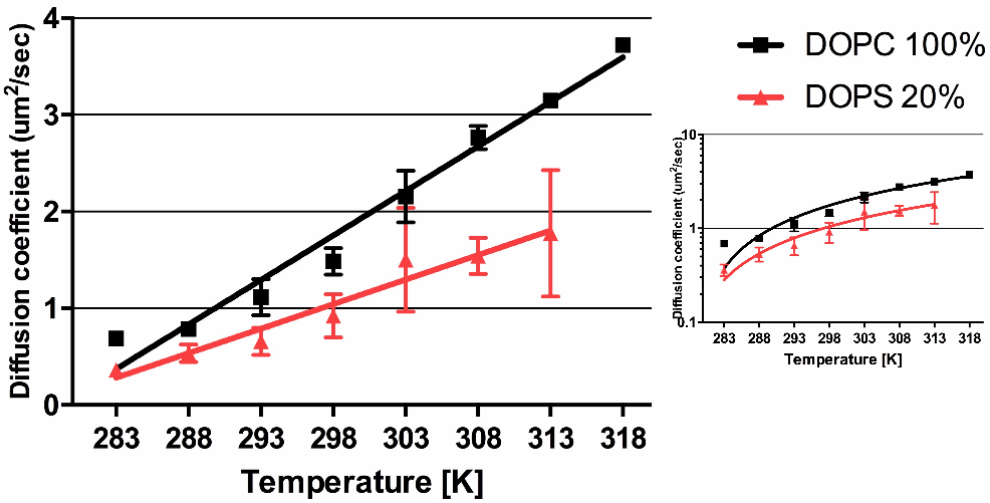

Figure 12: Diffusion coefficient vs temperature. For DOPC 100% (black squares) and DOPS 20% (red triangles) SLBs. SLBs were made by VF, had RhoPE tracer on base piranha treated glass substrate. Data was fitted with a linear regression fit.

Regarding the DOPS 20% charged lipid bilayer, the lipid bilayer remained homogeneous throughout the whole temperature range (see **Figure 13**). However, the oscillation artifact started occurring from 303 degrees K and kept presenting itself during the following temperatures (**Figure 13 e - g**). After 313 K, FRAP experiments were no longer possible as the amplitude of the oscillation was increased too high to obtain representative FRAP curve. In **Figure 13 g** the oscillation artifact is displayed; the top half of the image has a lower intensity than the bottom half, as the lipid bilayer is out of focus. The oscillation artifact has not been reported before by others that have used a similar assay [13]. It is speculated that bilayer internal curvature instability must be occurring.

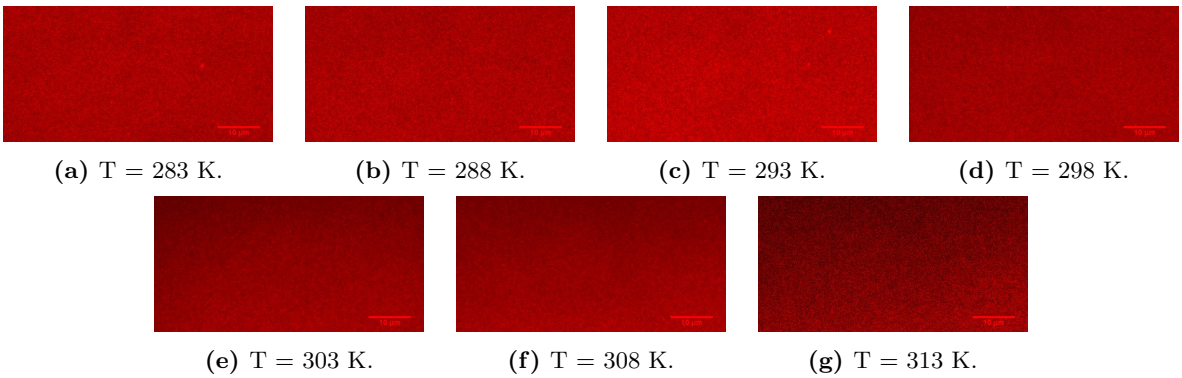

(a) T = 283 K. **(b)** T = 288 K. **(c)** T = 293 K. **(d)** T = 298 K.

(e) T = 303 K. **(f)** T = 308 K. **(g)** T = 313 K.

Figure 13: Symmetric DOPS 20% SLBs with varying temperatures. Images were acquired after temperature incubation time of 5 minutes after the sample heater reached steady state. All experiments were carried out in F-buffer at room temperature. Scale bar is 10 μm.

Linear dependence of temperature to D_{LL} was also observed in the 20% charged lipid bilayer (see **Figure 12**). However, D_{LL} increased less with increasing temperature than for the neutral lipid bilayer. Furthermore, at 303 K and higher variation of D_{LL} was larger than for its neutral counterpart.

Linearity of the relation between temperature and D_{LL} in bare lipid bilayers, shown in these results, suggests that the viscosity term (μ), presented in equation 3, must have a linear dependence to temperature. This implies that viscosity cannot explain the exponential relation of temperature and D_{LL}, reported in live cells. This dependence has not been reported before in other SLB temperature assays [13, 20].
Although both charged and neutral lipids both showed a linear increase of diffusion with temperature, there was a remarkable difference: lipids in a charged membrane had a lower diffusion coefficient at all measured temperatures compared to lipids embedded in a neutral membrane.

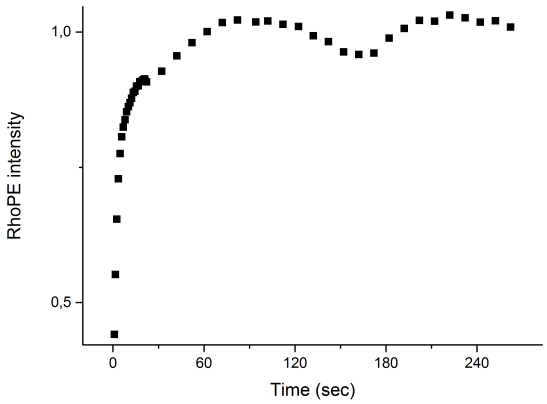

Figure 14: FRAP curve with oscillating recovery. Typical FRAP curve of 20% charged lipid bilayer at 303 K, corresponding to the lipid bilayer imaged in the movie, see **Supplementary information**.

4 Results: Increasing lipid charge decreases lipid diffusivity

4.1 Lipid charge dependence of SLB diffusion

To confirm the influence of lipid head group charge on D_{LL}, neutral and 20% charged SLBs were analyzed at room temperature, for many different samples. RhoPE tracer molecule was used as a probe for lipid bilayer diffusivity. Only mobile lipid bilayers, with an immobile fraction smaller than 3%, were taken into consideration.

Under the before explained conditions, both types of lipid bilayer demonstrated similar homogeneous landscapes (see **Figure 15 a and b**).

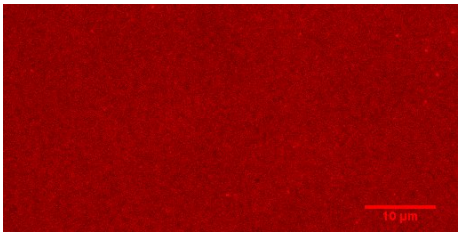

(a) Representative fluorescence image of DOPC 100% SLB. Homogeneous neutral bilayer (1 mol% RhoPE labeled.) manufactured by VF on base piranha cleaned glass cover slips.

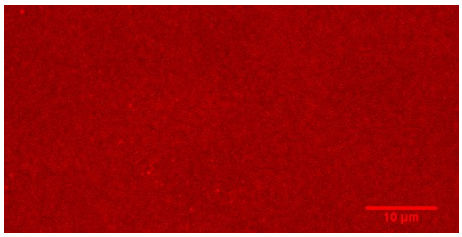

(b) Representative fluorescence image of DOPS 20% SLB. Homogeneous negatively charged bilayer (1 mol% RhoPE labeled.).

Figure 15: Representative fluorescence images of SLBs. Images were acquired before photobleaching with FRAP. Both conditions were situated in F-buffer at room temperature. Scale bar is 10 μm.

D_{LL}, however, was significantly different (Welch's t-test P<0.0001), as expected from the temperature results (see section 3). Regarding the mean values of the neutral, 1.02 μ^2/sec, and 20% charged, 0.74 μ^2/sec, lipid bilayer shows around 30% drop in lipid diffusion. More independent experiments were performed for the 20% charged lipid bilayer due to a wide spread in values that are uncorrelated in terms of channel, sample or surface treatment. For neutral lipid bilayers spread was noted to a lesser extent, therefore fewer data point were required for this condition.

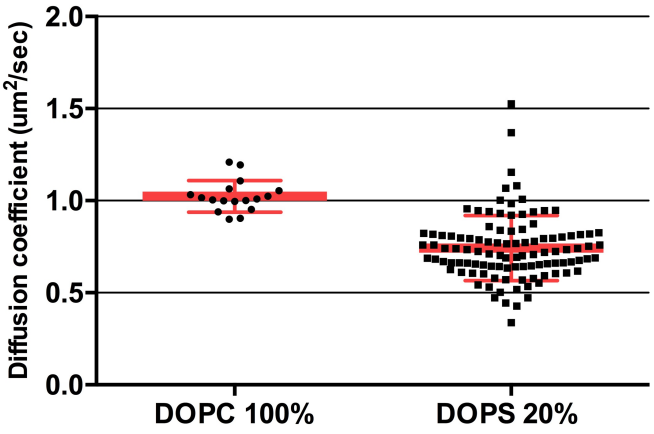

Figure 16: Effects of neutral and 20% negative lipid charge on diffusion of SLBs. Diffusion coefficients for DOPC 100% (left, n=17) vs DOPS 20% (right, n=105) containing supported lipid bilayers. All lipid bilayers were fashioned by the vesicle fusion method. Glass substrates were cleaned by base piranha surface treatment for both charge conditions. Lipid tracers included RhoPE and NBD-PC for Avanti #1 DOPC 100% and only RhoPE for all lipid batches DOPS 20%. DOPC 100% included 4 samples with 6 channels, DOPS 20% included 26 samples with 45 channels, all data was independent of a specific channel or sample.

Due to this significant drop in diffusion caused by charged headgroups, the influence of charge was further explored by increasing the concentration of charged lipids. Drop of lipid diffusion was noted in earlier research for 50% charged SLBs associated with alpha-synuclein [38]. Therefore 50% charged lipid bilayers were also investigated for

this research.

As explained in section 2.2 optimal surface treatment for homogeneous 50% lipid bilayers was obtained by ethanol cleaning (see **Figure 17a**), rather than base piranha cleaning. Lipid bilayers taken into account were always at least as homogeneous as displayed in **Figure 17b**. When making a comparison between 20% and 50% charged lipid bilayers, it is noted that 50% charged lipid bilayers have the tendency to result more easily into less homogeneous landscapes than 20%, however a well-formed 50% lipid bilayer is completely homogeneous, as seen in **Figure 17b**. This is not due to the surface treatment as base piranha cleaning results in much more 50% charged lipid bilayer heterogeneous landscape than displayed here (see section 4.1.2).

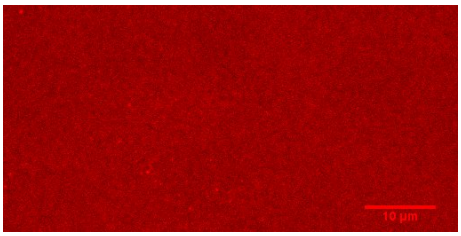

(a) Representative fluorescence image of DOPS 20% SLB. Same picture as displayed in **Figure 15b**. Homogeneous 20% negatively charged bilayer (1 mol% RhoPE labeled.).

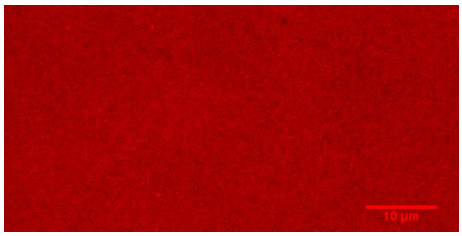

(b) Representative fluorescence image of DOPS 50% SLB. Homogeneous 50% negatively charged bilayer (1 mol% RhoPE labeled.).

Figure 17: Representative fluorescence images of SLBs. Images were acquired before photobleaching with FRAP. Both conditions were situated in F-buffer at room temperature. Scale bar is 10 μm.

Increasing the lipid charge even further, by 30% more, decreased D_{LL} to 0.40 μm^2/sec, which is another 34% drop, see **Figure 18**. Performing statistical analysis shows significant difference between diffusion data (Welch's t-test P< 0.0001). If this is compared with the D_{LL} of the neutral bilayer, the drop in diffusion is nearly 60%, which suggests a strong correlation between lipid charge and D_{LL}.

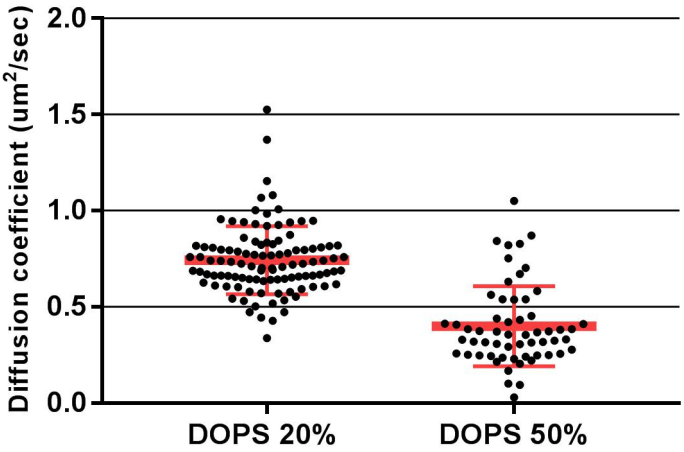

Figure 18: Effects of different densities of negative lipid charge on diffusion of SLBs. Diffusion coefficients for 20%-DOPS (left, n=105) vs 50%-DOPS (right, n=58) containing supported lipid bilayers. All lipid bilayers were fashioned by the vesicle fusion method. Glass substrates were cleaned by base piranha or ethanol surface treatment for both conditions. Lipid tracer was RhoPE for both conditions and all lipid batches are included. DOPS 20% included 26 samples with 45 channels and DOPS 50% included 14 samples with 27 channels, all data was independent of a specific channel or sample.

The effect of lipid charge on lipid diffusion is displayed quite clearly in the previous graphs (see **Figure 16** and **18**). Additionally interesting was the wide variance in D_{LL} obtained for the charged lipid bilayers. A large data set was necessary to draw conclusions on charge dependence, ±50 data points or higher. To explore the underlying cause of this variation, parameters potentially influencing lipid diffusion were investigated.

4.1.1 Lipid batches

Purchased lipids have an expiry date after which they can lose the distinctness of their properties. Predominantly for this study, weakening of lipid charge could be at hand, causing variations in D_{LL} per lipid vesicle batch. To investigate this variable, another batch of identical lipids were ordered, Avanti # 2 and another lipid batch from a different manufacturer were tested, Sigma # 1.
To better quantify the relation between lipid charge and the various lipid batches, the lipids were tested in 20% and 50% charged conditions (**Figure 19**).

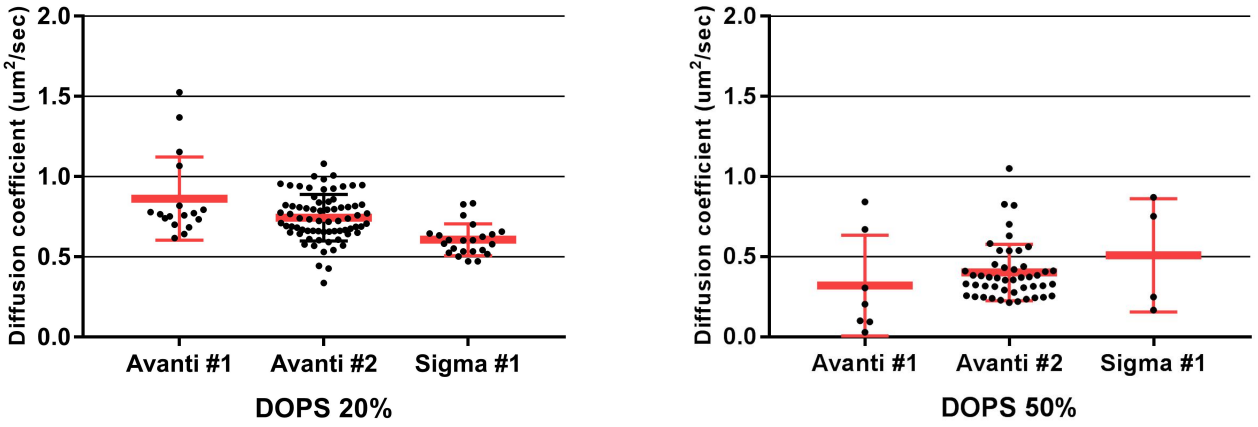

Figure 19: Comparison between brands and lots of DOPC and DOPS composed lipid bilayers. Diffusion coefficients for 20%-DOPS (left, n=17, 72, 16) vs 50%-DOPS (right, n= 7, 47, 4) containing supported lipid bilayers, fluorescent tracer Rhodamine-PE. Two different lots by Avanti are displayed and one for Sigma for each type of membrane. All lipid bilayers were fashioned by the vesicle fusion method. Glass substrates containing both types of charge were cleaned by or base piranha or ethanol surface treatment. Both conditions are included in this data. For DOPS 20%: Avanti #1 included 4 samples with 8 channels, Avanti #2 included 16 samples with 32 channels, and Sigma #1 included 5 samples and 7 channels, all data was independent of a specific channel or sample. For DOPS 50%: Avanti #1 included 2 samples with 4 channels, Avanti #2 included 11 samples with 24 channels, and Sigma #1 included 2 samples and 2 channels, all data was independent of a specific channel or sample.

Surprisingly, the batches showed different degrees of influence of lipid charge on D_{LL}. Avanti # 1 showed a strong dependence of charge to lipid diffusion, when regarding the difference in D_{LL} between 20% and 50% lipid bilayers. For the following lipid batches, the difference becomes smaller, where the Sigma lipid hardly seems to show an effect of lipid charge on lipid diffusion.
Here is again clearly noticeable the necessity of a large data set. The variance for the 50% charged lipid bilayers is extremely large for batches Avanti # 1 and Sigma # 1, and can therefore hardly serve as grounds for a conclusion.
Regarding only the results for 20% charged lipid bilayers, it is statistically significant that the batches induce different degrees of influence on D_{LL} (Kruskal-Wallis P<0.0001). Where it is feasible to say that Sigma # 1 lipids induce the strongest lipid slow down.
The data sets for both charged conditions of Avanti # 2 are sufficiently large to compare. However, although the D_{LL} follows the trend of charge dependent lipid slow down, the variance is still quite large.

Taking into account that both Avanti # 2 and Sigma # 1 were fresh lipids, the large variance in the displayed data cannot be due to aged lipids. Another variable, which has been studied extensively to influence lipid diffusion [20, 38], is surface treatment of the substrate.

4.1.2 Influence of surface treatment on membrane diffusion

To make the highest quality lipid bilayers, the optimal substrate cleaning method for both conditions had to be defined. Both types of charged lipid bilayers were tested on base piranha (see section 2.2.1) and ethanol (see section 2.2.2) cleaned substrates.
The effect on lipid bilayer homogeneousness of ill-favoured surface treatment is displayed in **Figure 20**. For the 20% charged lipid bilayer, surface treatment was not so much of an issue, the lipid bilayer showed a fairly homogeneous

landscape with exception of some darker and lighter intensity patches of around 20 microns in diameter (see **Figure 20a**).

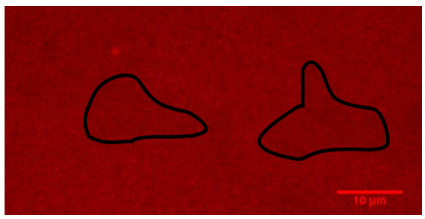

(a) Representative fluorescence image of DOPS 20% SLB on a ethanol treated substrate (1 mol% RhoPE labeled.).

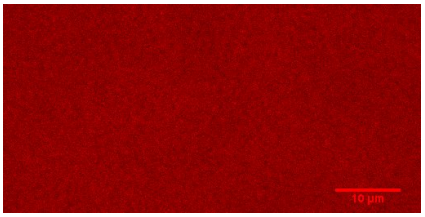

(b) Representative fluorescence image of a *mobile* DOPS 50% SLB on a base piranha treated substrate (1 mol% RhoPE labeled.).

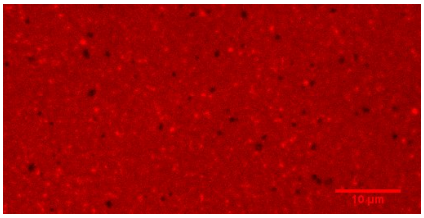

(c) Representative fluorescence image of an *immobile* DOPS 50% SLB on a base piranha treated substrate (1 mol% RhoPE labeled.). Note that this lipid bilayer has a heterogeneous landscape, indicating a strong likelihood for an immobility.

Figure 20: Representative fluorescence images of SLBs on substrate with ill-favoured surface treatment for the lipid bilayer charge composition. Images were acquired before photobleaching with FRAP. Both conditions were situated in F-buffer at room temperature. Scale bar is 10 μm.

By contrast, higher concentrations of charged lipids corresponded to increased specificity of preferred surface treatment. Although 50% charged lipid bilayer could be formed onto base piranha treated substrate, the reproducibility was very low. Lipid bilayers could result in homogeneous mobile lipid bilayers, see **Figure 20b**, or heterogeneous immobile lipid bilayers, see **Figure 20c**. **Figure 21** shows that the number of data points for 50% charged lipid bilayers on base piranha substrate is far lower than for the other conditions (n = 7 vs. 81, 24 and 54), due to failure of many lipid bilayers in these conditions. Interestingly, D_{LL} was higher on base piranha surfaces, compared to ethanol cleaned surfaces, for both 20% and 50% charged lipid bilayers.

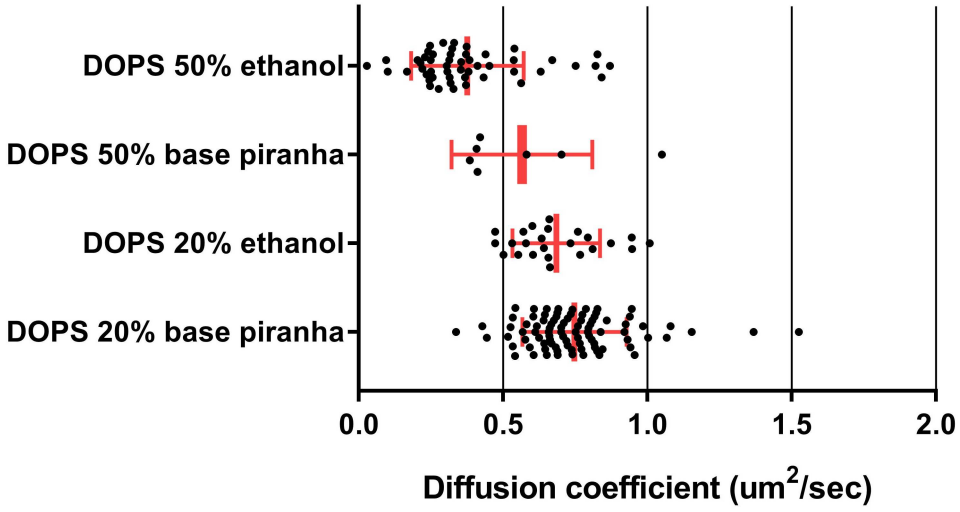

Figure 21: Surface treatment effect on lipid diffusion, base piranha vs ethanol. Diffusion coefficients for 20%-DOPS (bottom, n = 81, 24) vs 50%-DOPS (top, n = 7, 51) containing supported lipid bilayers, tracer Rhodamine-PE. Lipid bilayers were created by the vesicle fusion method and all lipid batches are included. For DOPS 20%: ethanol included 5 samples and 10 channels, base piranha included 21 samples and 35 channels. For DOPS 50%: ethanol included 12 samples and 23 channels, base piranha included 2 samples and 4 channels.

Even though the D_{LL} averages of both surface treatments showed similar results in 20% charged lipid bilayers (Welch's t test P = 0.0938 >0.05), base piranha surface treatment was preferred for this condition, based on landscape homogeneity.
For all conditions of lipid charge combined with the two types of surface treatment, D_{LL} variance was spread out.

This analysis gave insight to optimizing protocols for lipid bilayer formation (sections 2.3.1.2 and 2.3.2.2). However, it could not explain the large distribution of obtained D_{LL}.
Therefore, comparison of different lipid bilayer preparation techniques was necessary to investigate whether the large variance in D_{LL} might be influenced by the preparation technique of the lipid bilayers.

4.1.3 SLB methods

Before, lipid bilayers were formed by the vesicle fusion method (section 2.3.1.2). Earlier research reported differences in DLL due to preparation techniques, where the vesicle fusion method was compared to the Langmuir-Blodgett/ Langmuir-Schaffer methods [20, 41, 42].
To compare the D_{LL} variance of both methods, symmetric lipid bilayers were formed. To analyse if the variance was also charge dependent, a comparison was made between both methods for both neutral and 20% charged lipid bilayers.

Lipid bilayers formed by LBVF method (see section 2.3.2.2) resulted in homogeneous mobile bilayers (see **Figure 22**), comparable to lipid bilayers formed by VF.

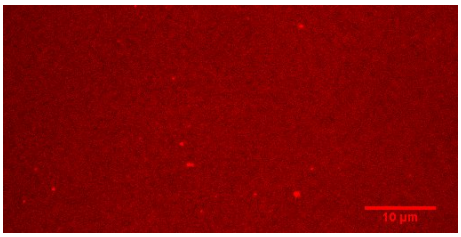

(a) Representative fluorescence image of a DOPC 100% SLB (1 mol% RhoPE labeled.).

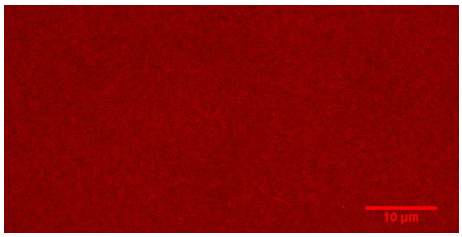

(b) Representative fluorescence image of a DOPS 20% SLB (1 mol% RhoPE labeled.).

Figure 22: Representative fluorescence images of SLBs, manufactured by the LBVF method. Images were acquired before photobleaching with FRAP. Both conditions were situated in F-buffer at room temperature. Scale bar is 10 μm.

Lipid diffusion, however, showed significant differences between LBVF and VF for both neutral and charged lipid bilayers. In the neutral lipid bilayers a significant difference in D_{LL} was shown (Welch's t t test $P < 0.0001$, see **Figure 23**). LBVF neutral lipid bilayers exhibited a higher D_{LL} than the VF lipid bilayers. However, both D_{LL} distributions showed minimal variance for neutral bilayers (see **Figure 23**). Contrarily, the 20% lipid bilayers again proved to present a large variance of D_{LL}, regardless of the preparation method.

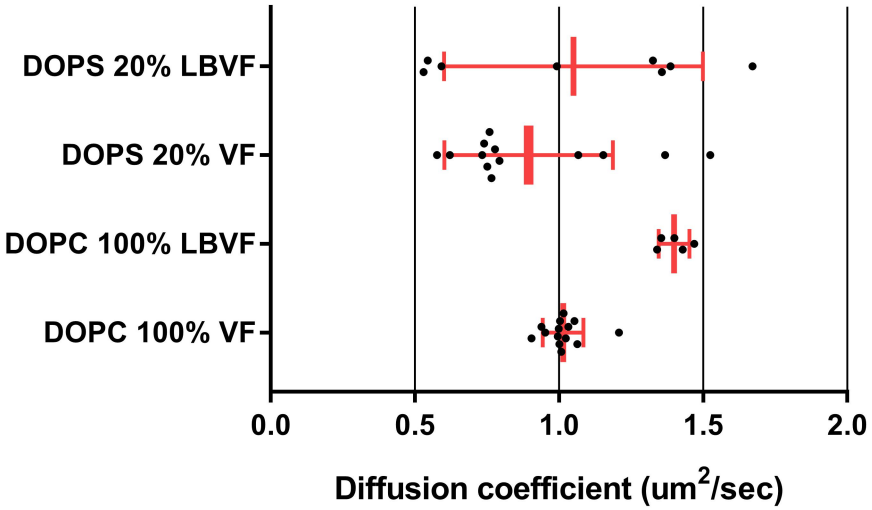

Figure 23: Effect on lipid diffusion caused by SLB production method. Diffusion coefficients for 100%-DOPC (left, n= 14, 5) vs 20%-DOPS (right, n= 13, 8) containing supported lipid bilayers, tracer Rhodamine-PE. Lipid bilayers were fashioned by the vesicle fusion method (VF) or by the Langmuir-Blodgett deposition combined with vesicle fusion (LBVF) using Avanti #1 lipids. Glass substrates were cleaned by base piranha surface treatment. DOPC 100% LBVF included 4 samples and 6 channels. DOPS 20% LBVF included 4 samples and 5 channels. VF data was taken from the first 4 samples of neutral and charged lipid bilayer experiments, which formed reproducible bilayers.

4.1.4 Influence of lipid tracers on membrane diffusion

To acquire more information about the charge dependent lipid diffusion, the charge effect per leaflet due to coupling was investigated. However, to correctly analyze the effect in each leaflet, the effect of different lipid tracers had to be defined. The fluorescent tracers used to visualize both leaflets of an asymmetrically charged lipid bilayer had their own charge; RhoPE is negatively charged and NBD-PC is neutral.

Neutral and charged lipid bilayers with both types of tracer were formed. All lipid bilayers were homogeneous, see **Figure 25**. Regarding D_{LL}, there was no significant difference between the charged RhoPE and neutral NBD-PC tracers in a neutral lipid bulk (Welch's t test $P = 0.5399 > 0.05$). However, the charged lipid bilayers revealed a significant difference in D_{LL} between the two tracers (Welch's t test $P = 0.0102 < 0.05$).

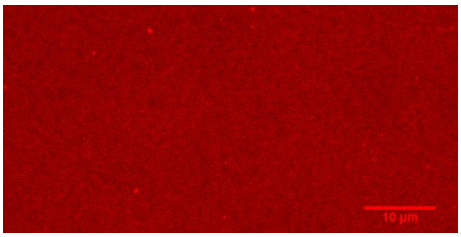

(a) Representative fluorescence image of a DOPC 100% SLB (1 mol% RhoPE labeled.).

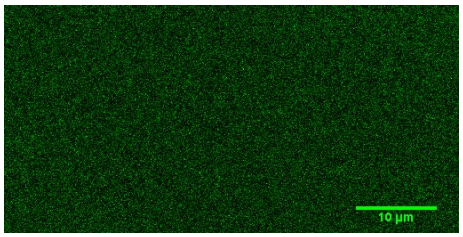

(b) Representative fluorescence image of a DOPC 100% SLB (1 mol% NBD-PC labeled.).

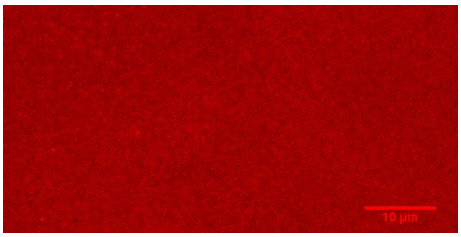

(c) Representative fluorescence image of a DOPS 20% SLB (1 mol% RhoPE labeled.).

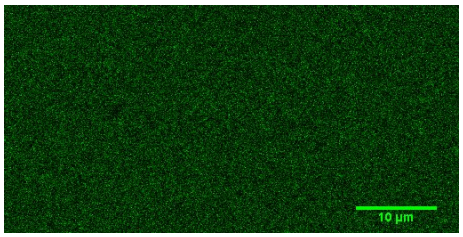

(d) Representative fluorescence image of a DOPS 20% SLB (1 mol% NBD-PC labeled.).

Figure 24: Representative fluorescent images of lipid tracers RhoPE and NBD-PC in neutral and charged SLBs. Images were acquired before photobleaching with FRAP. Both conditions were situated in F-buffer at room temperature. Scale bar is 10 μm.

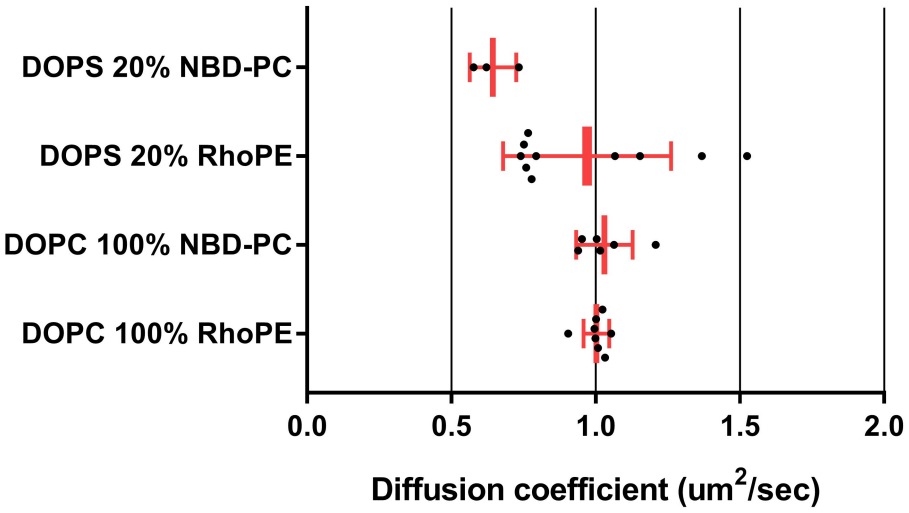

Figure 25: Rhodamine-PE vs NBD-PC tracer molecule on differently charged lipid bilayers. Diffusion coefficients for 100%-DOPC (left, n= 8, 6) vs 20%-DOPS (right, n= 10, 3) containing supported lipid bilayers. Lipid bilayers were fashioned by the vesicle fusion method. Glass substrates were cleaned by base piranha surface treatment. Only Avanti #1 lipids were used here. Also only lipid bilayers with RhoPE used on the same samples as NBD-PC lipid bilayers were regarded in this comparison. DOPC 100% RhoPE included 2 samples and 3 channels, NBD-PC 2 samples and 3 channels. DOPS 20% RhoPE included 2 samples and 2 channels, NBD-PC 2 samples and 3 channels.

Again the variance for the charged lipid bilayers is large compared to the neutral lipid bilayers. Furthermore, the charged NBD-PC tagged lipid bilayers only present three data points.

4.2 Asymmetric membrane diffusion in SLBs

A clear dependence of lipid diffusion to lipid charge can be stated on basis of the before mentioned data. To further explore this dependence, asymmetrically charged lipid bilayers were formed, by LBVF, to observe the magnitude of

lipid charge influence per leaflet.

Physiologically the plasma membrane is not symmetrical in charge, so it was interesting to investigate this effect of asymmetrical leaflet charges. Earlier research has found that typical D_{LL} values for SLBs are lower, DOPC 100% 3.1 ± 0.3 μm^2/sec [43], than values found in GUVs, DOPC 100% 7.8 ± 0.8 μm^2/sec [43]. This difference is most probably explained by the interaction between substrate and lipid bilayer in SLBs, causing lipid slow-down. Hypothetically, if no coupling of leaflets is present, the distal leaflet (facing the flow channel) could have D_{LL} values as high as seen in GUVs [7]. The proximal leaflet will attain a D_{LL} similar to that seen in symmetric SLBs [7].
Primarily, however, it is interesting to investigate if one leaflet is affected by the lipid charge composition of the opposing leaflet. In asymmetric lipid bilayers this influence can be defined by comparing D_{LL} of different composition combinations.

Proximal leaflets were dyed with RhoPE and distal leaflets with NBD-PC. Both leaflets had a visually homogeneous landscape in all conditions in the presented data, see **Figure 26**.

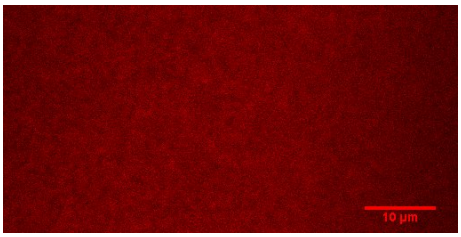

(a) Example of RhoPE labelled proximal leaflet of the SLB. In this case a DOPC 100% neutral leaflet. Imaged at 561 nm laser beam with confocal microscope set-up. Leaflet presents a homogeneous layer.

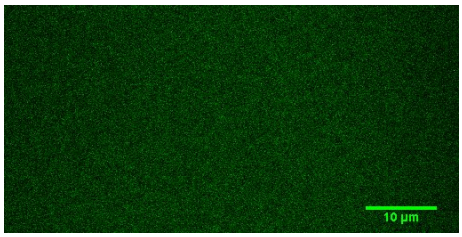

(b) Example of NBD-PC labelled distal leaflet of the SLB. In this case a DOPC 20% charged leaflet. Imaged at 561 nm laser beam with confocal microscope set-up. Leaflet presents a homogeneous layer.

Figure 26: Representative fluorescence images of leaflets of a LBVF created asymmetric lipid bilayer. Images were acquired before photobleaching with FRAP. Both conditions were situated in F-buffer at room temperature. Scale bar is 10 μm.

Considering the charge dependence of D_{LL}, the asymmetric lipid bilayers displayed some interesting results. Primarily, the leaflets seem coupled for a few reasons, see **Figure 27**. Firstly, the D_{LL} of the proximal leaflet decreases as a function of the distal leaflet's charge density, whilst keeping the proximal leaflet's composition constant, **Figures 27b, 27c and 27d**. Secondly, an increase in proximal leaflet charge, lowers all D_{LL} of corresponding distal leaflets (**Figure 27b, 27c and 27d**).
Lastly, although only the proximal leaflet interacts with the glass substrate, lipid diffusion closer to typical SLB values, 3.1 ± 0.3 μm^2/sec [43], was observed for both leaflets. Uncoupled leaflets would show D_{LL} values of the distal leaflet closer to 7.8 ± 0.8 μm^2/sec [43], which is found in free-standing GUVs. From these values found by Przybylo et al. (2006)[43], GUV D_{LL} values are twice as high as values for SLBs. Based on this report and taking the average D_{LL} of our data into account, we could hypothesize that in an uncoupled system, our distal leaflets would show D_{LL} of around 2.0 μm^2/sec.

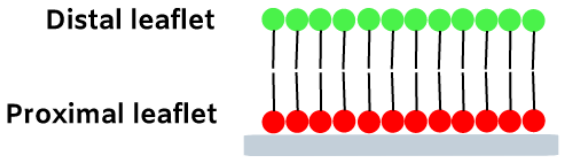

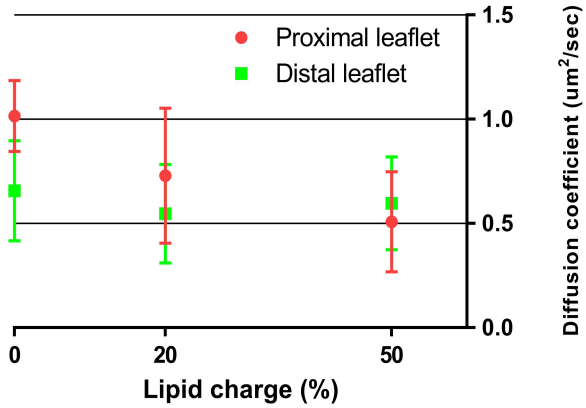

(a) Lipid diffusion in proximal and distal leaflets of asymmetric SLBs for various charges. Data is grouped together based only leaflet position and charge, not on opposite leaflet properties. Diffusion coefficients for 100%-DOPC (left, $n_{prox} = 12$, $n_{dis} = 9$), 20%-DOPS (middle, $n_{prox} = 10$, $n_{dis} = 10$) and 50%-DOPS (right, $n_{prox} = 8$, $n_{dis} = 10$).

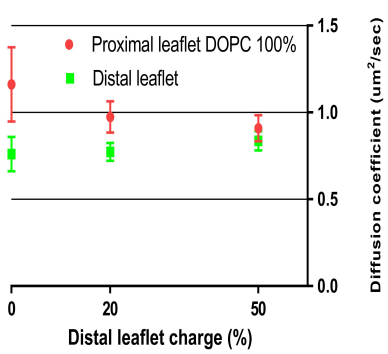

(b) Lipid diffusion for a proximal neutral DOPC 100% leaflet and varying charge of distal leaflets. Diffusion coefficients for distal DOPC 100% (left), DOPS 20% (middle) and DOPS 50% (right), all n = 4.

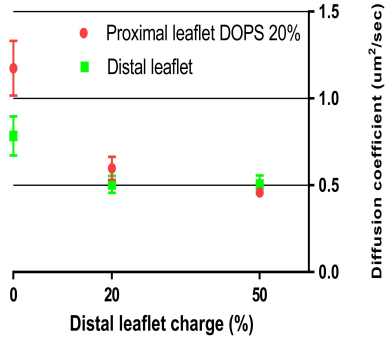

(c) Lipid diffusion for a proximal charged DOPS 20% leaflet and varying charge of distal leaflets. Diffusion coefficients for distal DOPC 100% (left, $n_{prox} = 3$, $n_{dis} = 3$), DOPS 20% (middle, $n_{prox} = 4$, $n_{dis} = 4$) and DOPS 50% (right, $n_{prox} = 4$, $n_{dis} = 3$).

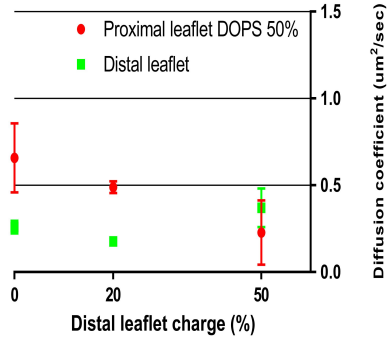

(d) Lipid diffusion for a proximal charged DOPS 50% leaflet and varying charge of distal leaflets. Diffusion coefficients for distal DOPC 100% (left, $n_{prox} = 4$, $n_{dis} = 2$), DOPS 20% (middle, $n_{prox} = 2$, $n_{dis} = 2$) and DOPS 50% (right, $n_{prox} = 2$, $n_{dis} = 3$).

Figure 27: Lipid diffusion for separate leaflets with different charge combinations. Tracer molecules are RhoPE for proximal leaflets, red circles, and NBD-PC for distal leaflets, green squares. Lipid bilayers were assembled by LBVF on base piranha treated cover slip.

Other surprising results are presented in this assay. The proximal leaflet exhibits faster lipid diffusion than the distal leaflet for neutral and 20% charged distal conditions (see **Figure 27b, 27c and 27d**). This is unexpected as the proximal leaflet is known to interact with the substrate and may therefore logically experience lipid slow down (see section 27). This trend is not followed for charged proximal leaflets combined with 50% charged distal leaflet. In these cases the distal leaflet is slightly faster than the lower proximal leaflet (see **Figure 27c and 27d** distal leaflet charge 50%).

As mentioned before, presence of a neutral composition gives rise to an increased D_{LL}, relatively to a charged counterpart. This is also true when only one leaflet in the bilayer has a neutral composition. Following the earlier noted charge dependence, the lowest values of D_{LL} are measured when a high 50% charged leaflet is part of the bilayer composition.

5 Results: Influence of septin on lipid diffusion

Septin is thought to act as a diffusion barrier in the plasma membrane, thereby causing subdiffusive behaviour of lipids [44, 25]. This protein diffusion barrier induced subdiffusive behaviour could explain the exponential relation between temperature and the diffusion coefficient, seen in live cells. To test whether septin directly causes diffusion barriers in lipid diffusion, diffusion in bare lipid bilayer was compared to diffusion in membranes with septin bound to it.
Unpublished data of the Koenderink lab showed that the protein binds to supported lipid bilayers containing PS headed lipids. In the following section, the effect of septin on lipid diffusion was investigated (section 5.1). To characterize the influence of septin on lipid diffusion, variables were modified to investigate the effect of septin and the lipid bilayer. The adjusted variables included; three lipid bilayer charge densities, three septin batches (see section 5.2), three septin concentrations (see section 5.3), two SLB preparation methods (see section 5.4) and a septin assay featuring charge asymmetric lipid bilayers (see section 5.5).

5.1 Influence of septin on differently charged membranes

A control experiment was performed to define the adhesion of septin to the SLBs. As mentioned above, septin is known to interact with the PS head-groups of lipids. Therefore, it was predicted that septin would not attach to neutral SLBs.
Fluorescent imaging showed no adhesion of septin to the neutral SLB, see **Figure 28d**. The accompanying lipid bilayer had a homogeneous landscape and was mobile, see **Figure 28a**. Furthermore, the corresponding septin FRAP curve showed full recovery, indicating septin had not adhered to the lipid bilayer surface or, in theory, initally adheres but dissociates very rapidly. In charged lipid bilayer conditions, septin shows a fluorescent homogeneous landscape adhered to the surface of the lipid bilayer, see **Figure 29b**. The corresponding septin curve shows a large immobile fraction as recovered fluorescent intensity does not exceed 50%, indicating adhesion to the lipid bilayer, see **Figure 29c**.

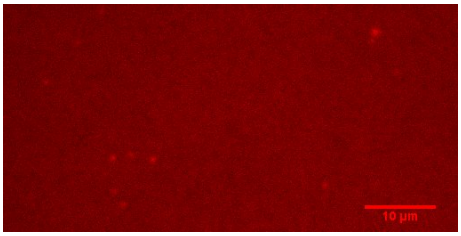

(a) Representative fluorescent image of RhoPE labelled DOPC 100% SLB. Imaged at 561 nm laser beam with confocal microscope set-up. Lipid bilayer presents a homogeneous membrane.

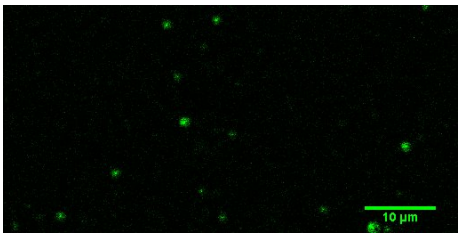

(b) Representative fluorescent image of 0.1 μM septin on a neutral lipid bilayer. Hardly any fluorescence is noted (GFP 488 nm), no adhesion of septin to the membrane was visible during imaging.

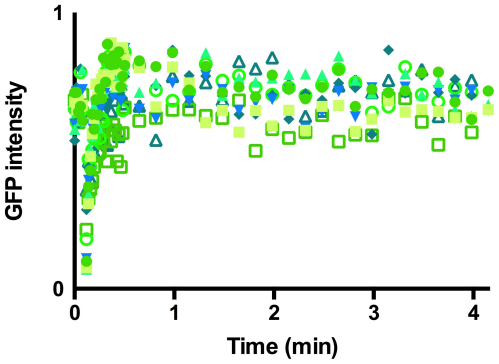

(c) Septin recovery curve from raw FRAP data of DOPC 100% SLB. Bleached area is $8\mu m$ in diameter. Each symbol is one FRAP recovery curve. All curves were obtained under equal conditions. Septin does not adhere to a completely neutral lipid bilayer, resulting in a complete fluorescence recovery of the diffusive septin present in the sample channel.

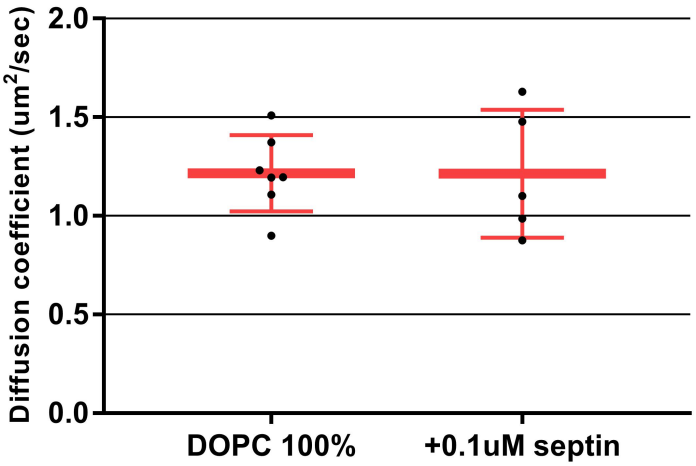

(d) Effect of septin on neutral, DOPC 100% lipid bilayer. Diffusion coefficients for DOPC 100% (left, n= 7) vs 100%-DOPC with 0.1uM septin (right, n= 5) containing supported lipid bilayers.

Figure 28: Effect of 0.1μM septin on a DOPC 100% symmetric lipid bilayer. Lipid bilayers were fashioned by the vesicle fusion method. Glass substrates were cleaned by base piranha surface treatment. All lipid batches are included. Septin batch #23 is displayed

FRAP experiments were performed on a lipid bilayer with and without septin. The D_{LL} of the bare neutral lipid bilayer was similar to that of a lipid bilayer with the presence of 0.5 μM septin (Welch's t test $P = 0.9909 > 0.05$), see **Figure 28d**. Furthermore, the D_{LL} values matched earlier neutral lipid bilayer results (see section 4.1). Therefore, these results could indicate that septin did not have an influence on the lipid diffusion of neutral lipid bilayers.
Next, DOPS 20% lipid bilayers were combined with septin. Two concentrations of septin were analyzed on the 20% charged lipid bilayers, 0.5μM (critical concentration, after which septin bundles [45]) and 0.1μM, which should result in a homogeneous carpet of septin on the lipid bilayer [Agata Szuba, unpublished work].

As shown in **Figure 29b**, at 0.5 μM septin binds, for the most part, as a homogeneous carpet. Some formation of bundles is also noted, due to prolonged polymerization time. The corresponding 20% charged lipid bilayer shows a homogeneous landscape and is mobile, see **Figure 29a**.

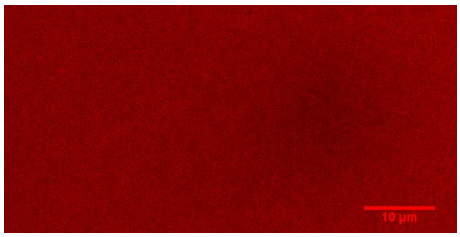

(a) Example of RhoPE labelled DOPS 20% SLB. Imaged at 561 nm laser beam with confocal microscope set-up. Lipid bilayer presents a homogeneous membrane.

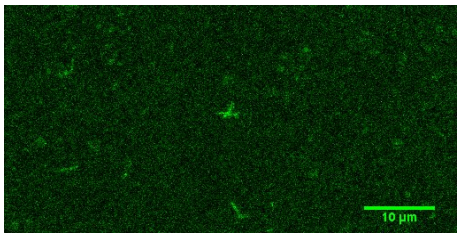

(b) Example of 0.5μM septin carpet situated on the upper surface of the SLB. Septin is tagged by GFP, imaged at 488 nm laser beam with confocal microscope set-up.

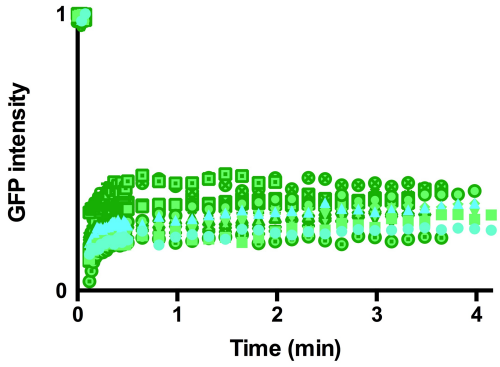

(c) Septin recovery curve from raw FRAP data of DOPS 20% SLB. Septin adheres to this 20% charged lipid bilayer, resulting in a 20-40 % fluorescence recovery of septin present in the sample channel.

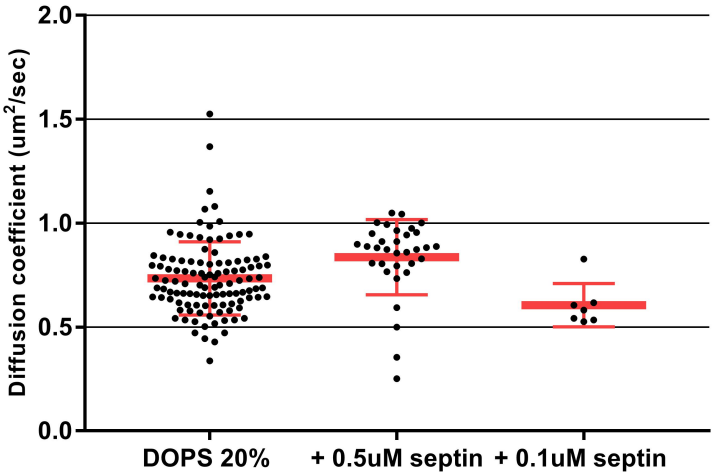

(d) Effect of septin on DOPS 20% charged lipid bilayer. Diffusion coefficients for DOPS 20% (left, n= 105) and with adhering septin at critical concentration (right, n= 33) DOPS 20% containing supported lipid bilayers, tracer Rhodamine-PE.

Figure 29: Effect of 0.5μM and 0.1μM septin on a DOPS 20% symmetric lipid bilayer. Lipid bilayers were fashioned by the vesicle fusion method. Glass substrates were cleaned by base piranha surface treatment. Septin batches #23 and #24 are displayed.

Regarding the effect of 0.5 μM septin on D_{LL}, it induced an increase of D_{LL} compared to the bare 20% charged lipid bilayer (see **Figure 29d**, Welch's t test $P = 0.0058 < 0.05$).
Contrastingly, 0.1 μM septin induced a drop in diffusion (see **Figure 29d**, Welch's t test $P = 0.0166 < 0.05$). However, when comparing the 0.1 μM septin results with only the bare membrane data of the same sample, septin induces an increase in diffusion [data not shown]. The mean D_{LL} is lower, 0.56 μm^2/sec, than D_{LL} with septin, which is 0.66 μm^2/sec. Therefore, septin does not induce a diffusion barrier at a concentration of 0.1 μM.

Next, septin at the critical concentration (0.5 μM) was combined with a 50% charged lipid bilayer, to examine the effect of septin on lipid diffusion even further.
The 50% charged lipid bilayers showed homogeneous landscapes (see **Figure 30a**), and septin bound to the lipid bilayer surface in a carpet structure (see **Figure 30b**).
Moreover, when bleached during FRAP, the septin carpet did not recover in intensity, suggesting proper adhesion of the septin to the lipid bilayer. This is also displayed in the septin FRAP curve, where GFP intensity quickly stabilizes and remains around 5-10% recovery, see **Figure 30c**.

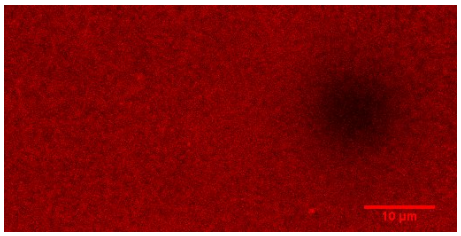

(a) Example of RhoPE labelled DOPS 50% SLB. Imaged at 561 nm laser beam with confocal microscope set-up. Lipid bilayer presents a homogeneous membrane.

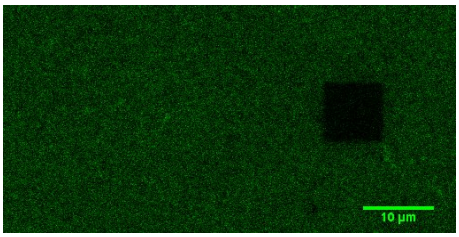

(b) Example of septin batch carpet situated on the upper surface of the SLB. Septin is tagged by GFP, imaged at 488 nm laser beam with confocal microscope set-up. Bleached area visible showing no recovery up to T_{end} , confirming septin adhesion.

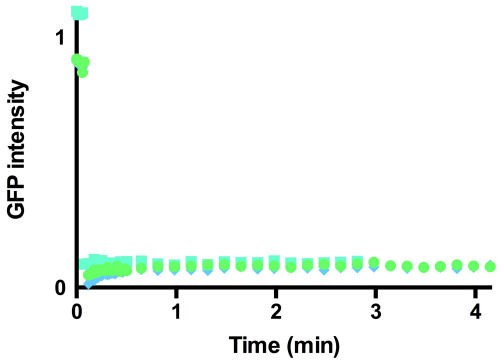

(c) Septin recovery curve from raw FRAP data of DOPS 50% SLB. When septin adhered as a homogeneous carpet to this 50% charged lipid bilayer, it resulted in a 10 % fluorescence recovery of septin.

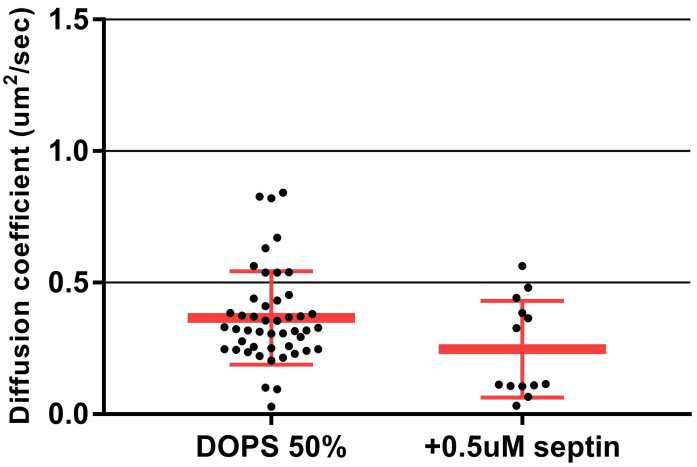

(d) Effect of septin on DOPS 50% charged lipid bilayer. Diffusion coefficients for DOPS 50%(left, n = 47) and with adhering septin at critical concentration (right, n = 13) DOPS 50% containing supported lipid bilayers, tracer Rhodamine-PE.

Figure 30: Effect of 0.5μM septin on a DOPC 50% symmetric lipid bilayer. Lipid bilayers were fashioned by the vesicle fusion method. Glass substrates were cleaned by ethanol surface treatment. Septin batches #21 and #23 were used.

Lipid diffusion measurements showed no significant effect of septin (see **Figure 30d**, Welch's t test P = 0.0526 > 0.05). Additionally, when investigating the raw data, on corresponding samples, the D_{LL} with septin was higher than for the bare lipid bilayer [data not shown]. Strikingly, it occasionally occurred that immobile lipid bilayers [data not shown in **Figure 30d**], became mobile in the presence of septin adhesion. Therefore, an increase in D_{LL} was noted for these assays.

5.2 Septin batches

The small enhancing effect of septins on lipid diffusion is opposite to the expected slow-down [25]. Therefore we decided that batch-specific faulty septin properties had to be excluded. Here, three batches of septin were compared. By eye lot #23 looked best; a homogeneous layer on the lipid bilayer surface with a few bundles was observed, see **Figure 31f**. Lot #22 seemed to adhere the worst, showing mainly large filament structures and clusters of septin, see **Figure 31e**. Lot #21 was of intermediate quality, having a combination of septin carpet and more bundles than in lot #23, see **Figure 31d**. Different imaging settings per sample and therefore intensities cannot be compared between pictures.

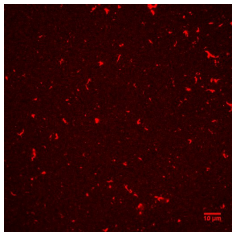

(a) Representative fluorescent image of DOPS 20% (lipid tracer 1 mol% RhoPE) lipid bilayer with high intensity spots that coincide with the lot #21 septin artifacts (see (d) below).

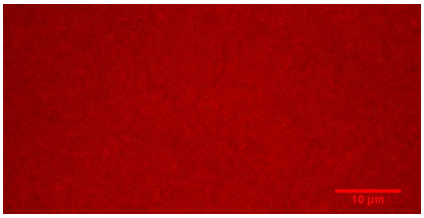

(b) Representative fluorescent image of DOPS 20% (lipid tracer 1 mol% RhoPE) homogeneous lipid bilayer with adhering lot #22 septin, displayed below (e).

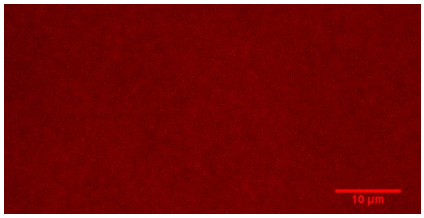

(c) Representative fluorescent image of DOPS 20% (lipid tracer 1 mol% RhoPE) homogeneous lipid bilayer with adhering lot #23 septin, displayed below (f).

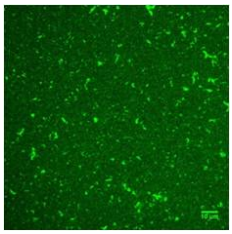

(d) Septin lot #21 showing carpet and bundels.

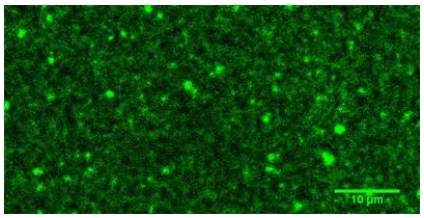

(e) Septin lot #22 showing mostly clots.

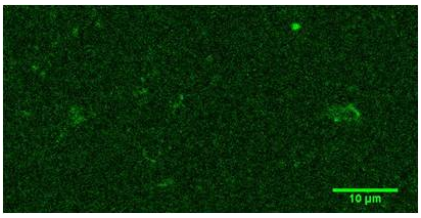

(f) Septin lot #23 showing carpet structure with a few bundels.

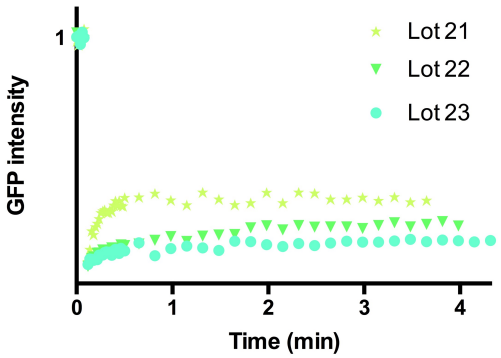

(g) Septin recovery curve from raw FRAP data of the various septin lots on a DOPS 20% SLB. For each lot one example is displayed. Recovery is the most for lot # 21 and the least for lot # 23.

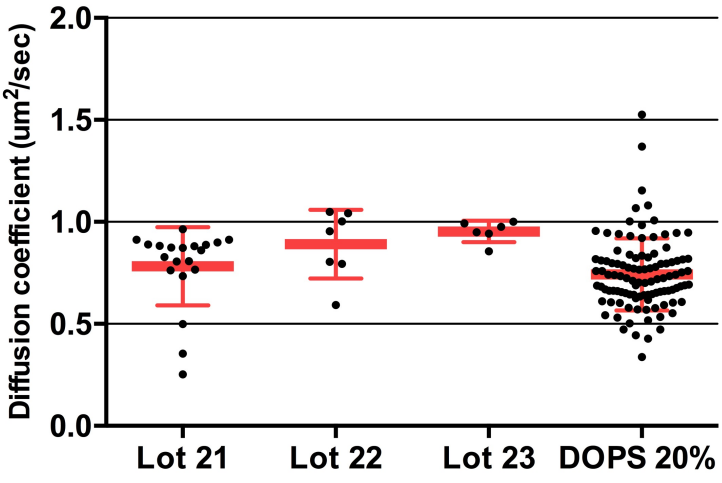

(h) DOPS 20% charged lipid bilayer composed by Langmuir-Blodgett Vesicle Fusion deposition vs equal conditions with critical concentration of septin. Diffusion coefficients for DOPS 20% with adhering septin at critical concentration 0.5μM, lipid tracer Rhodamine-PE. Comparison of various septin batches, purified in house fly septin; lot 21 (left, n=20), lot 22 (middle, n=7) and lot 23 (right, n=6).

Figure 31: Effects of three septin lots on lipid diffusion. Glass substrates were cleaned by base piranha surface treatment. Septin carpet and clots situated on the upper surface of the SLB. Septin is tagged by GFP, imaged at 488 nm laser beam with confocal microscope set-up. Scale bars are 10 mircons.

When comparing D_{LL} per septin batch, it was interesting to remark significant differences between all septin batches (see **Figure 31h**, Kruskal-Wallis test $P = 0.0234 < 0.05$).

5.3 Septin concentrations

To further characterize the behaviour of septin, different concentrations, below critical concentration, were analyzed. Concentrations of 0.05 μM, 0.1 μM and 0.5 μM on DOPS 20% lipid bilayers were compared.

Regarding the lipid bilayers and corresponding septin layers visually (see **Figure 32**), a number of artifacts were present that might explain the diffusion results. The lipid bilayer with 0.05 μM septin (**Figure 32b and 32e**) shows large defects. Coinciding these defects is a local increase in septin concentration, possibly because septin sticks to the glass underneath the lipid bilayer defect. For the 0.1 μM septin condition, hardly any septin is bound to the lipid bilayer surface (see **Figure 32c and 32f**) and remarkably, the D_{LL} in **Figure 33d** is closer to that for bare SLBs, unlike for the other septin concentrations tested. Different from the images acquired for 0.05 μM septin, for 0.1 uM septin, the lipid bilayer defects do not coincide with the septin clusters shown. Finally, the 0.5 μM condition shows a homogeneous lipid bilayer and the septin carpet layer is present (see **Figure 32d and 32g**). However, yet again some septin clusters occur on the septin layer, although there are no lipid bilayer artifacts.

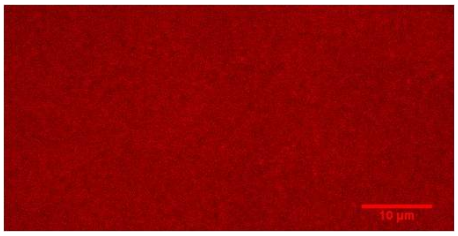

(a) DOPS 20% Sigma lipid bilayer, lipid tracer Rhodamine-PE.

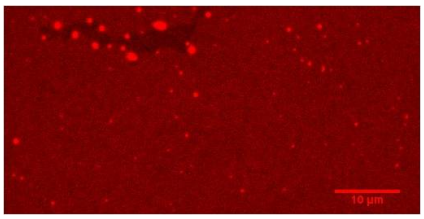

(b) DOPS 20% lipid bilayer with 0.05uM septin layer. Defects of the membrane colocalize with preferred septin adhesion sites. On homogeneous patches of membrane the septin is formed in vaguely bundled structures.

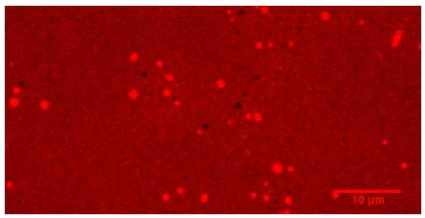

(c) DOPS 20% lipid bilayer with 0.1uM septin layer. Defects of the membrane do not colocalize with septin clotted structures. On homogeneous patches of membrane the adhered septin structure is not visible.

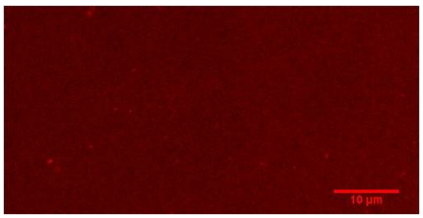

(d) DOPS 20% lipid bilayer with 0.5uM septin layer. Small defects in the membrane colocalize with septin clotted structures. On homogeneous patches of membrane the adhered septin has a carpet structure.

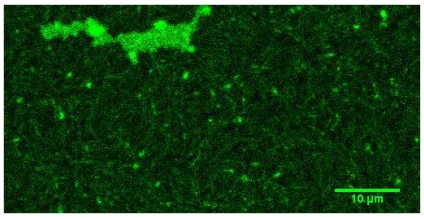

(e) See figure 32b.

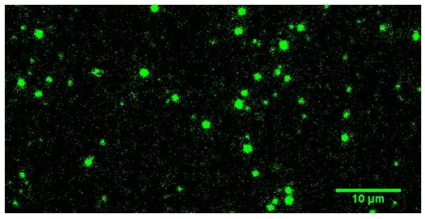

(f) See figure 32c.

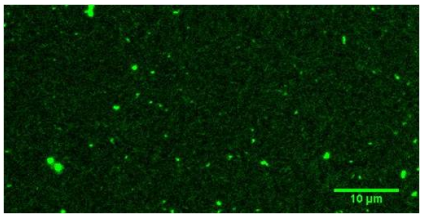

(g) See figure 32d.

Figure 32: DOPS 20% charged lipid bilayers combined with 0.05μM, 0.1μM and 0.5μM concentrations of septin #22. Septin carpet and clots situated on the upper surface of the SLB. Septin is tagged by GFP, imaged at 488 nm laser beam with confocal microscope set-up. All scale bars are 10 microns.

We observed increased (0.05 and 0.5 μM) or similar (0.1 μM) values of D_{LL} to the bare DOPS 20% lipid bilayer (see **Figure 33d**). Interestingly, D_{LL} with 0.1 μM was lower than at 0.05 and 0.5 μM, possibly due to the lack of septin binding.

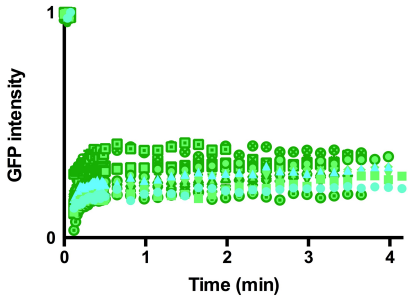

(a) Septin recovery curve from raw FRAP data of DOPS 20% SLB. When 0.5 μM septin adhered as a homogeneous carpet to this 20% charged lipid bilayer, it resulted in a 20-40 % fluorescence recovery of septin.

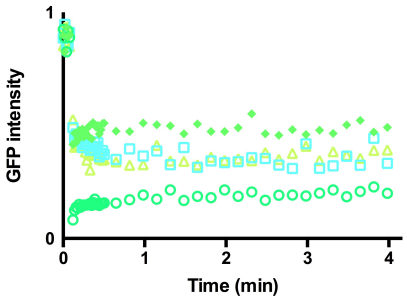

(b) Septin recovery curve from raw FRAP data of DOPS 20% SLB. When 0.1 μM septin adhered as a homogeneous carpet to this 20% charged lipid bilayer, it resulted in a 20-50 % fluorescence recovery of septin.

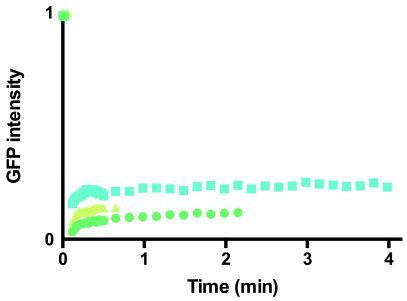

(c) Septin recovery curve from raw FRAP data of DOPS 20% SLB. When 0.05 μM septin adhered as a homogeneous carpet to this 20% charged lipid bilayer, it resulted in a 10-30 % fluorescence recovery of septin.

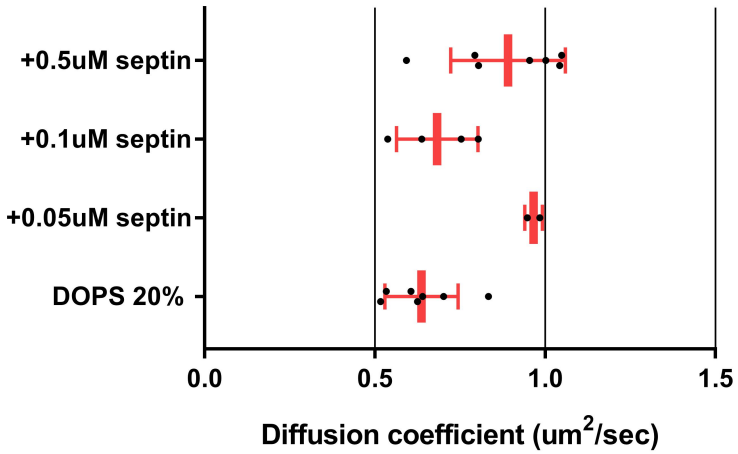

(d) Diffusion coefficients for DOPS 20% with different concentrations of adhering septin, 0.05 μM (n=2), 0.1 μM (n=4) and 0.5 μM (n=7), lipid tracer Rhodamine-PE. Septin concentration increases per data column up to critical level of septin 0.5 μM.

Figure 33: DOPS 20% charged lipid bilayers combined with 0.05 μM, 0.1 μM and 0.5 μM concentrations of septin #22. Glass substrates were cleaned by base piranha surface treatment.

5.4 Effect of septin on two SLB methods

To test whether the membrane preparation method has an affect on the adhesion of septin to the lipid bilayer, the SLB formation method was changed from VF to LBVF. Lipid bilayers formed by LBVF resulted in a very inhomogeneous septin layer (**Figure 34d**) and no change in D_{LL} on a DOPS 20% lipid bilayer (**Figure 34b**).

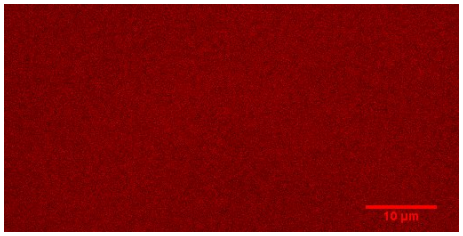

(a) Representative fluorescent image (RhoPE 1 mol%) of homogeneous DOPS 20% lipid bilayer, manufactured by LBVF.

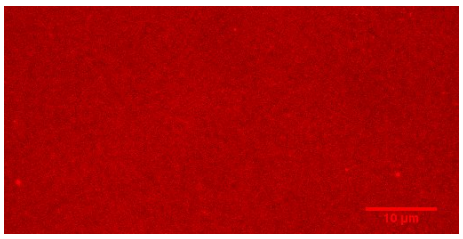

(b) Representative fluorescent image (RhoPE 1 mol%) of homogeneous DOPS 20% lipid bilayer, manufactured by LBVF with adhering 0.5 μm septin. No defects on the lipid bilayer clearly visible, whereas the septin layer is full of clusters (see c).

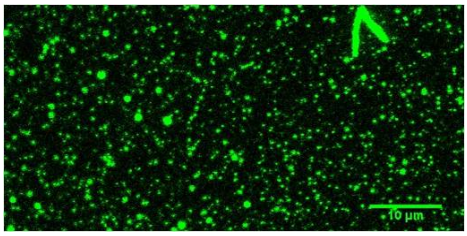

(c) Example of septin batch #21 carpet and clots situated on the upper surface of the SLB. Septin is tagged by GFP, imaged at 488 nm laser beam with confocal microscope set-up.

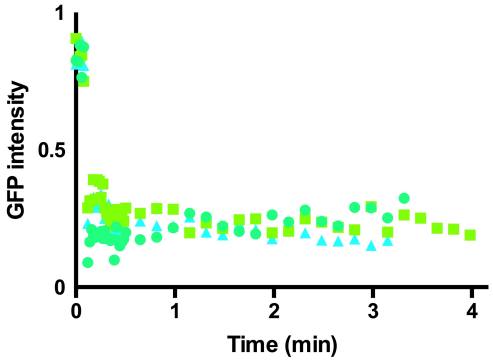

(d) Septin recovery curve from raw FRAP data of DOPS 20% SLB, manufactured by LBVF. When septin adhered to this 20% charged lipid bilayer, it resulted in a ± 25% fluorescence recovery of septin.

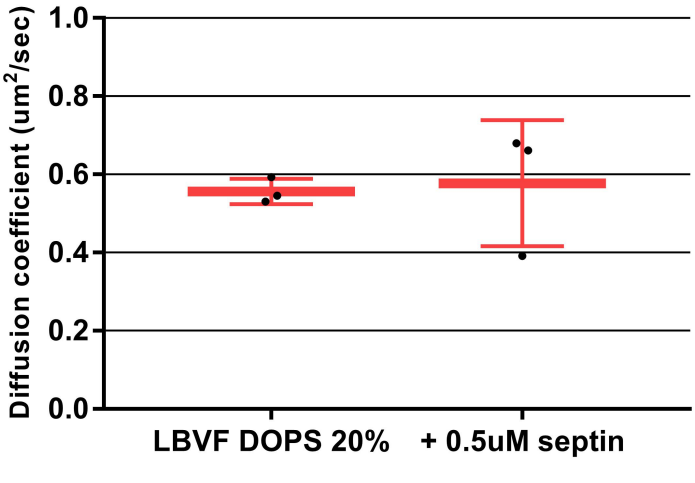

(e) DOPS 20% charged lipid bilayer composed by Langmuir-Blodgett / vesicle Fusion deposition with critical concentration of septin. Diffusion coefficients for DOPS 20% (left, n= 3) and with adhering septin at critical concentration (right, n=3) DOPS 20% containing supported lipid bilayers, lipid tracer Rhodamine-PE. Glass substrates were cleaned by base piranha surface treatment.

Figure 34: Symmetric lipid bilayer preparation according to the LBVF method combined with 0.5 μM septin batch #21.

5.5 Influence of septin on asymmetrically charged membranes

Septin is a peripheral membrane protein, which only directly interacts with the inner leaflet of the plasma membrane. In SLBs, septin binds to the charged PS head-groups of the lipids in the distal leaflet, which is facing the flow channel

environment. However, to understand the extent of the influence of septin on lipid diffusion, it was interesting to analyze the proximal and distal leaflets separately.
Similar to the asymmetrically charged lipid bilayers (see section 4.2), an increase of lipid diffusion from neutral to 50 % charged lipid bilayer was observed (see **Figure 36**). Again similar to earlier results (**Figure 27**), D_{LL} of the lipid bilayers with adhered septin was increased compared to the bare lipid bilayers, with an exception for the proximal DOPS 50% leaflet, which was comparable to its corresponding bare lipid bilayer.

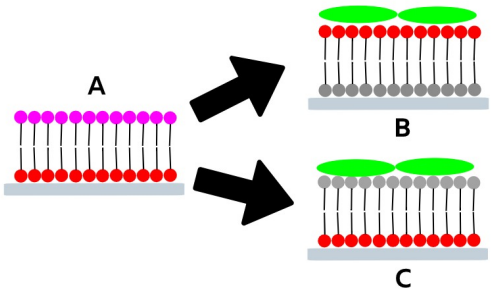

Figure 35: Comparison of displayed data and experimental situation. A) Situation presented in following results; proximal leaflet is coloured red and distal leaflet is coloured pink. B) Acquisition of FRAP curves for distal leaflets was achieved by only adding dye to the distal leaflet and leaving the proximal leaflet dark. Septin was tagged with GFP. C) To visualize the proximal leaflet, only this leaflet was dyed. Thereby leaving the distal leaflet dark.

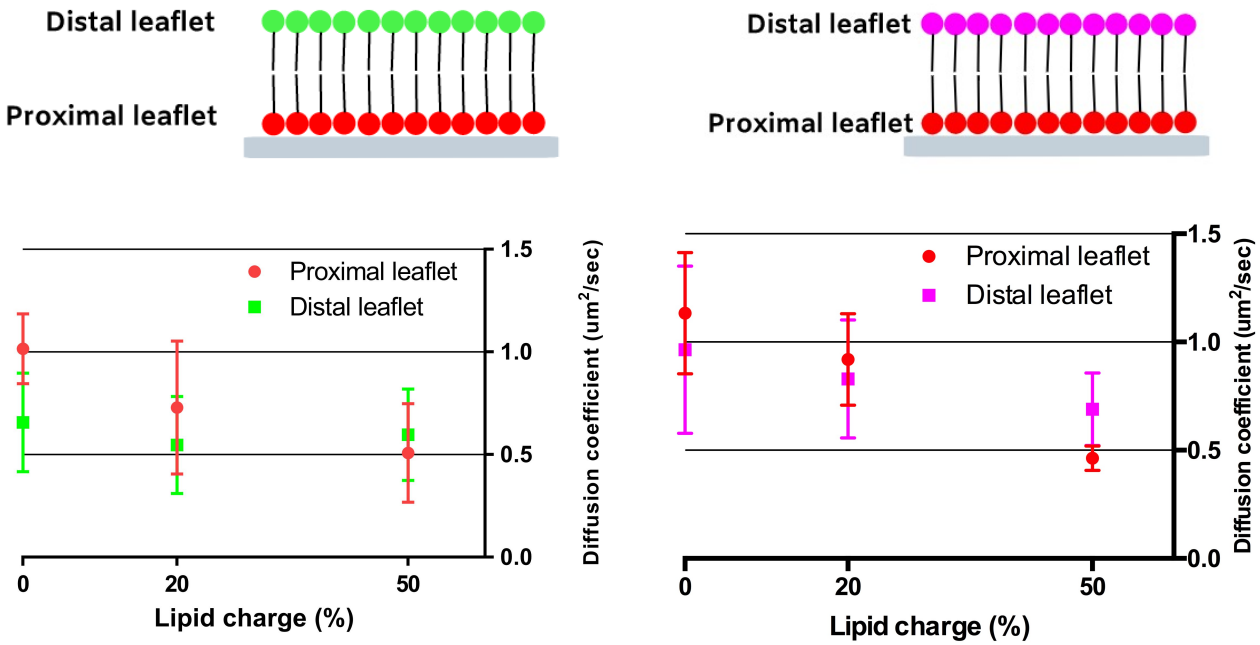

Figure 36: Effect of 0.1 μM septin batch #24 on proximal and distal leaflets for DOPC 100%, DOPS 20% and DOPS 50%. Displayed on the left, copy of D_{LL} for asymmetric leaflets without septin (see section 4.2). On the right, with 0.1 μM septin for proximal and distal leaflets in 0 ($n_{prox} = 20$, $n_{dis} = 16$), 20 ($n_{prox} = 11$, $n_{dis} = 16$) and 50% ($n_{prox} = 10$, $n_{dis} = 11$) charged conditions. Lipid bilayers were made by LBVF on base piranha treated glass. All leaflets in the septin graph (right) are RhoPE labelled.

It is even more interesting to regard the D_{LL} based on division by proximal leaflet charge. On a DOPC 100% proximal leaflet with an equally neutral distal leaflet, no attachment of septin occurs (see **Figure 38c**). However, the D_{LL} of both leaflets increase relatively to their bare lipid bilayer counterpart (see **Figure 39**). With a DOPS

20% distal leaflet, the proximal neutral leaflet presents the same D_{LL}, wheras the distal leaflet increases in diffusion. Septin attaches well in a carpet layer to the DOPS 20% distal leaflet (see **Figure 38f**). For a DOPS 50% distal leaflet, the proximal neutral leaflet increases in D_{LL} and the charged distal leaflet reduces in D_{LL}. Onto the DOPS 50% the septin does attach but not quite as homogeneously as for the DOPS 20% distal leaflet (see **Figure 38i**).

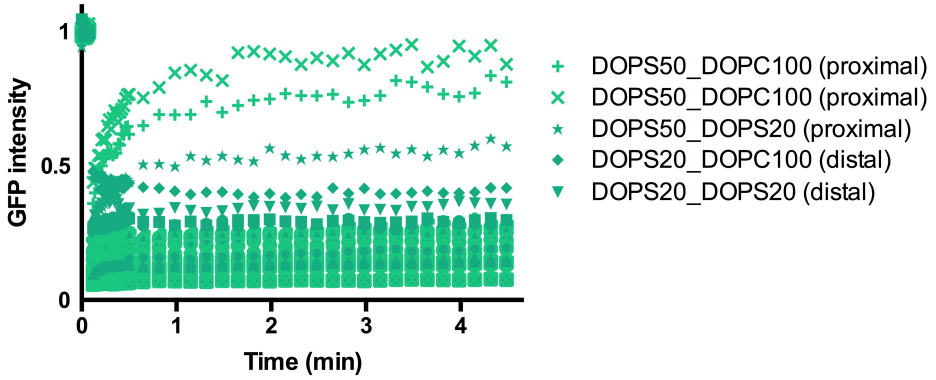

Figure 37: Septin batch #24 FRAP curves for all asymmetric leaflets, proximal and distal. Most septin fluorescent recovery curves reach around 5-40 %. Except for leaflets shown in the legend, which show more or even complete recovery. These are leaflets of 100% neutral lipid bilayers, or with a distal neutral leaflet, or a leaflet where septin did not bind correctly to.

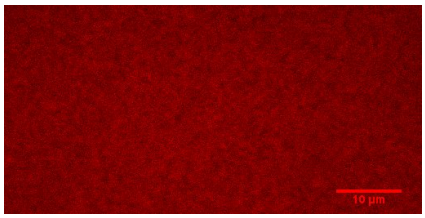

(a) Proximal DOPC 100% leaflet, RhoPE labelled.

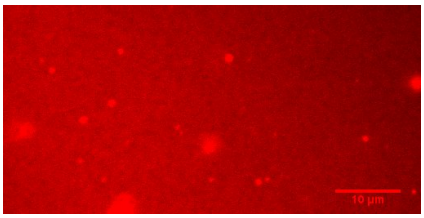

(b) Distal DOPS 100% leaflet, RhoPE labelled.

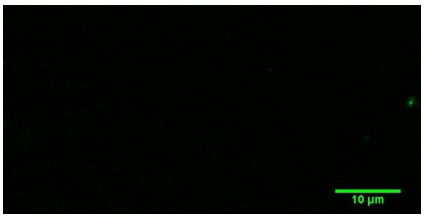

(c) Septin 0.1 μM on neutral lipid bilayer.

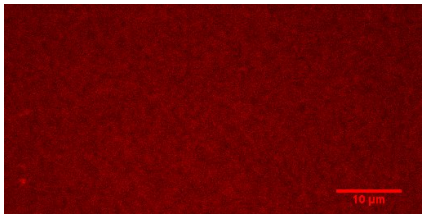

(d) Proximal DOPC 100% leaflet, RhoPE labelled.

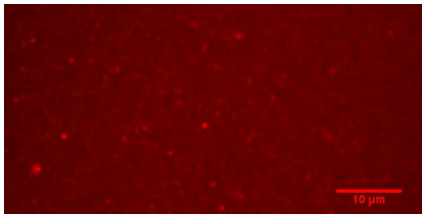

(e) Distal DOPS 20% leaflet, RhoPE labelled.

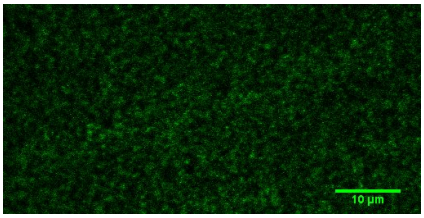

(f) Septin 0.1 μM on neutral proximal leaflet and 20% charged distal leaflet.

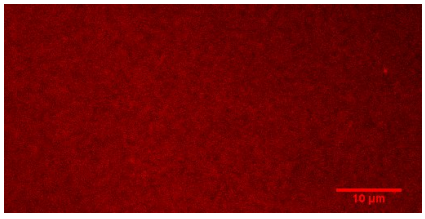

(g) Proximal DOPC 100% leaflet, RhoPE labelled.

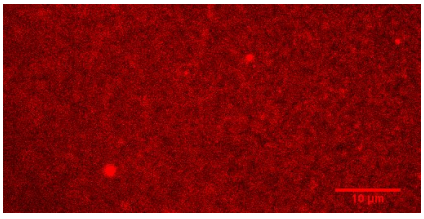

(h) Distal DOPS 50% leaflet, RhoPE labelled.

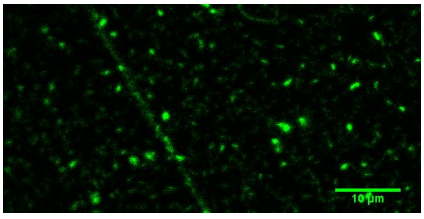

(i) Septin 0.1 μM on neutral proximal leaflet and 50% charged distal leaflet.

Figure 38: Representative fluorescent images (RhoPE for lipid leaflets and NBD-PC for 0.1 μm septin batch #24.) of proximal DOPC 100% based asymmetric lipid bilayers. Bilayers were manufactured by LBVF on a base piranha glass cover slip. Images were acquired before FRAP experiments took place. All conditions contained F-buffer, at room temperature, filled channel at the time of image acquisition. Scale bar is 10 μm.

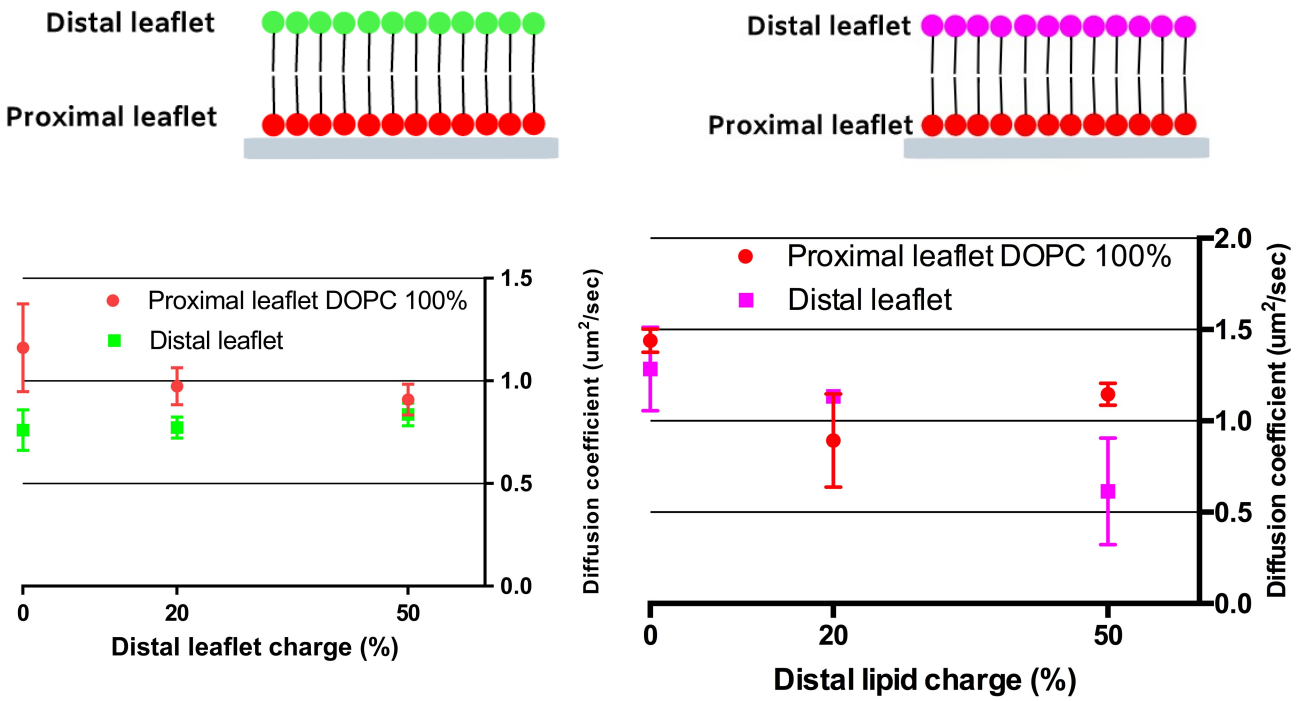

Figure 39: Effect of 0.1 μM septin on a DOPC 100% proximal leaflet and DOPC 100% (n_{prox} = 6, n_{dis} = 6), DOPS 20% (n_{prox} = 8, n_{dis} = 3) and DOPS 50% (n_{prox} = 6, n_{dis} = 2) distal leaflets. Displayed on the left, copy of D_{LL} for asymmetric leaflets with a DOPC 100% proximal leaflet without septin (see section 4.2). On the right, same conditions but with 0.1 μM septin. Lipid bilayers were made by LBVF on base piranha treated glass. All leaflets in the septin graph (right) are RhoPE labelled.

On a charged DOPS 20% proximal leaflet with a neutral DOPC 100% distal leaflet, adhesion of septin occurs even though this is not to be expected. The septin carpet layer is not completely homogeneous, some septin clusters occur (see **Figure 40c**). The 20% charged proximal leaflet is decreased in D_{LL} and the distal neutral leaflet is slightly increased in D_{LL}. In the symmetric DOPS 20% lipid bilayer, septin is well attached, forming a homogeneous carpet layer (see **Figure 40f**). Here, both leaflets have an increased diffusion (see **Figure 41**). For a higher, 50%, charged distal leaflet an increased D_{LL} was obtained. No data was measured for the proximal 20% charged leaflet. Also on this lipid bilayer septin attached as carpet, although not as homogeneously as the symmetric 20% charged lipid bilayer (see **Figure 40i**).

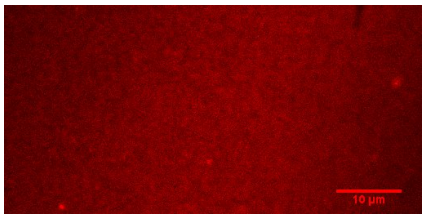

(a) Proximal DOPS 20% leaflet, RhoPE labelled.

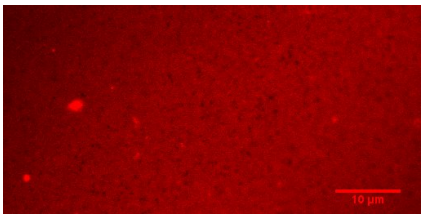

(b) Distal DOPC 100% leaflet, RhoPE labelled.

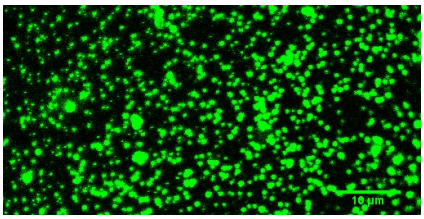

(c) Septin 0.1 μM on 20% charged proximal leaflet and neutral distal leaflet.

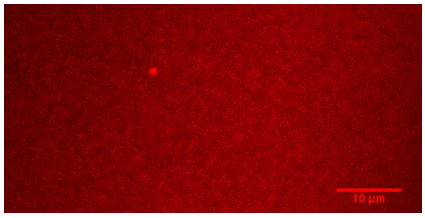

(d) Proximal DOPS 20% leaflet, RhoPE labelled.

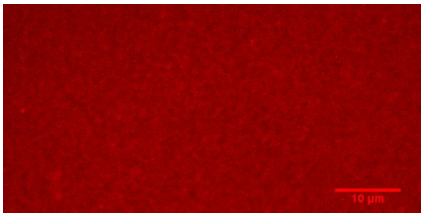

(e) Distal DOPS 20% leaflet, RhoPE labelled.

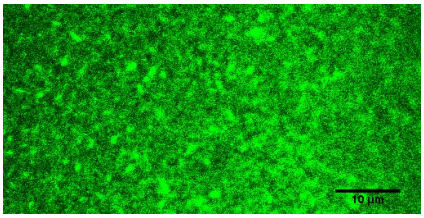

(f) Septin 0.1 μM on 20% charged proximal leaflet and 20% charged distal leaflet.

(g) Missing.

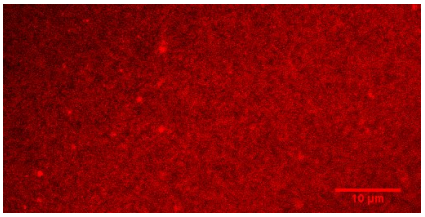

(h) Distal DOPS 50% leaflet, RhoPE labelled.

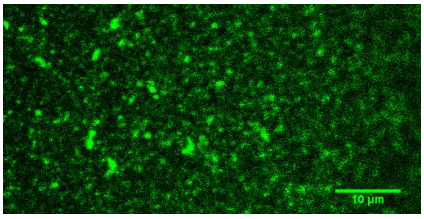

(i) Septin 0.1 μM on 20% charged proximal leaflet and 50% charged distal leaflet.

Figure 40: Representative fluorescent images (RhoPE for lipid leaflets and NBD-PC for 0.1 μm septin batch #24.) of proximal DOPC 20% based asymmetric lipid bilayers. Bilayers were manufactured by LBVF on a base piranha glass cover slip. Images were acquired before FRAP experiments took place. All conditions were contained F-buffer, at room temperature, filled channel at the time of image acquisition. Scale bar is 10 μm.

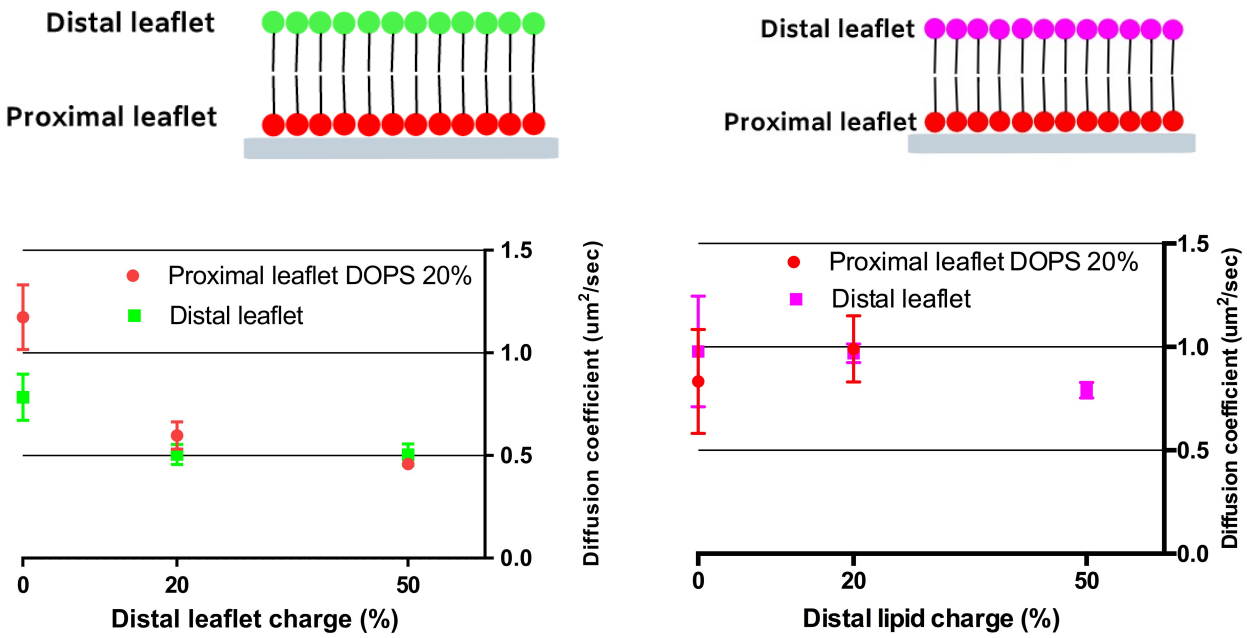

Figure 41: Effect of 0.1 μM septin on a DOPC 20% proximal leaflet and DOPC 100% (n_{prox} = 5, n_{dis} = 6), DOPS 20% (n_{prox} = 6, n_{dis} = 6) and DOPS 50% (n_{prox} = 0, n_{dis} = 7) distal leaflets. Displayed on the left, copy of D_{LL} for asymmetric leaflets with a DOPC 20% proximal leaflet without septin (see section 4.2). On the right, same conditions but with 0.1 μM septin. Lipid bilayers were made by LBVF on base piranha treated glass. All leaflets in the septin graph (right) are RhoPE labelled.

Also on a 50% charged proximal leaflet combined with a neutral DOPC 100% leaflet, septin showed attachment in a carpet structure. Vaguely filaments can be defined, but for the most part the septin layer is homogeneous (see **Figure 42c**). D_{LL} for the proximal charged leaflet was reduced and for the neutral distal leaflet increased. Therefore resulting in an equal diffusion for both leaflets (see **Figure 43**). With a DOPS 20% leaflet, septin adhered well (see **Figure 42f**). The D_{LL} for the proximal 50% leaflet stayed equal to its bare leaflet counterpart. The DOPS 20% distal leaflet increased in D_{LL}, thereby rising above the D_{LL} of the proximal leaflet (see **Figure 43**). Lastly, for the symmetrical DOPS 50% lipid bilayer, the distal leaflet remained equal to a situation without septin. The septin adhered to the lipid bilayer as a carpet structure with a few septin clusters (see **Figure 42i**). No further data on this condition was acquired.

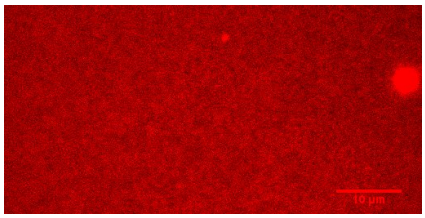

(a) Proximal DOPS 50% leaflet, RhoPE labelled.

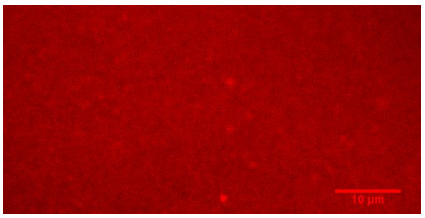

(b) Distal DOPC 100% leaflet, RhoPE labelled.

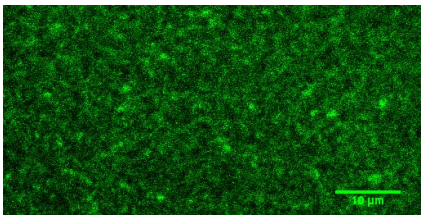

(c) Septin 0.1 μM on 50% charged proximal leaflet and 100% neutral distal leaflet.

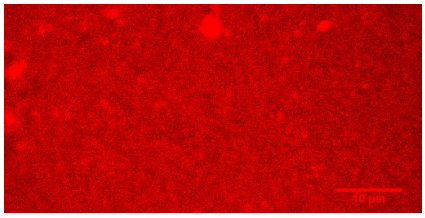

(d) Proximal DOPS 50% leaflet, RhoPE labelled.

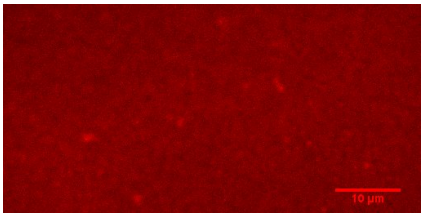

(e) Distal DOPS 20% leaflet, RhoPE labelled.

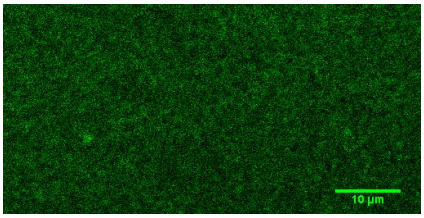

(f) Septin 0.1 μM on 50% charged proximal leaflet and 20% charged distal leaflet.

(g) Missing.

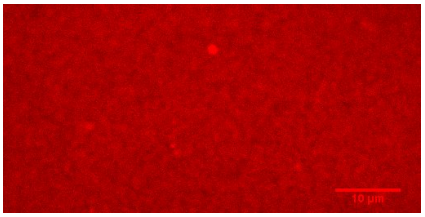

(h) Distal DOPS 50% leaflet, RhoPE labelled.

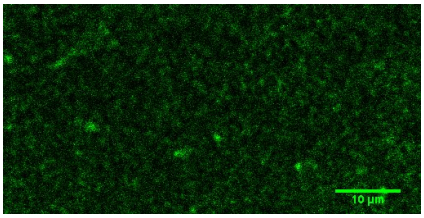

(i) Septin 0.1 μM on 50% charged proximal leaflet and 50% charged distal leaflet.

Figure 42: Representative fluorescent images (RhoPE for lipid leaflets and NBD-PC for 0.1 μm septin batch #24.) of proximal DOPS 50% based asymmetric lipid bilayers. Bilayers were manufactured by LBVF on a base piranha glass cover slip. Images were acquired before FRAP experiments took place. All conditions were contained F-buffer, at room temperature, filled channel at the time of image acquisition. Scale bar is 10 μm.

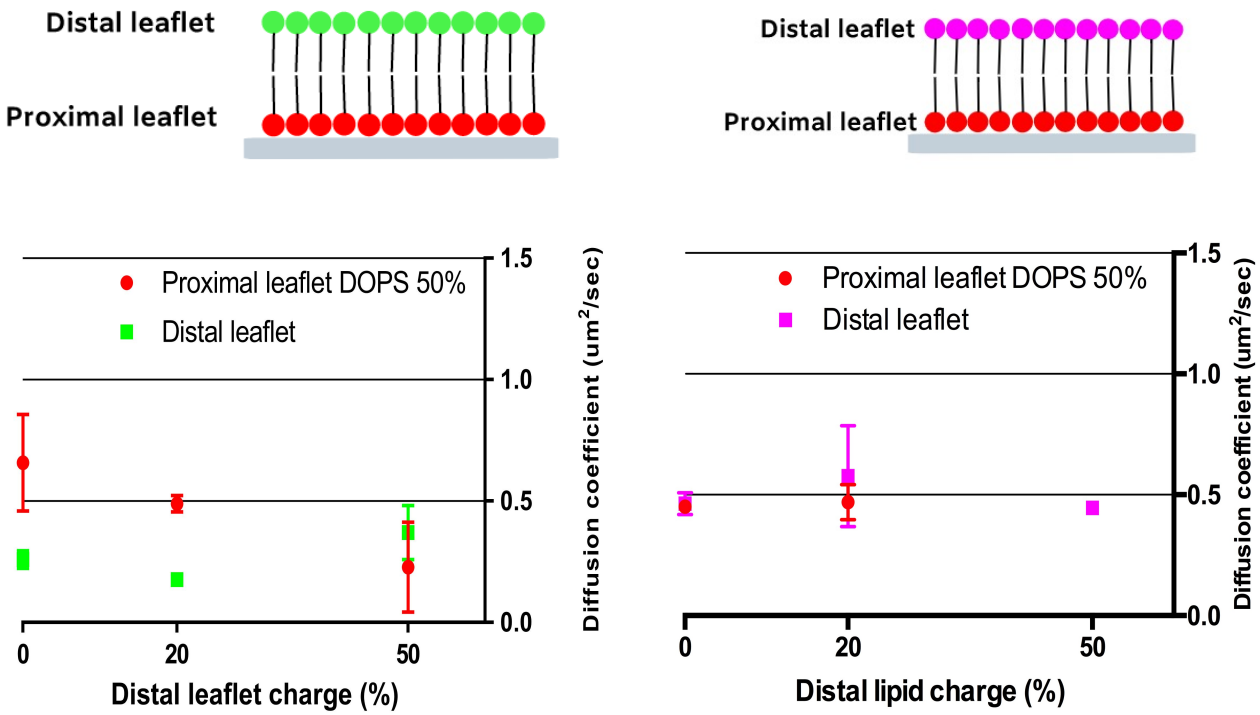

Figure 43: Effect of 0.1 μM septin on a DOPC 50% proximal leaflet and DOPC 100% ($n_{prox} = 3$, $n_{dis} = 4$), DOPS 20% ($n_{prox} = 7$, $n_{dis} = 7$) and DOPS 50% ($n_{prox} = 0$, $n_{dis} = 2$) distal leaflets. Displayed on the left, copy of D_{LL} for asymmetric leaflets with a DOPC 50% proximal leaflet without septin (see section 4.2). On the right, same conditions but with 0.1 μM septin. Lipid bilayers were made by LBVF on base piranha treated glass. All leaflets in the septin graph (right) are RhoPE labelled.

6 Discussion

6.1 Linear relation between lateral lipid diffusion and temperature

As temperature dependent diffusion, not affected by phase transitions, has not been examined before, information regarding a viscous effect on lateral lipid diffusion was lacking. In the first section of this research, the aim was therefore to explore the possibility that a viscous effect could cause the reported exponential relationship between lateral lipid diffusion and temperature, in live cells. This relation was investigated by subjecting a minimal model membrane system to temperature variations. The minimal model membrane system solely consisted of a SLB that had neutral or partially charged lipid composition. This experimental set-up eliminated the occurrence of potential diffusion barriers, thereby characterizing the viscous behaviour of the bare membrane, not influenced by more complex interactions with proteins. Collectively, the acquired data suggests a linear relation between D_{LL} and temperature, see **Figure 12**, where both neutral and charged SLBs follow a linear dependence.
The linear relation shows an increase in D_{LL} as temperature increases. This increase of D_{LL} could be explained by the change in fluidity of the SLB. When increasing temperature, the fluidity of the SLB increases, this in turn decreases the degree of lipid packing. Decreased lipid packing is associated to increased D_{LL}, which is predicted in the free area model, see equation 3 and measured for various lipids by Lindblom et al. [16]. Furthermore, for bilayers with charged headgroups, such as DOPS, the total free area volume per lipid is smaller and so lipid packing density is higher in these charged conditions than for neutral SLBs [16, 46]. Coinciding with our results, in **Figure 12**, charged SLBs exhibit a lower D_{LL}, at the measured temperatures (283 - 318 K), than neutral bilayers with larger free area volumes per lipid.

During the experiments, an undulation of the SLB was observed specifically at 303 K and at temperatures above 313 K for both neutral and charged lipid compositions. The undulation is reflected by the large variance of D_{LL} at these temperatures. Data acquisition proved more difficult and was limited to a smaller temperature range for charged than for neutral SLBs. This indicates a stronger undulation effect in the charged SLBs. The repulsive electrostatic forces between charged lipid headgroups and the negatively charged glass substrate [38] provide a plausible explanation for this difference in undulation severity.
A possibility to explain this non-intuitive undulation result could be that unfused vesicles, undesirably remaining in the experimental channel, are provoked to fuse to the bilayer, by the increasing temperature. These remaining vesicles could be present due to insufficient washing of the channel. An adverse mechanism to temperature initiated vesicle fusion, however, could also explain the undulation. At these higher temperatures (above 303 K) the SLB may collapse, causing generation of vesicles, which constantly changes the area of the SLB. During imaging, unfused vesicles are sometimes visible as high intensity spots. These were occasionally present in our experiments but did not completely disappear at high temperatures. Furthermore, extensive rinsing was performed with an amount of buffer exceeding three times the channel volume. Therefore, SLB area change leading to undulation by remaining vesicles would seem an unlikely cause.
Another option possibly causing the undulation would be via local heating by the photobleaching laser [39]. Axelrod et al. [39], however, proved that this effect is negligible in FRAP experiments. Even so, supposing laser heating would influence our experiments, this undulation would have been observed in all FRAP measurements, at all temperatures, which was not the case.
The undulation could also be related to temperature induced reduced lipid packing, resulting into membrane instability. In the charged plasma membrane, increase of temperature decreases membrane stability, which is compensated by recruitment of more charged lipids [46]. However, in our minimal model membrane system recruitment of lipids is not possible, resulting in an increasingly unstable SLB. Neutral SLBs are one component, membrane models, ensuring optimal lipid packing and maximum stability [16]. For charged model SLBs, the already lowered lipid packing (due to two lipid components) could be optimized by adjusting charge concentration with increasing temperature. In our model membrane system, charge concentration was constant throughout experiments. Therefore reduced SLB stability could not be amended, causing the undulation. This reasoning would imply that undulation is not present in neutral SLBs, contradicting our results.
The increased undulation on charged SLBs could likewise be explained by lipid packing. When combining two types of lipids, such as DOPC and DOPS, lower packing density can be obtained, therefore bilayer instability could be induced, leading to the undulation.
Yet another explanation could be sought outside the SLB. Behavior of the water layer between substrate and bilayer has been known to influence lipid behavior [35]. Within the temperature range observed in this research, it would be implausible to suggest that increased solute molecule activity is the cause of the undulation. Water-based buffers would show a significant change in behaviour close to the boiling point of water at 373 K.

The influence of the substrate, with its accompanying undulation artifact, could be bypassed by using GUVs, as a membrane model system, instead of SLBs [47].

The undulation was not the only artifact present in the SLB during temperature variation. When lowering temperature, SLBs showed dark spots in the neutral, but charged RhoPE tagged, SLB. Lowering temperature might have partially separated the bulk lipid from the tracer lipid as lipid mobility decreases, increasing stability. This therefore could imply a dominant effect of lipid packing over charge stability. Another, more likely, explanation could be that lipid mobility decreases, due to decreasing temperature, resulting into inhomogeneously distributed lipids that cause holes in the membrane.

The diffusion-temperature relation (between 283 - 318 K) trend observed for a neutral SLB coincides with D_{LL} trend found by Bag et al. for a smaller temperature range (298 - 313 K), however exact D_{LL} values reported by this author are ± 0.5 μm^2/sec higher under equal circumstances [13]. Bag et al. only regarded this relation as a starting point to observe phase transition with cholesterol mixed SLBs. Further lipid diffusion-temperature relation research has been performed on model membranes, however only to describe lipid compositions undergoing phase separation [20] or phase transition [13]. The lipid compositions used here do not have phase separating properties, nor gel-fluid phase transition as the transition temperature of DOPC and DOPS is at 256 K [48].

Our results imply that D_{LL} scales linearly to temperature in a model membrane system in the absence of phase separation. Therefore, the exponential relation reported in live cells is probably induced by hindrance of diffusion barriers, such as associating proteins or lipid phase separation.

6.2 Lipid charge induces lipid slow-down

As lipid diffusion of partially charged membranes was found to be generally slower than for neutral SLBs, this implied lipid charge dependence of D_{LL}. To characterize the lipid charge dependence, three degrees of lipid charge were compared in SLBs.

A clear influence of the lipid charge can be noted on D_{LL}. This can be explained by lipid slow down induced by reduced free area volume of charged lipids, as mentioned previously, lipid-lipid interactions or interactions between charged lipids and the glass substrate. By investigating D_{LL} in the absence of a substrate, the contribution of the latter could be defined. Methods to achieve such a model system already exist, for instance GUVs [43], oil-water monolayers [49] or black lipid membranes [14].

D_{LL} value of 1.0 μm^2/sec found for DOPC neutral SLBs is slower than reported results, namely ± 3.1-3.8 μm^2/sec (BODIPY and DiD tracers on mica) [43], 4.0 ± 0.5 μm^2/sec (Rhodamine Red-X tracer on borosilicate glass) [50], ± 2.5 μm^2/sec (Rho-PE tracer on glass) [13]. The larger differences may be due to a difference in solid support material, as Przybylo et al.[43] used mica, whereas this study uses glass substrates. However, Benda et al. [50] and Bag et al. [13] used conditions most similar to this research, unfortunately their D_{LL} does not coincide with ours, 4.0 ± 0.5 μm^2/sec and ± 2.5 μm^2/sec vs 1.0 μm^2/sec. D_{LL} results found under the exact same conditions with POPC lipids were reported between 1.0 ± 0.5 μm^2/sec [51] for neutral SLBs, which coincide with our results.
The influence of substrates on D_{LL} has often been debated and explored [20, 52, 53]. Substrate materials each interact in a specific way with lipid bilayers. Mica is characterized by an atomically smooth surface and therefore has a stronger ionic interaction with the lipid bilayer [20]. Glass substrates are more rough and therefore a larger aqueous subphase is present between the substrate and lipid bilayer, as well as less local adhesion potential [20]. To resolve the significant influence of a substrate on D_{LL}, GUVs can be used as a model membrane system alternative for D_{LL} measurements.
Furthermore, large variations of diffusivity were presented between lipid batches, surface treatments, SLB formation methods and lipid tracers, which could not be pinpointed to one cause, see **Figures 19, 21, 23, and 25**.

Difference in tracer charge would suggest a reduced diffusion in the charged tracer. Contradictingly, the results suggest otherwise, the charged RhoPE exhibits higher D_{LL} than the neutral NBD-PC. Charged RhoPE has also been seen to increase diffusion in earlier research [Doekes, 2017, Internship report], independent of leaflet composition. In literature, D_{LL} has however been reported to be independent of the lipid tracer used for diffusion measurements by Almeida et al. [12]. The tracer effect on D_{LL} could be circumvented by restricting usage to one tracer type. Another option could be to first characterize the difference in D_{LL} of various tracer types, see section 7. This would

be beneficial for future experiments, where various tracers could be used simultaneously.
Surprisingly, a large variance in data for charged SLBs was shown by the D_{LL} results. In earlier research this has never been so evidently present [13, 43, 50]. During the course of this research, variables were analyzed and optimized to minimize the variance in diffusion data. Regarding all results in section 4 more minimization of D_{LL} variance in this membrane model does not seem probable. To avoid the necessity of large data sets for charged SLBs, another membrane model system could be used to investigate the lipid charge dependence of D_{LL}.

Even though large variations in data points were present in this research, large enough data sets were obtained to confirm the lipid charge dependence of lateral D_{LL}.

6.3 Comparison of LBVF and VF

To explore the option of an effect of SLB formation methods on D_{LL}, both LBVF and VF techniques were compared. Moreover, LBVF was necessary to produce asymmetric bilayers, so it was necessary to compare results of both techniques.

Results show that LBVF SLBs typically have a slightly higher D_{LL} than VF formed SLBs, see **Figure 23**. Additionally, LBVF has the advantage of producing asymmetric SLBs (section 4.2). However, VF is a much more straightforward technique (section 2.3.1.2) and both SLB systems show similar variances for charged SLB compositions.

Neutral bilayers showed small variance (>0.5 $\mu m^2/sec$) of D_{LL} in both methods, whereas variance increased as a function of larger charge lipid concentrations. In this research, LBVF method exhibits higher D_{LL} compared to VF for both neutral and charged conditions, although the charged data is not significantly different. Some literature results confirm this difference; Scomparin et al found 2-10 μm^2/sec for Langmuir-Blodgett method and 2-4 $\mu m^2/sec$ for VF (DMPC on glass substrate), Starr et al. found 1.4±0.2 $\mu m^2/sec$ for Langmuir-Blodgett (LB) method and 0.62±0.18 $\mu m^2/sec$ (POPC on fused silica substrate) [20, 54]. Others have reported no differences between Langmuir-Blodgett method and VF methods in diffusion; Harms et al. found 3.5 μm^2/sec (POPC and DPPC mix on glass) and Kalb et al. found 3.5±0.5 μm^2/sec (POPC on quartz substrate) for both LB and VF methods [55, 56].
Especially significant differences were observed when fusion to the substrate occurred in different subphase conditions [20, 57]. The presence of cations, occurring in buffer, which is increased by addition of salt, is known to enhance vesicle fusion by an increased ionic strength which allows higher adsorption of vesicles to the substrate. This affects the typical size of homogeneous areas but could also have an effect on D_{LL}. Regarding our bilayer formation methods, the aqueous subphase between bilayer and substrate for LB deposition is deionized water and for VF is F-buffer. This would mean that the VF bilayers should be higher in diffusion, due to a higher salt subphase, than LBVF, which is not the case.
Another influencing factor could be the thickness of the water layer between substrate and bilayer. Scomparin et al. [20] found that VF bilayers have a thicker water layer than LBVF deposited layers. Again, this would result in higher D_{LL} of VF formed bilayers than LBVF, contradicting the obtained results.

Although differences were observed between methods, the increasing variance as function of lipid charge concentration is clearly present in both conditions. The overall D_{LL} is generally higher for LBVF, however the charge induced drop in diffusion follows the same trend in both LBVF and VF.

6.4 Leaflet coupling

To characterize the extent of charge influence on D_{LL}, an analysis was made on separate leaflets of the SLB.

Our results show that the leaflets influence each other dependent on lipid composition. When the proximal leaflet was highly charged the diffusion of the distal leaflets would show a drop in diffusion, independent on their own leaflet composition, see **Figure 27**, and vice versa. This implies an effect of charge composition on both leaflets through leaflet coupling. Furthermore, D_{LL} values of corresponding leaflets differed less than 0.5 μm^2/sec from each other, **Figures 27b, 27c and 27d**.

Surprisingly, the asymmetric bilayers mostly showed faster diffusion in the proximal leaflet. Contradicting literature, where two diffusion coefficients were measured; a fast and slow component [20]. Based on transfer ratio's of

Langmuir-Blodgett depositions, defined by the decrease in lipid film area during deposition divided by substrate area pulled through the lipid film, Scomparin et al. suggested that the slower D_{LL} would correspond to the proximal leaflet and the faster D_{LL} on to the distal leaflet. This was justified by the known strong ionic interaction between the proximal leaflet and the substrate [35], which results in higher experience of lipid slow-down than in the distal leaflet. Furthermore this reasoning was suggested to be validated by numerical simulations [58]. Reason for this contradiction to literature could be due to all the proximal leaflets being tagged by RhoPE, which influences D_{LL} in charged compositions, compared to NBD-PC, see section 4.1.4. It would be worthwhile to repeat experiments with switched lipid tracers, to check whether the proximal leaflet is truly characterized by increased D_{LL} or that it is merely a lipid tracer effect.
Interestingly, the diffusion trend in the distal leaflets, only when associating with a neutral proximal leaflet, increases with increased distal charge. Another unexpected finding is that the D_{LL} of 50% charged proximal leaflets are lower than their associating distal leaflets. This could suggest that higher charge concentration dominates over the effect induced by the higher RhoPE D_{LL} compared to NBD-PC, see **Figure 27d**. To test the influence of the tracer, the leaflets should be tagged with the same tracer, the other leaflet with no tag, and then compared to the present data.

The proximal leaflet affects D_{LL} of the distal leaflet and vice versa. Therefore, it is suggested that the leaflets are coupled. This is confirmed by the fact that the D_{LL} of both proximal and distal analyzed leaflets have values closer to typical values for SLBs (2.4-4.6 μm^2/sec) [50, 59, 43], and not GUVs (7.8± 0.8 μm^2/sec) [43].

6.5 Septin increases lateral lipid diffusion

Septins have been implicated to effect D_{LL} by acting as a diffusion barrier in the plasma membrane of living cells [60]. They are known to bind to PS lipids via electrostatic interactions, and therefore may induce slow-down. The exponential relation between temperature and D_{LL}, seen in live cells and described by equation 4, may be induced by an energy barrier caused by peripheral membrane proteins such as septin.

On the SLBs analyzed in this research, a contradictory effect was seen, where septin does not induce lipid slow-down by acting as a diffusion barrier. The effect of septin interaction even seems to increase D_{LL}, see **Figures 28d, 29d and 30d**. Increased lipid diffusivity remained a reproducible result throughout changing of variables, such as SLB charge density and septin concentration, see **Figures 28d, 29d, 30d and 33d**. Strikingly, all batches of septin increased D_{LL}. Such an increase in diffusion in a minimal model is highly unexpected, as no active systems (for instance cytoskeletal components) are present to enhance the diffusivity of lipids.

Other peripheral membrane proteins have shown to also effect D_{LL}, such as alpha-synuclein [51]. This protein induces lipid slow-down by increasing lipid packing at protein cluster sites. Due to the denser lipid packing, membrane fluidity decreases and therefore mobility is reduced by this lipid-protein interaction.
Septin forms a fairly homogeneous layer on top of the SLB when imaged by confocal microscopy [unpublished work from the Koenderink lab]. However, on molecular scale, it is composed of filaments [25]. In this research, clusters and filaments have shown to not cover the whole area of the membrane homogeneously but with less dense septin between filaments. When bundled, these filaments might have small linear regions of interaction sites (of the amino acid residues, see section 1), where most polar lipids are recruited to. In this manner the remaining part of the membrane becomes less packed, therefore increasing D_{LL}. The largest part of the bilayer will thereby become less packed, resulting in an increased general diffusivity.

These results imply that septin does not cause a diffusion barrier that can explain the exponential relation between D_{LL} and temperature. We hypothesize that septin induces an increase in diffusion by an effect on lipid packing.

6.6 The binding of septin

Septin is known to form as a homogeneous carpet layer on a charged SLB or as bundles, in the absence of interactions with charged lipids. However, bundles can also result from prolonged polymerization time before septin - membrane contact, which is why often small bundles were noted on top of a septin carpet layer (see **Figure 31**).

During experiments septin was observed to not only bind as bundles or carpet structure but also in clusters. This sometimes occurred within a filament/carpet structure, **Figure 31** or when no other observable septin adhesion was present, **Figure 28d**. Septin clusters did not always coincide with SLB defects. A homogeneous SLB was sometimes

accompanied by associated septin clusters.

Poor adhesion of septin, as seen in **Figure 33d**, compared to the homogeneous septin carpet results of Agata Szuba, to the charged lipids could be due to degradation of the lipid stock that result in weaker electrostatic interactions. In general, stronger localization of septin was observed in comparison to homogeneous SLBs, due to defects in the substrate (see **Figure 38i**, lines of higher fluorescence intensity), or where the SLB had artifacts (see **Figure 32b**) or was immobilized (data not shown). Therefore, it is more likely that the weak interaction is due to a SLB quality problem.

To induce better adhesion, septin was combined with 50% charged SLBs. These SLBs have shown to bind septin but not as homogeneously as on 20% charged SLBs. Moreover, SLB charge affected both the amount and homogeneity of septin bound to the membrane.

6.6.1 Septin and SLB formation methods

Especially poor adhesion of septin was noted for VF assembled SLBs. Often no adhesion occurred or only clusters of septin. At first, for symmetric bilayers of lipid batch Avanti #2, these same clusters were noted. However when using the Sigma #1 batch in LBVF for the asymmetric SLBs, septin lot # 24 bound as a homogeneous carpet layer. This suggests the electrostatic interaction is inhibited by a change in the polar lipids, not in septin.

The LBVF technique resulted in SLBs that induced more and homogeneous septin adhesion, where septin FRAP curves showed a large immobile fraction (see **Figures 28c, 29c and 30c**). With the LBVF method, it is possible to tune the lipid packing by adjusting the surface pressure of the subphase before lipid deposition. Lipid packing might therefore be denser than for SLBs formed by VF. Increased lipid packing results in higher concentration of charged lipids, which in turn could enhance the lipid-septin interaction.

6.6.2 The effect of septin through leaflet coupling

To further zoom in on the interaction between the PS lipids and septin, an interesting result was found: although septin only binds to the distal leaflet, an increase of D_{LL} was seen in both leaflets, see **Figures 36, 39, 41 and 43**. The increase of D_{LL} was higher in the distal leaflets, which would be expected due to the leaflet-septin interaction. This finding would suggest that via leaflet coupling septin affects both leaflets. In charged symmetric SLBs the diffusion of both leaflets increase an equal amount, confirming again that septin influences both leaflets, see **Figures 39, 41 and 43**.

Not only does septin influence the leaflets, but we also found that the proximal leaflet influences septin. A charged proximal leaflet combined with a neutral distal leaflet showed stronger binding of septin than when both leaflets are neutral, see **Figure 38 a-c and 40 a-c**. Although the septin binds in clusters and not homogeneously, significant binding was observed, see **Figure 40 a-c**. An effect of flip-flop might explain a change in D_{LL} and the unexpected adhesion of septin to the neutral leaflet.

Lipid flip-flop could induce a change in D_{LL}, by increasing or decreasing the net lipid charge density of the leaflet. With a higher percentage of charged lipids, the leaflet's D_{LL} is reduced compared to a neutral condition. Therefore, if the leaflet's charged is increased by flip-flop, the D_{LL} of this leaflet will decrease.
Regarding the septin associated lipid bilayers, septin also influences D_{LL}, which according to our results show increased D_{LL} compared to bare membranes. Septin only associates to the distal leaflet and therefore we must regard just the proximal leaflet, assuming septin does not influence the proximal leaflet. To test the occurrence of flip-flop we suggest an increase in D_{LL} for a charged leaflet and a decrease in D_{LL} for neutral leaflets with respect to the bare asymmetric counterparts.
Figures 39, 41 and 43 show that this does not occur, therefore this change in D_{LL} of the proximal leaflet could suggest that a flip-flop mechanism is not in play. However, to completely eliminate the chance of flip-flop other experiments could be performed, explained in the following section.
Regarding the unpredicted result of septin binding to a neutral distal leaflet when the proximal leaflet was charged, see **Figures 40c and 42c**. Flip-flop may provide a reasonable explanation for this unexpected outcome. Charged lipids could be present in the distal leaflet by flip-flop, so that septin can bind to the SLB. To test the presence of flip-flop, an experiment can be performed by flushing dithionite over the SLB. Dithionite blocks out the fluorescence of the top layer of the SLB. If flip-flop occurs, the bilayer fluorescence intensity will drop faster than without dithionite

[61]. Such experiments have been preformed by the author [Doekes, 2017, Internship report], where it was reported that no flip-flop occurred one hour after SLB synthesis in any case. Experiments in this research could last up to four hours. Therefore it would be interesting to perform the dithionite experiment during an extended experimental time.

Regarding the fully neutral bilayer, where no septin seems to bind, an increase of D_{LL} is seen in both leaflets, in the presence of septin. The increase of D_{LL} is stronger on the distal leaflet.
These effects could possibly be due to a difference in buffer condition, although is hardly different for the bare SLB (F-buffer) and septin-bilayer combination (septin buffer), as the difference is only addition of PCA, PCD and MgATP, anti-bleach factors, in the septin buffer.

In earlier research, leaflet coupling has occurred in model membrane systems [62, 63, 64, 65]. However, mostly in membrane composed of PS with sphingomyelin, where they proposed that the sphingomyelin could induce changes in the lateral interactions of the surrounding lipids [62, 65]. Although others suggested that PS could also influence coupling between the outer leaflet and the cytoskeleton [62, 66], predominantly actin, as it is known to interact with cytoplasmic proteins [62, 67].

7 Conclusion

This work defines, for the first time, the viscous behaviour of the lipid membranes by demonstrating the linear relation of lateral lipid diffusion to temperature, in the absence of a phase transition temperature. It has been proven that membrane viscosity can be excluded from inducing the exponential relation of lipid diffusion and temperature found in live cells.

Interestingly, lipid charge appeared to induce lipid slow-down; this was further investigated to characterize this mechanism. It was found that neutral symmetric lipid bilayers exhibit faster lipid diffusion than charged lipid bilayers. Lipid diffusion of neutral bilayers agreed with values found in literature, whereas charged lipid bilayers have been known to show faster lipid diffusion than found in this research. The diffusion coefficient was found to decrease with an increasing concentration of lipid charge and therefore displayed a decreasing diffusion coefficient as function of increased lipid charge. We hypothesize that charge dependent lipid slow-down may be due to interactions with the glass substrate and a decreased free area volume of charged lipids.
Charge concentration showed a dependence on specific substrate surface treatment to ensure optimized lipid mobility. DOPS 20% lipid bilayers express the highest diffusion rate on base piranha treated glass, whereas membrane homogeneity and the diffusion coefficient of DOPS 50% lipid bilayers were optimized on ethanol treated glass.

Asymmetric lipid bilayer results proved leaflet coupling by showing an effect of change in charge composition on the opposing leaflet. The lipid diffusion values of both leaflets were furthermore of similar magnitude, whereas for an uncoupled system it would be expected that the distal leaflet shows lipid diffusion similar to GUV diffusion data.

Regarding the associating septin, it can be concluded that septin increases the net lipid diffusion of a bilayer. We suggest that this may be explained by locally enhanced lipid packing, which causes a net decrease in lipid packing for the whole lipid bilayer. Lipid packing could be measured by combining fluorescence anisotropy and lipid diffusion experiments to determine how lipid order is affected by septin. Septin has shown to affect the distal leaflet more in terms of diffusion than the proximal leaflet, which is expected as septin only interacts with the distal leaflet. However septin has shown to slightly affect the proximal leaflet, maybe through the coupling of the leaflets.

As septin interacts via the charged headgroups of lipids, it has been suggested that no adhesion of septin would take place on a completely neutral lipid bilayer. Visually, this has been confirmed, however, an effect on lipid diffusion has been registered on the neutral leaflet in the presence of non-associating septin in the channel solution.
Furthermore, septin has been found to adhere well to LBVF created lipid bilayers compared to VF bilayers. Especially on charged symmetric bilayers and bilayers with charged distal leaflets, septin binds as a homogeneous carpet to the lipid bilayer.
Reports in literature regarding septin have shown septin to function as a diffusion barrier. The obtained results, however, do not indicate such a mechanism as lipid diffusion reproducibly enhances lipid diffusion.

In this research, SLBs were used as model membrane system to understand changes in lipid diffusion. SLBs have given a lot of insight on lipid diffusion and have provided an easy platform to vary parameters, pinpoint contributions of single components and to adapt the model system to various experimental conditions. However, this situation is strongly simplified compared to the plasma membrane.
Although this research has given an insight on contributions of lipid charge in a membrane and the coupling of leaflets, many questions still remain. Concerning septin more questions remain unanswered to properly describe the influence and behavior of this peripheral membrane protein.
We propose several interesting follow-up experiments to gain further understanding in lipid diffusion and septin characterization:

- To get more insight in the undulation artifact, the substrate material could be changed to mica. Substrate surfaces consisting of mica are more atomically smooth. The lipid bilayer therefore has a stronger adhesion potential with the substrate than with a glass substrate [20]. Presence or absence of the undulation under these conditions could provide more information on the contribution of substrate - lipid interactions. To eliminate the undulation artifact GUVs could be used instead of SLBs.
- By switching from SLBs to GUVs, the main objection of the significant influence of the substrate on lipid diffusion is eliminated, as well as substrate defects. Nevertheless, the limitations of GUVs lie in more complex methods of preparation and complicated addition of proteins [43].

- The dark spots observed in the lipid bilayers at lower temperatures could be further characterized by reducing the temperature lower than 283 K at 5 K intervals, after which the lipid bilayers could be analyzed by AFM [48]. AFM could determine if the bilayer collapses, leading to holes or that the lipid bilayer is still intact but the fluorescence is heterogeneously distributed.
- Due to the inconsistency of lipid diffusion results and large variability compared to literature, different lipids (such as DMPC or DPPC) could be measured by using the same preparation and imaging methods. Thereby giving more information on the cause of the difference in lipid diffusion results.
- To define if the difference in lipid tracer diffusion exhibited by their neutral or charged properties, lipid diffusion of NBD-PC could be compared to the charged NBD-PS. These tracers only differ in charge, therefore a significant difference in lipid diffusion could suggest tracer charge dependence of lipid diffusion.
- To eliminate the effect of tracer charge influencing lipid diffusion results in asymmetric SLBs, experiments should be done with one type of tracer, for instance RhoPE, instead of two. However, experimental time to obtain results will significantly be doubled, as only one leaflet can be imaged per experiment, rather than both leaflets simultaneously.
- Investigate the association of septin to neutral distal leaflets and whether it has an effect on D_{LL} in neutral membranes. This could potentially be defined by performing an extended (>2 hrs) dithionite flip-flop experiment [61]. Additionally, occurrence of flip-flop could be checked by adding annexin V, instead of septin, to the channel buffer. This protein is characterized to specifically adhere to PS lipids in the presence of calcium ions [68]. For such an experiment, the SLB would have a charged proximal leaflet and neutral distal leaflet. If flip-flop occurs, the annexin V will gradually adhere to the surface of the SLB.
- The effect of septin on lipid packing should be further explored. This could also be measured by the before mentioned fluorescence anisotropy experiment, to define if inducing an increase in lipid diffusion is possible by heterogeneous lipid packing.

Once septin acts as a diffusion barrier on lipid diffusion, this research can be taken one step further by adding a component to the model membrane system. Instead of using a planar substrate, the membrane could be synthesized on a curved substrate. Septin has been reported to occur at curved sites of plasma membrane [25]. Therefore, it would be interesting to investigate the contributions of septin combined with curved substrate. More details on this proposal and a preliminary experiment can be found in the **Supplementary information**.

References

[1] Jeroen Leeuwenburgh Sander Jansen John Bosco, Ruggero Van Den Beucken. Surface engineering for bone implants: A trend from passive to active surfaces. *Coatings*, 2(3):95–119, 2012.

[2] Olivier Degidi Marco Pontes Ana Emilia Parias Piattelli Adriano Rompen, Eric Domken. The effect of material characteristics, of surface topography and of implant components and connections on soft tissue integration: A literature review. *Clinical Oral Implants Research*, 17(2):55–67, 2006.

[3] Kishore Upadhya Nagaraja Shammas Mohammed Krishna Ravi Rama Sekhar Ravichandra Krishna Alla, Rama Ginjupalli. Surface roughness of implants: A review. *Trends in Biomaterials and Artificial Organs*, 15(3):112–118, 2011.

[4] Pablo A. Iglesias Tianzhi Luo, Krithika Mohan and Douglas N. Robinson. Molecular mechanisms of cellular mechanosensing. *Nature Materials*, 12(11):1064–1071, 2013.

[5] Mark Ahearne. Introduction to cell hydrogel mechanosensing. *Interface Focus*, 4(2), 2014.

[6] Julian Lewis Martin Raff Keith Roberts Bruce Alberts, Alexander Johnson and Peter Walter. *Molecular Biology of the Cell, 4th edition*. Molecular Biology of the Cell. New York: Garland Science, 2002.

[7] Ilpo Poyry, Sanja Vattulainen. Role of charged lipids inmembrane structures — insight given by simulations. *Biochimica et Biophysica Acta - Biomembranes*, 1858(10):2322–2333, 2016.

[8] Andrei L Lomize, Irina D Pogozheva, Mikhail a Lomize, and Henry I Mosberg. The role of hydrophobic interactions in positioning of peripheral proteins in membranes. *BMC structural biology*, 7(October 2016):44, 2007.

[9] Richard A.L. Jones. *Soft Condensed Matter*. Oxford Master Series in Condensed Matter Physics. Oxford University Press, 2003.

[10] Julio L. Simons, Kai Sampaio. Membrane organization and lipid rafts. *Cold Spring Harbor Perspectives in Biology*, 3(10):1–17, 2011.

[11] Mykyta V. Chubynsky and Gary W. Slater. Diffusing diffusivity: A model for anomalous, yet Brownian, diffusion. *Physical Review Letters*, 113(9):1–5, 2014.

[12] P.F.F. ALMEIDA and W.L.C. VAZ. Lateral diffusion in membranes. *Handbook of Biological Physics*, 1:305 – 357, 1995.

[13] Darilyn Hui Xin Wohland Thorsten Bag, Nirmalya Yap. Temperature dependence of diffusion in model and live cell membranes characterized by imaging fluorescence correlation spectroscopy. *Biochimica et Biophysica Acta - Biomembranes*, 1838(3):802–813, 2014.

[14] Andreas Van Qui Kramer Stefanie Gregor Ingo Enderlein Jörg Weiß, Kerstin Neef. Quantifying the diffusion of membrane proteins and peptides in black lipid membranes with 2-focus fluorescence correlation spectroscopy. *Biophysical Journal*, 105(2):455–462, 2013.

[15] A. Ramadurai, S. Holt. Lateral diffusion of membrane proteins. *Journal of the American Chemical Society*, 131(35):12650–12656, 2009.

[16] Göran Lindblom and Greger Orädd. Lipid lateral diffusion and membrane heterogeneity. *Biochimica et Biophysica Acta - Biomembranes*, 1788(1):234–244, 2009.

[17] Suvrajit Polley Anirban Huang Hector Mayor Satyajit Rao Madan Groves Jay T. Lee, Il Hyung Saha. Live cell plasma membranes do not exhibit a miscibility phase transition over a wide range of temperatures. *Journal of Physical Chemistry B*, 119(12):4450–4459, 2015.

[18] Shi Ying Gupta Anjali Bag Nirmalya Wohland Thorsten Huang, Shuangru Lim. Plasma membrane organization and dynamics is probe and cell line dependent. *Biochimica et Biophysica Acta (BBA) - Biomembranes*, Article In Press, 2016.

[19] Débora M Clausen Mathias P Eggeling Christian Lagerholm, B Christoffer Andrade. Convergence of lateral dynamic measurements in the plasma membrane of live cells from single particle tracking and sted-fcs. *Journal of Physics D: Applied Physics*, 50(6):063001, 2017.

[20] M. Ferreira T. Charitat B. Tinland C. Scomparin, S. Lecuyer. Diffusion in supported lipid bilayers: Influence of substrate and preparation technique on the internal dynamics. *The European Physical Journal E*, 28:211–220, 2009.

[21] Takahiro K Fujiwara, Kokoro Iwasawa, Ziya Kalay, Taka A Tsunoyama, Yusuke Watanabe, Yasuhiro M Umemura, Hideji Murakoshi, Kenichi G N Suzuki, Yuri L Nemoto, Nobuhiro Morone, and Akihiro Kusumi. Confined diffusion of transmembrane proteins and lipids induced by the same actin meshwork lining the plasma membrane. *Molecular biology of the cell*, 27:11–81, 2016.

[22] Chen Tamm Lukas K. Kiessling, Volker Wan. Domain coupling in asymmetric lipid bilayers. *Biochimica et Biophysica Acta - Biomembranes*, 1788(1):64–71, 2009.

[23] Senthil Arumugam and Patricia Bassereau. Membrane nanodomains: contribution of curvature and interaction with proteins and cytoskeleton. *Essays in biochemistry*, 57:109–19, 2015.

[24] Alexander L. Lyubartsev, Alexander P. Rabinovich. Recent development in computer simulations of lipid bilayers. *Soft Matter*, 10:1154111547, 2011.

[25] Pascale Mostowy, Serge Cossart. Septins: the fourth component of the cytoskeleton. *Nat Rev Mol Cell Biol*, 13(3):183–194, 2012.

[26] Makato Takiguchi Kingo Tanaka-Takiguchi, Yohko Kinoshita. A cost–benefit analysis of the physical mechanisms of membrane curvature. *Nature Publishing Group*, 15(9):1019–1027, 2013.

[27] Hua Jin Matthew P. Scott Maxence V. Nachury Elias T. Spiliotis Qicong Hu, Ljiljana Milenkovic and W. James Nelson. A septin diffusion barrier at the base of the primary cilium maintains ciliary membrane protein distribution. *Science*, 329(5990):436–439, 2010.

[28] Tomoko Petersen Jennifer D. Racz Bence Sheng Morgan Choquet Daniel Ewers, Helge Tada. A septin-dependent diffusion barrier at dendritic spine necks. *PLoS ONE*, 9(12):1–19, 2014.

[29] Makato Takiguchi Kingo Tanaka-Takiguchi, Yohko Kinoshita. Septin-mediated uniform bracing of phospholipid membranes. *Current Biology*, 19(2):140–145, 2009.

[30] John R. Lew Daniel J. Gladfelter, Amy S. Pringle. The septin cortex at the yeast mother-bud neck. *Current Opinion in Microbiology*, 4(6):681–689, 2001.

[31] Michael Casamayor, Antonio Snyder. Molecular dissection of a yeast septin: distinct domains are required for septin interaction, localization, and function. *Molecular and cellular biology*, 23(8):2762–2777, 2003.

[32] Chen Xie Hong McPherson Peter S. Grinstein Sergio Trimble William S. Zhang, Jianshe Kong. Phosphatidylinositol polyphosphate binding to the mammalian septin h5 is modulated by gtp. *Current Biology*, 9(24):1458–1467, 1999.

[33] F. C. Koenderink G. H. Mavrakis, M. Tsai. Purification of recombinant human and drosophila septin hexamers for tirf assays of actin–septin filament assembly. *Methods in Cell Biology*, 136:199–220, 2016.

[34] Suman Sengupta Parijat Maiti Sudipta Sahoo, Bankanidhi Nag. On the stability of the soluble amyloid aggregates. *Biophysical Journal*, 97(5):1454–1460, 2009.

[35] E. Evans E. Merkel, R. Sackmann. Molecular friction and epitactic coupling between monolayers in supported bilayers. *Journal de Physique*, 50(12):1535–1555, 1989.

[36] Guy Cox. Biological confocal microscopy. *Elsevier Science Ltd.*, 2002.

[37] D.M. Soumpasis. Theoretical analysis of fluorescence photobleaching recovery experiments. *Biophysical Journal*, 41(1):95–97, 1983.

[38] Aditya Iyer, Nathalie Schilderink, Mireille M A E Claessens, and Vinod Subramaniam. Membrane-Bound Alpha Synuclein Clusters Induce Impaired Lipid Diffusion and Increased Lipid Packing. *Biophysical journal*, 111(11):2440–2449, 2016.

[39] D. E. Schlessinger J. Elson E. Webb W. W. Axelrod, D. Koppel. Mobility measurement by analysis of fluorescence photobleaching recovery kinetics. *Biophysical Journal*, 16(9):1055–1069, 1976.

[40] Andrey V. Tataurov. Measurement of lateral diffusion in lipids. *University of Pittsburgh*, Master Thesis, 2005.

[41] Volker Tamm Lukas K. Crane, Jonathan M. Kiessling. Measuring lipid asymmetry in planar supported bilayers by fluorescence interference contrast microscopy. *Langmuir*, 21(4):1377–1388, 2005.

[42] Lj Girard-Egrot, Ap Blum. Langmuir-blodgett technique for synthesis of biomimetic lipid membranes. *Langmuir*, page Ch. 2, 2007.

[43] Jana Humpolickova Ales Benda Anna Zan Magdalena Przybylo, Jan Sykora and Martin Hof. Lipid diffusion in giant unilamellar vesicles is more than 2 times faster than in supported phospholipid bilayers under identical conditions. *International Journal of Molecular Sciences*, 22(22):9096–9099, 2013.

[44] K I Lee, W Im, and R W Pastor. Langevin dynamics simulations of charged model phosphatidylinositol lipids in the presence of diffusion barriers: toward an atomic level understanding of corralling of PIP2 by protein fences in biological membranes. *BMC Biophys*, 7:13, 2014.

[45] Feng-Ching Tsai Jose Alvarado Aurelie Bertin Francois Iv Alla Kress Sophie Brasselet Gijsje H. Koenderink Manos Mavrakis, Yannick Azou-Gros and Thomas Lecuit. Septins promote f-actin ring formation by crosslinking actin filaments into curved bundles. *Nature Cell Biology*, 16:322–334, 2014.

[46] Howard Goldfine. Bacterial membranes and lipid packing theory. *Journal of Lipid Research*, 25:1501–1507, 1984.

[47] Petra García-Sáez, Ana J. Schwille. Fluorescence correlation spectroscopy for the study of membrane dynamics and protein/lipid interactions. *Methods*, 46(2):116–122, 2010.

[48] Youngjik Choi Simon J. Attwood and Zoya Leonenko. Preparation of dopc and dppc supported planar lipid bilayers for atomic force microscopy and atomic force spectroscopy. *International Journal of Molecular Sciences*, 14:3514–3539, 2013.

[49] Brid Cronin Matthew A. Holden William L. Hwang, Min Chen and Hagan Bayley. Droplet interface bilayers. *Journal of American Chemical Society*, 130(18):5878–79, 2008.

[50] V. Marecek A. Lhotsky W. Th. Hermens A. Benda, M. Benes and M. Hof. How to determine diffusion coefficients in planar phospholipid systems by confocal fluorescence correlation spectroscopy. *Langmuir*, 19(10):4120–4126, 2003.

[51] Mireille M.A.E. Claessens Aditya Iyer, Nils O. Petersen and Vinod Subramaniam. Amyloids of alpha-synuclein affect the structure and dynamics of supported lipid bilayers. *Biophysical Journal*, 106(12):2585–2594, 2014.

[52] Edward S. Allgeyer Sharon L. Ashworth Sarah M. Sterling, Ryan Dawes and David J. Neivandt. Comparison actin- and glass-supported phospholipid bilayer diffusion coefcients. *Biophysical Journal*, 108:1946–1953, 2015.

[53] Martin Machan, Radek Hof. Lipid diffusion in planar membranes investigated by fluorescence correlation spectroscopy. *Biochimica et Biophysica Acta - Biomembranes*, 1798(9):1377–1391, 2010.

[54] Nancy L. Thompson Tammy E. Starr. Formation and characterization of planar phospholipid bilayers supported on tio2 and srtio3 single crystals. *Langmuir*, 16(26):10301–10308, 2000.

[55] G. J. Schutz H. J. Gruber G. S. Harms, M. Sonnleitner and Th. Schmidt. Single-molecule anisotropy imaging. *Biophysical Journal*, 77:2864–2870, 1999.

[56] Sammy Frey Edwin Kalb and Lukas K. Tamm. Bacterial membranes and lipid packing theory. *Biochimiea et Biophysica Acta*, 1103:307–316, 1992.

[57] Paul S. Cremer and Steven G. Boxer. Formation and spreading of lipid bilayers on planar glass supports. *Journal of Physical Chemistry B*, 103:2554–2559, 1999.

[58] Chenyue Xing and Roland Faller. Interactions of lipid bilayers with supports: A coarse-grained molecular simulation study. *Journal of Physical Chemistry B*, 112(23):7086–7094, 2008.

[59] Granick Steve Zhang Liangfang. Slaved diffusion in phospholipid bilayers. *Proceedings of the National Academy of Sciences of the United States of America*, 102(26):9118–9121, 2008.

[60] Yves Caudron, Fabrice Barral. Septins and the lateral compartmentalization of eukaryotic membranes. *Developmental Cell*, 16(4):493–506, 2009.

[61] Sandra L. Pucadyil, Thomas J. Schmid. Real-time visualization of dynamin-catalyzed membrane fission and vesicle release. *Cell*, 135(7):1263–1275, 2008.

[62] Toyoshi Fujimoto and Ingela Parmryd. Interleaflet coupling, pinning, and leaflet asymmetry—major players in plasma membrane nanodomain formation. *Frontiers in Cell and Developmental Biology*, 4(1):1–12, 2017.

[63] Kiessling V. Wan, C. and L. K. Tamm. Coupling of cholesterol- rich lipid phases in asymmetric bilayers. *Biochemistry*, 47:2190–219, 2008.

[64] Chiantia S. Visco, I. and P. Schwille. Asymmetric supported lipid bilayer formation via methyl-beta-cyclodextrin mediated lipid exchange: influence of asymmetry on lipid dynamics and phase behavior. *Langmuir*, 30:7475–7484, 2014.

[65] Q. Lin and E. London. Ordered raft domains induced by outer leaflet sphingomyelin in cholesterol-rich asymmetric vesicles. *Biophysical Journal*, 108:2212–2222, 2015.

[66] Zasada A. Mabuchi K. Krauze K. Wang C. L. Makuch, R. and R. Dabrowska. Phosphatidylserine liposomes can be tethered by caldesmon to actin filaments. *Biophysical Journal*, 73:1607–161, 1997.

[67] C. L. Stace and N. T. Ktistakis. Phosphatidic acid- and phosphatidylserine-binding proteins. *Biochemical Biophysical Acta*, 1761:913–926, 2006.

[68] Ryuji Osaki Toshihisa Akiyoshi Kazunari Takeuchi Shoji Kamiya, Koki Kawano. Cell-sized asymmetric lipid vesicles facilitate the investigation of asymmetric membranes. *Nature Chemistry*, 8(June):4–6, 2016.

[69] William S. Trimble and Sergio Grinstein. Barriers to the free diffusion of proteins and lipids in the plasma membrane. *Journal of Cell Biology*, 208(3):259–271, 2015.

[70] Damián Lobato-Márquez and Serge Mostowy. Septins recognize micron-scale membrane curvature. *Journal of Cell Biology*, 213(1):5–6, 2016.

[71] C. Patrick Collier. Bilayer membrane interactions with nanofabricated scaffolds. *Chemistry and Physics of Lipids*, 192(1):75–86, 2015.

[72] Dale L. Sasaki Darryl Y. Longo Marjorie L. Ogunyankin, Maria O. Huber. Nanoscale patterning of membrane-bound proteins formed through curvature-induced partitioning of phase-specific receptor lipids. *Langmuir*, 29(20):6109–6115, 2013.

[73] Chih Jung Capraro Benjamin R. Wu Tingting Chen Chi Mon Yang Shu Baumgart Tobias Hsieh, Wan Ting Hsu. Curvature sorting of peripheral proteins on solid-supported wavy membranes. *Langmuir*, 28(35):12838–12843, 2012.

[74] Jennifer L McMahon, Harvey T Gallop. Membrane curvature and mechanisms of dynamic cell membrane remodelling. *Nature*, 438(7068):590–596, 2005.

[75] Jones Tsai, Eileen Sun, Yuan Gao, James C. Hone, and Lance C. Kam. Non-Brownian diffusion of membrane molecules in nanopatterned supported lipid bilayers. *Nano Letters*, 8(2):425–430, 2008.

[76] S Boxer. Molecular transport and organization in supported lipid membranes. *Current Opinion in Chemical Biology*, 4(6):704–709, 2000.

[77] C. W. Hagen. The future of focused electron beam-induced processing. *Applied Physics A*, 117:1599–1605, 2014.

[78] W. F. van Dorp and C. W. Hagen. A critical literature review of focused electron beam induced deposition. *Applied Physics A*, 104:081301, 2008.

[79] Sander Dobbenga. The plasma membrane: Nature's touch screen. *Unpublished work TU Delft*, 2017.

[80] Roberto Dominguez and Kenneth C. Holmes. Actin structure and function. *Annual Review Biophysical Journal*, 40(6):169–186, 2011.

[81] Sandrine Dufrêne Yves F El Kirat, Karim Morandat. Nanoscale analysis of supported lipid bilayers using atomic force microscopy. *Biochimica et biophysica acta*, 1798(4):750–765, 2010.

[82] J. H. Cherstvy A. G. Metzler, R. Jeon. Non-brownian diffusion in lipid membranes: Experiments and simulations. *Biochimica et Biophysica Acta - Biomembranes*, 1858(10):2451–2467, 2016.

[83] P Montal, M Mueller. Formation of bimolecular membranes from lipid monolayers and a study of their electrical properties. *Proceedings of the National Academy of Sciences of the United States of America*, 69(12):3561–3566, 1972.

[84] Naoki Yamanaka Tomoko Noji Hiroyuki Watanabe, Rikiya Soga. High-throughput formation of lipid bilayer membrane arrays with an asymmetric lipid composition. *Scientific reports*, 4:7076, 2014.

[85] Thomas Keyser Ulrich Mahendran Kozhinjampara R Winterhalter Mathias Gutsmann, Thomas Heimburg. Protein reconstitution into freestanding planar lipid membranes for electrophysiological characterization. *Nature protocols*, 10(1):188–98, 2015.

[86] Noura Sayed Dosoky Muhammad Shuja Khan and John Dalton Williams. Engineering lipid bilayer membranes for protein studies. *International Journal of Molecular Sciences*, 14:21561–21597, 2013.

[87] Dennis R. Voelker Gerrit van Meer and Gerald W. Feigenson. Membrane lipids: where they are and how they behave. *Nature Reviews Molecular Cell Biology*, 9:112–124, 2008.

[88] Arnd Honigmann, Alf Pralle. Compartmentalization of the cell membrane. *Journal of Molecular Biology*, 428(24):4739–4748, 2016.

[89] M. J. D. Rickayzen G. Evans W. a. B. Powles, J. G. Mallett. Exact analytic solutions for diffusion impeded by an infinite array of partially permeable barriers. *Proceedings of the Royal Society A: Mathematical, Physical and Engineering Sciences*, 436(1897):391–403, 1992.

[90] Stefanos Sethna James P. Veatch Sarah L. Machta, Benjamin B. Papanikolaou. Minimal model of plasma membrane heterogeneity requires coupling cortical actin to criticality. *Biophysical Journal*, 100(7):1668–1677, 2011.

[91] Regina Bailey. Article: Cell membrane. *Encyclopedia Britannica Online*, 2007:Retrieved from: https://www.thoughtco.com/cell–membrane–373364, 2017.

[92] John L Tymoczko Jeremy M Berg and Lubert Stryer. *Biochemistry, 5th edition.* Biochemistry. New York: W H Freeman, 2002.

[93] Molecular Biophysics, Stony Brook, I Introduction, B Marcks, V Future Directions, a Membrane Targeting, and B Computational Studies. The Role of Electrostatic and Nonpolar Interactions in the Association of Peripheral Proteins with Membranes. *Current topics in membranes*, 52:277–307, 2002.

[94] J E Johnson and R B Cornell. Amphitropic proteins: regulation by reversible membrane interactions (review). *Molecular membrane biology*, 16(3):217–35, 1999.

[95] Rohit Jain and Kizhakeyil L. Sebastian. Diffusion in a Crowded, Rearranging Environment. *Journal of Physical Chemistry B*, 120(16):3988–3992, 2016.

[96] Darryl Y. Sasaki Subhash H. Risbud Wade F. Zeno, Alice Rystov and Marjorie L. Longo. Crowding-induced mixing behavior of lipid bilayers: Examination of mixing energy, phase, packing geometry, and reversibility. *Langmuir*, 32(18):?, 2016.

[97] Maximilian S. Oakes Patrick W. Occhipinti Patricia Gladfelter Amy S. Bridges, Andrew A. Jentzsch. Micron-scale plasma membrane curvature is recognized by the septin cytoskeleton. *Journal of Cell Biology*, 213(1):23–32, 2016.

[98] Aldo Orwar Owe Czolkos, Ilja Jesorka. Molecular phospholipid films on solid supports. *Soft Matter*, 7(10):4562, 2011.

[99] Barbara J. Weitz D. A. Pautot, Sophie Frisken. Production of unilamellar vesicles using an inverted emulsion. *Langmuir*, 19(7):2870–2879, 2003.

Supplementary information

Curvature

A trial experiment was performed as a start of the next phase in the assay to characterize the contributions of septin and curvature in lipid slow-down.

Curved substrates have been shown in vitro to form phase-separating membrane domains, which could be potentially accompanied by inducing lipid slow-down. Especially at sharp curved regions of the membrane and bilayer height mismatches, could a change in diffusion occur [69, 25, 70].
Regarding substrate topography interactions, lipids are proposed to diffuse differently due to the interaction between substrate and lipid. Therefore, a curved substrate could directly form a diffusion barrier for lipids. Evidence for this is absent, however phase separation, curvature sorting, and barrier induced lipid pathways have been reported [71, 72, 73, 74, 75, 76].

The used patterned substrate consists of two 8 μm diameter rings (see section 45a). The 200 nm high rings were made by EBID technology [77, 78] on ITO glass substrate with platinum and carbon, which was finished off with sputtered glass to make lipid bilayer formation possible. This process was setup and optimized earlier [79].

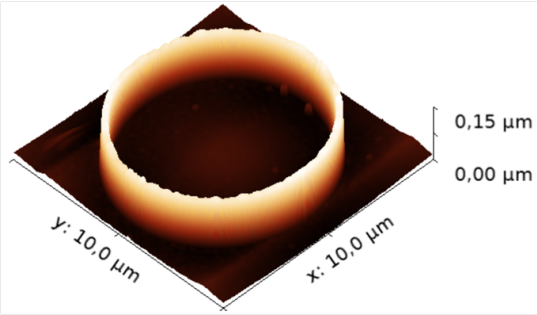

Figure 44: AFM image of ring patterned on substrate.

In the assay combining a patterned substrate, 20% charged symmetric lipid bilayer and 0.1 μM septin, a few results are presented. The lipid bilayer forms over the patterned rings (see figure 45b). Septin, however, did not adhere in this sample to the lipid bilayer (see figure 45c). Strikingly, septin does not show any sign of acknowledging these topographic features in the substrate and membrane.

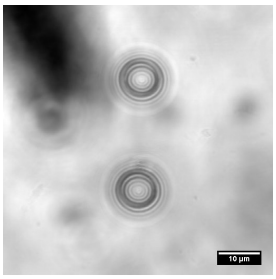

(a) Image of the surface of the patterned substrate by ND filter with 488 nm laser. Imaged with 40x objective on a confocal microscope.

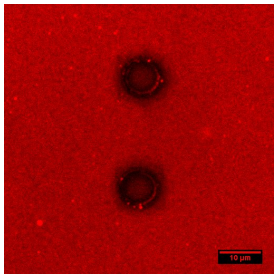

(b) Image of the membrane, labelled by RhoPE, where the patterned substrate is visible by 561 nm laser. Imaged with 40x objective on a confocal microscope.

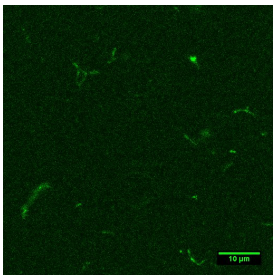

(c) Image of septin, tagged by GFP, on/above the membrane and substrate. Imaged with 488 nm laser and 40x objective on a confocal microscope.

Figure 45: Patterned substrate consisting of two 8 μm rings with DOPS 20% lipid bilayer and 0.1 μM septin.

Septin, in this assay, remarkably does not acknowledge patterns in the substrate, even though patterns are visible

in membrane and could therefore be identified as a membrane defect. Septin prefers to bind to defects due to its 'sticky' nature. The lipid bilayer was created by vesicle fusion, which has been shown to result in heterogeneous or absence of septin binding to the lipid bilayer.
Therefore, it is proposed that the experiment should be repeated with LBVF formed lipid bilayers to ensure better binding of septin. Experiment repetition was delayed due to unavailability of new patterns. The lipid bilayer seems to form over and inside of the barrier ring. Intensity within the ring was lower than the surrounding membrane. This could suggest less packing or that the barrier inhibits lipid diffusion causing the photobleached lipids to stay there together and therefore the area is darker. FRAP experiments could not be performed due to time constraints. However, possibility of external curvature inducing a diffusion barrier should be explored, especially when defining the contribution of septin as diffusion barrier in the plasma membrane.

Glossary

actin Is a globular filament forming protein that is most abundant in cells. Two of its main functions is to aid in cell mobility and maintain cell shape [80].

actin polymerization The change of actin structure; from dissolved particles to actin filaments. The polymerization is triggered by lowered salt concentrations in vitro.

actomyosin cortex Layer of cytoskeletal proteins attached to the inner surface of the plasma membrane. It mediates mechanical stimuli exerted on the membrane to the cells interior.

AFM Atomic force microscopy, AFM, is an imaging technique that uses a very-high resolution scanning probe. The obtained resolution has the order of nanometer scale, resulting in 300 times larger accuracy than the optical diffraction limit. The nanoscale structure of a membrane can be also explored in real-time with high speed AFM. Additionally, height profile images can be generated directly in aqueous solution [81].
Different AFM imaging modes are available, which differ in the way the tip is moving over the sample. For imaging soft biological samples the tapping mode is most preferable, where an oscillating tip scans over the sample surface. Lateral forces during this mode are greatly reduced [81].
The main advantage of AFM is that the sample is observed at a nanometer resolution [81]. In a membrane, the structure, molecular forces, chemical properties and receptor sites can be obtained from an AFM analysis. The required firm attachment of a sample to the solid support is a great limitation of AFM. This association results in alteration of sample properties such as material elasticity, fluidity and lipid or protein diffusion, decreasing the biological relevance of AFM results [81]. Furthermore, AFM only provides information on height and stiffness of structure but there is no option to specifically track certain target lipids or proteins.

alpha-synuclein Is a protein known to locally impair lipid diffusion by increasing lipid packing [38].

amino acid residues Part of the amino acid that defines it from other amino acids. Amino acids are the building blocks of proteins. The basic structure of amino acids are the all same; amine group, carbon chain, carboxylic acid and a residue part, which characterizes the amino acid, for instance with charge or not.

annexin V Is a peripheral membrane protein that has been found to specifically bind to PS lipids [38, 68]. In the cell it is involved in vesicle fusion [38].

anomalous diffusion Every deviation from this free diffusion movement is anomalous diffusion. In membranes anomalous diffusion is the slow-down of lipids and proteins. Slow-down occurs when lipids are affected in some way. Therefore, their diffusivity decreases. For example, lipids can interact with proteins or cytoskeletal components, be trapped in specific membrane domains or forced to follow a certain trajectory. These general forms of lipid hindrance causing lipid slow-down are grouped as diffusion barriers. Diffusion barriers have a large variety of causes and characteristic effects on lipid diffusion.
In contrast to normal diffusion, anomalous diffusion has a sublinear relation of MSD to time or has a non-Gaussian diffusion pattern[21, 82]. Lipid slow-down related to sublinearity, is also known as subdiffusion.
The non-linear dependence of the MSD to time, in anomalous diffusion, is described by an adapted version of equation 9, and can be used as theoretical starting point of a simulation to analyze FRAP [82]. The following equation is therefore the general equation to describe sub- and superdiffusion:

$$MSD = \langle x^2(t) \rangle = K_\beta t^\beta \tag{8}$$

, where the diffusivity of the particle K_β (in $\mu m/sec^\beta$) is dependent on the anomalous diffusion exponent β. For subdiffusive systems $0 < \beta < 1$ applies, whereas for superdiffusive systems (induced by active mechanisms, such as the cytoskeleton) $\beta > 1$ applies. To provide a more propitiate simulation analyze experimental membrane diffusion data, a length scale dependent term must be incorporated, as typical membrane diffusion differs at short and long length scales.
Anomalous lipid trajectories can be analyzed by direct methods. Single particle tracking lipid trajectories provide information on the properties of the occurring diffusion barrier [20] .

artifact An unexpected or undesired abnormality in behaviour of the lipid bilayer or septin in the biomimetic system..

bare membrane Lipid bilayer without any proteins adhering to the surface or embedded into the membrane.

bio-compatibility A material used for an implant that resides in a living tissue may not invoke an immune reaction by being toxic, injurious, or physiologically reactive.

black lipid membranes Black lipid membranes, initially designed by Montal and Mueller [83], form a lipid bilayer over an aperture. Classically, the lipid bilayer is composed of two compartments. Recently, these membranes have been designed on high-throughput wells [84] or produced by the patch pipette technique [85]. As the workable membrane is free standing, results are not influenced by an additional interaction, for instance a glass substrate. Additionally, as a free-standing membrane, transmembrane proteins can be incorporated. Disadvantages of this technique are small bilayer area, heterogeneous membrane structure and chance of multiple lipid layers. Due to insufficient surface tension the lifetime of the bilayer is less than an hour [86, 71].

bulk lipid The lipids of which the lipid bilayer is composed, disregarding the lipid tracer .

bundles Several filaments can be assembled and crosslinked into bundles.

cell cortex Also known as actomyosin cortex Layer of cytoskeletal proteins attached to the inner surface of the plasma membrane. It mediates mechanical stimuli exerted on the membrane to the cells interior .

cholesterol Is a type of lipid called a sterol and is regularly present in plasma membranes. The properties of the membrane are altered by cholesterol. At high temperatures cholesterol stabilizes the membrane and at lower temperatures it prevents other lipids from clustering and stiffening [6, 10].

clusters A group of multiple proteins, in or on the plasma membrane.

cortical protein Cortical proteins are situated on the cytosolic surface of the membrane. These proteins couple the cytoskeleton to the plasma membrane, thereby connecting the plasma membrane to cytoskeletal mechanics. Additionally, cortical proteins play a large role in intracellular signaling [6].

cytoplasm The cells interior environment [87] .

cytoskeleton The cellular structure in the cytoplasm that maintains the structure, shape and organization of the cell. It offers mechanical support that allows the cell to divide and migrate. It is composed of several larger and smaller filament components that operate in sync [6].

defect Imperfection of the substrate.

deionized water Water in its purist form, without ions.

differentiate Cellular differentiation is the process where a cell changes its' cell type.

diffusion barrier In membranes anomalous diffusion is the slow-down of lipids and proteins. Slow-down occurs when lipids are affected in some way. Therefore, their diffusivity decreases. For example, lipids can interact with proteins or cytoskeletal components, be trapped in specific membrane domains or forced to follow a certain trajectory. These general forms of lipid hindrance causing lipid slow-down are grouped as diffusion barriers. Diffusion barriers have a large variety of causes and characteristic effects on lipid diffusion.

distal leaflet In the SLB the leaflet of the lipid bilayer facing the aqueous surrounding environment of the experimental channel or interacting with a peripheral protein.

dithionite Specifically converts the fluorescent NBD-PC lipid to a non-fluorescent compound. Dithionite cannot pass the lipid bilayer and therefore will only bleach fluorescent lipids in the outer leaflet [41].

DMPC 1,2-dimyristoyl-sn-glycero-3-phosphocholine .

DPPC 1,2-dipalmitoyl-sn-glycero-3-phosphocholine.

extracellular environment Environment outside the cell [87] .

extracellular matrix The ECM is composed of all structures that inhabit the environment outside the cell. It provides a scaffold for the cells and initiates several signalling pathways [6].

filaments Linear polymer of globular subunits.

flip-flop Flip-flop is transverse diffusion of lipids through the membrane. In this type of diffusion, a lipid switches from the proximal (cytosolic) leaflet, moving along the z-axis, to the distal (noncytosolic) leaflet [6]. Flip-flop is especially important to the noncytosolic leaflet of the membrane, as it allows for its lipid turnover [6]. Nonexistence of flip-flop would result in no formation and regeneration of new membranes [6]. In a pure lipid bilayer, flip-flop is very slow. Therefore, in the plasma membrane, enzymes are necessary to catalyze the process [6]. If the lipid turnover rate is too slow, the noncytosolic leaflet will loose its ability to properly function.

focal adhesions Focal adhesions are the connection between the cells interior and extracellular matrix. They are known to transmit mechanical signalling though transmembrane proteins, integrins, and intracellular protein clusters that are connected to the actin cytoskeleton [6].

heterogeneous Any deviation from a homogeneous landscape. A heterogeneous landscape can be desired, due to lipid domains, or undesired, due to defects.

homogeneous A homogeneous landscape of a membrane is absent of defects and lipid domains. The membrane is imaged as a surface with equal fluorescence intensity through out the membrane area.

hop diffusion Long-range movement of lipids to a new confined section of a membrane leaflet, is termed hop diffusion. Hop diffusion results from an increased level of hindrance along the lipid trajectory [23]. Diffusion barriers inducing hopping can also induce non-random reorganization of lipids [88, 21]. Consequently, the lipids distribute heterogeneously throughout the membrane, while experiencing hop diffusion [88, 44].
A model used to explain barrier-induced hop diffusion is the picket-fence model [23]. Idealized hop diffusion can be fitted with a model developed for an infinite array of partially permeable barriers by Powles et al. (1992)[89]. This model was used by Fujiwara et al. (2016)[21] to confirm their SPT subdiffusion results to coincide with the hop diffusion mechanism. This analytical solution regards the diffusion coefficient of a particle within an environment of semi-permeable barriers at an equal distance, which is the assumption that causes idealization. Due to regarding an infinite array, only long-term diffusion coefficient over long length scales can be explained. Hop diffusion has mostly been simulated, as no complete analytical solution is available at present. Hop diffusion can be simulated by molecular dynamics, typically by using Kawasaki dynamics [90].

immobilized The lipids of the lipid bilayer experience no to minimal diffusion. There is no fluorescent recovery when an area is bleached by the laser during FRAP.

integrins Are the principle receptors that bind extracellular matrix proteins to the cell. They are transmembrane proteins [6].

Langmuir-Blodgett (LB) method Langmuir-Blodgett (LB) based methods involve transfer of the first lipid monolayer, or leaflet, from a water subphase by a vertical motion onto the substrate [41, 42]. The upper monolayer can be fashioned in a similar manner or by the Langmuir-Schaeffer technique. In the latter technique the upper monolayer is obtained by horizontal deposition onto the subphase [41, 42]. An advantage of these techniques is the ability to create asymmetric lipid bilayers. On the other hand the techniques are time consuming and have many factors, such as position of cover slip and surface pressure on the subphase, that can influence the quality of the lipid bilayer [41, 42].
LB methods can be combined with the vesicle fusion method to make asymmetric bilayers [41, 42]. Here, a LB monolayer is created, followed by vesicle fusion that forms an upper leaflet.

lateral lipid diffusion One diffusional process is transfer of ions and proteins across the membrane. The other is diffusional motion of lipid and proteins within the membrane, often referred to as lateral diffusion.
A biological membrane can be viewed as a two-dimensional fluid [6]: molecules exhibit lateral diffusion [6]. This is 'sideways' diffusion of lipids within their leaflet.
Lateral diffusion of lipids in the cell membrane expresses anomalous diffusion. However, lipid diffusion can be divided into a first normal diffusion trajectory and a second anomalous trajectory. These are coupled to two diffusion coefficients that describe these different pathways. Normal, or Brownian, diffusion occurs on a 'short-range' , occurring within a confined membrane area. A second, smaller, effective diffusion, **Figure 46** is associated with so-called 'long-range' motion, occurring over membrane diffusion barriers [75, 21].

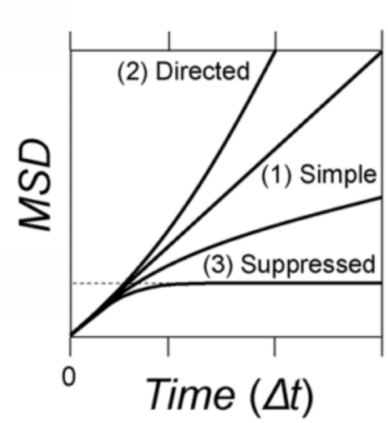

Figure 46: Types of lateral diffusion. The dotted line shows the transition between short-range diffusion and long-range diffusion. During anomalous diffusion, (2) or (3), there is a difference in slope between the two ranges [21].

When imaging on long time scales (>1 sec), anomalous membrane dynamics can not be characterized. This results in false interpretation of membrane dynamics being Brownian. However, when imaging at shorter time scales (millisecond), short-range lipid diffusion is visualized. Typically in membranes, this anomalous diffusion caused hop diffusion.

leaflet A phospholipid bilayer forms the basic structure, fifty percent of the membrane [10].Composed of two lipid leaflets, the bilayer is divided into a cytosolic, or inner, leaflet and extracellular, or outer, leaflet, see **Figure 47**.

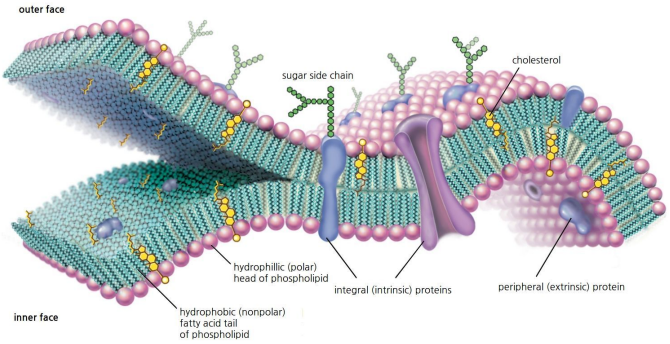

Figure 47: Graphical example of the complex plasma membrane. The plasma membrane is consists of a lipid bilayer with embedded and adhered proteins, sugars and cholesterol [91].

.

leaflet coupling The suggestion that one leaflet can influence the other leaflet in terms of diffusion and domain formation, in absence of interfering proteins [62].

lipid bilayer A lipid bilayer is lipids assembled as two planar structures on top of each other in an aqueous environment, creating a hydrophobic core and hydrophilic outer shell [10], see **Figure 48**.

lipid charge Membrane lipids and proteins are recognized to interact via electrostatic interactions. This occurs when peripheral membrane proteins have a positive charge, whereas membrane lipids have a partially negative charge. Lipid charge is defined by the atomic composition of the headgroup of the lipid.

lipid domains Lipids constantly reorganize themselves within the membrane by lateral lipid diffusion. This reorganization leads, in live cells, to demixing of the several lipid components. In vitro, phase separation of lipids has been registered, creating domains on a nanoscale.

lipid organization The distribution of different types of lipids throughout a leaflet. Usually related to lipid domain discussions.

lipid packing How densely lipids exist next to each other in a membrane leaflet/how large the free area volume is per lipid.

lipid slow-down In membranes anomalous diffusion is the slow-down of lipids and proteins. Slow-down occurs when lipids are affected in some way. Therefore, their diffusivity decreases.

lipid tracer Lipids with fluorescent molecules, to image membranes.

lipids Lipids are fatty amphiphatic molecules [6]. This means they exist of hydrophilic, or polar head, and hydrophobic, or non-polar, tail (**Figure 48**). The fatty acid tail can differ in length and saturation [6]. Unsaturated tail kinks are formed by a cis-double bond in the chain. Conversely, a saturated tail is straight and does not have a double bond [6]. Membrane lipids are often characterized by large hydrocarbon volume, short tail length and optimal head area for lipid packing [10].

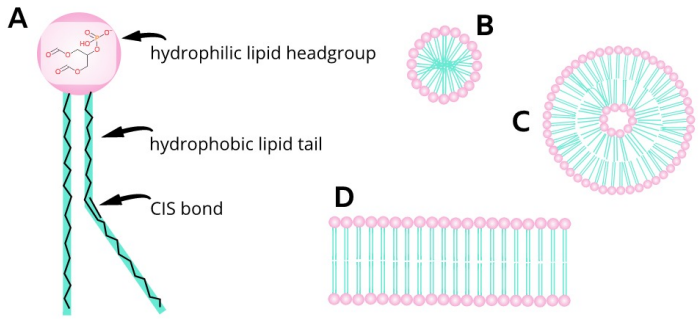

Figure 48: Structure and self-assembly of lipids. A) Structure of lipid molecule with a hydrophilic headgroup that can intact with the aqueous surroundings and a hydrophobic tail. Tails can saturated and are then straight, as shown in the left chain or can be unsaturated by a CIS double bond, shown in the right chain. **B)** Example of a spherical micell, with a hydrophobic core and hydrophilic outside. **C)** Example of a vesicle, made up of two sheets of lipids in a spherical form, thereby resulting in an aqueous center compartment, hydrophobic core layer and hydrophilic shell. **D)** Example of a lipid bilayer, with two hydrophilic planar shells and hydrophobic core.

Polar heads of lipids can form hydrogen bonds with water molecules [6]. However, the uncharged hydrophobic tails are insoluble in water [6]. The combination of soluble heads with insoluble tails result in the self-assembly of lipids. This ensures stability of the lipids, as in this manner lipids are able to suspend in aqueous surroundings [92]. Lipids can self-assemble into structures such as spherical or cylindrical micelles, bilayers and vesicles, see **Figure 48** [9]. A membrane is assembled as a bilayer, creating a hydrophobic core and hydrophilic outer shell [10].
Important lipid types are phospholipids, phosphoglycerides, sphingomyelin, glycolipids, cholesterol, and sphingolipids [6, 93, 94] .

live cell In this research, live cells are referred to intact alive animal cells that are used individually for experimental purposes. Therefore in vivo for this type of research are live cells, although in clinical research this is called in vitro. Here, by in vitro is meant model systems of cells.

migrate Migration of cells involve all processes that lead to the displacement of a cell from one location to another.

monolayers One leaflet component of a bilayer. Only one area of lipid headgroups and tails, instead of two.

multi-lamellar vesicles Vesicles with many smaller vesicles inside.

non-cytosolic leaflet The outside leaflet of plasma membrane, facing the extracellular environment.

normal diffusion Normal diffusion is the continuous free movement of particles within a bulk of homogeneous Newtonian fluid medium, where there is no form of hindrance, other than continuous drag [11]. The movement has no net direction and no net displacement. This movement can be displayed as a Gaussian distribution.
The diffusion coefficient that puts a value to diffusion is calculated from the mean squared displacement (MSD). For normal diffusion, the MSD has a linear relation to time, this is referred to as Fickian diffusion [95]. The linear dependence is given by [82]:

$$MSD = \langle x^2(t) \rangle = K_1 t \tag{9}$$

, where x is the position of a particle at time t and K_1 is a constant regarding the diffusivity of the particle. This diffusivity can be expressed by the Saffman and Delbrück model, which explains Brownian diffusion within membranes. The continuum hydrodynamic model assumes an infinite two-dimensional (2D) lipid bilayer plane, consisting of infinite viscous fluid domains that separate domains of water-like fluid [14, 15]:

$$D_{SD} = \frac{k_B T}{4\pi\mu_m h}\left(ln\frac{1}{\varepsilon} - \gamma\right) \tag{10}$$

, where D_{SD} is the diffusion coefficient, k_B is the Boltzmann constant, T is temperature in Kelvin, μ_m is the membrane viscosity, h is the bilayer height, γ is the Euler's constant and ε is defined by:

$$\varepsilon = \frac{R\mu_s}{h\mu_m} \tag{11}$$

, where R is the radius of the cylindrical molecule, representing a protein within the planar medium, and μ_s is the viscosity of the surrounding medium. However the molecular radius of a protein for which this model is valid is limited to 10 nm, due to hydrophobic mismatches between proteins and lipid tails [14, 15]. This limitation results from the strong dependence of the diffusion coefficient to the molecule radius. The Saffman-Delbrück theoretical model on membrane diffusion has been suggested to hold by experimental data, that focuses on concentration and size dependence diffusion of proteins in relevant physiological circumstances [15].

peripheral protein Proteins that interact with one leaflet by non-covalent interactions, are peripheral membrane proteins. They adhere to lipids directly by interacting with the hydrophilic headgroups or indirectly by binding to integral membrane proteins. The interaction is weaker, thus reversible, whereas integral proteins bind irreversibly to the hydrophobic membrane core.
A type of peripheral membrane proteins are cortical proteins. Cortical proteins are situated on the cytosolic surface of the membrane. These proteins couple the cytoskeleton to the plasma membrane, thereby connecting the plasma membrane to cytoskeletal mechanics. Additionally, cortical proteins play a large role in intracellular signaling [6]. Example of a peripheral membrane protein is synuclein, which is suggest to maintain regulate lipid turnover and stability. On the extracellular side, peripheral membrane proteins are mainly involved in cell-cell signaling and cellular adhesion [6].

phase separated domains The membrane can organize into different phases, namely: liquid ordered (Lo), liquid disordered (Ld) and as solid gel. The plasma membrane is proposed to maintain a state close to Lo-Ld phase separation system. This concept is often referred to as the 'lipid raft model' [23]. The raft model represents lipid organization on a nanoscale. Therefore lipid rafts are also referred to as nanodomains.
Lipids constantly reorganize themselves within the membrane by lateral lipid diffusion. This reorganization leads, in live cells, to demixing of the several lipid components. In vitro, phase separation of lipids has been registered, creating domains on a nanoscale. Lipid phase separation is subject to the lipid composition, specifically head group properties, tail saturation and length, and temperature [96]. Each lipid has its own structure, mechanical and chemical properties. Therefore, lipids can prefer to assemble in regions of favourable lipid types, instead of distributing homogeneously. Inhomogeneous organization can also be enhanced by an associating membrane molecule or by membrane curvature [23].

phase separation The membrane can organize into different phases, namely: liquid ordered (Lo), liquid disordered (Ld) and as solid gel. The plasma membrane is proposed to maintain a state close to Lo-Ld phase separation system. This concept is often referred to as the 'lipid raft model' [23]. The raft model represents lipid organization on a nanoscale. Therefore lipid rafts are also referred to as nanodomains.
Lipids constantly reorganize themselves within the membrane by lateral lipid diffusion. This reorganization leads, in live cells, to demixing of the several lipid components. In vitro, phase separation of lipids has been registered, creating domains on a nanoscale. Lipid phase separation is subject to the lipid composition, specifically head group properties, tail saturation and length, and temperature [96]. Each lipid has its own

structure, mechanical and chemical properties. Therefore, lipids can prefer to assemble in regions of favourable lipid types, instead of distributing homogeneously. Inhomogeneous organization can also be enhanced by an associating membrane molecule or by membrane curvature [23].

phase transitions Transition of a lipid domain from one state to the other, for instance from solid gel state to fluid state. Phase transition is catalyzed by change in temperature.

POPC lipids 1-palmitoyl-2-oleoyl-sn-glycero-3-phosphocholine. Neutral lipid.

proliferate Cell growth and division that lead to an increase of cell count.

proteins There are countless proteins interacting with the plasma membrane in a cellular environment. Proteins embedded into the membrane are integral proteins. Peripheral proteins are situated on one side of the membrane [6].

Integral proteins are characterized by hydrophobic side chains that associate with the hydrophobic core of the lipid bilayer. Most integral proteins are transmembrane proteins that span the entire bilayer length. Some transmembrane proteins transport ions, proteins or sugars across the membrane. However, a integral protein can also be partially embedded in the membrane. Typically, the protein is anchored into a leaflet by fatty acids that bind to the hydrophobic core, named hydrophobic insertion. As it is only partially anchored, as the inner polypeptide chain of the protein does not insert in the bilayer core [6].

Proteins that interact with one leaflet by non-covalent interactions, are peripheral membrane proteins. They adhere to lipids directly by interacting with the hydrophilic headgroups or indirectly by binding to integral membrane proteins. The interaction is weaker, thus reversible, whereas integral proteins bind irreversibly to the hydrophobic membrane core.

A type of peripheral membrane proteins are cortical proteins. Cortical proteins are situated on the cytosolic surface of the membrane. These proteins couple the cytoskeleton to the plasma membrane, thereby connecting the plasma membrane to cytoskeletal mechanics. Additionally, cortical proteins play a large role in intracellular signaling [6]. Example of a peripheral membrane protein is synuclein, which is suggest to maintain regulate lipid turnover and stability. On the extracellular side, peripheral membrane proteins are mainly involved in cell-cell signaling and cellular adhesion [6].

proximal leaflet In the SLB the leaflet of the lipid bilayer interacting with the substrate.

septin Septin is a small, 30 - 65 kDa [25], cortical protein that is sometimes also classified as a cytoskeletal component, next to actin, microtubules and intermediate filaments [25]. It belongs to the GTP-binding proteins family, which are proteins that are involved in communicating information from outside the cell to its interior [32]. They can assemble into higher order structures such as filaments, linear or spiral bundles, ring structures or as a two-dimensional array of septin and are not polar [25]. Septin can bind via its central core domain, consisting of a polybasic region, directly to phosphoinositides (PS plasma membrane lipids), PIP lipids [32, 31]. This region is a cluster of basic amino acid residues (at the N-terminus), near the phosphate loop which is adjacent to the GTP-binding motif, located at the proteins' surface [31]. Septins' structure is dependent on which cellular component it interacts with. When interacting with phospholipids, it has been proposed septin assembles into filaments [25].

Septin structures have been registered to function as cortical network on the plasma membrane to organize and retain associating membrane protein distribution [29]. Furthermore, septins have been found to influence the rigidity of the cell when interacting with phospholipids of the plasma membrane [29]. Cell rigidity contributes to determining cell shape and cell directional movement [29].

Septins have been known to act as diffusion barriers that compartmentalize membrane molecules into membrane domains [25, 26]. These septins are usually associated with a highly curved section of the membrane [97], where the cell has a different specialized function than the rest of the cell, for instance the cilia in mammalian cells [27] and at the base of dendritic membrane spines [28]. By FRAP experiments the presence of diffusion barriers were proposed, additionally, in experiments with suppressed septin expression, compartmentalization was observed to be lost [25]. However, the exact contribution of septin and of a proposed diffusion barrier effect of curvature remain to be defined .

small unilamellar vesicles A type of unilamellar vesicles that is unsuitable for analyzing membrane lipid diffusion. Between 30-50 nm diameter, they have a too small size to visualize the membrane organization, as this occurs below diffraction limit. Although an image of micrometer size can be obtained, the lateral membrane dynamics cannot be imaged. However SUVs are used in vesicle fusion to form lipid bilayers. When they are flushed onto a substrate, the SUVs collapse and fuse to form lipid bilayers.

sonicated Sonication uses sound waves to agitate particles in a substance. Here, multi-lamellar vesicles are turn into SUVs by this wave energy.

state domains Gel and fluid state domains refer to domains defined by specific compositions of lipids that exhibit different fluidic properties; liquid and solid gel.

subphase 1. The layer of water between the lipid bilayer and the substrate. 2. The upper film of water on the air-water interface on the Langmuir-Blodgett trough.

substrate Underlying piece of material on which the model membrane system is formed.

supported lipid bilayer A common method of lipid bilayer assembly is on planar solid substrates. Supported lipid bilayers (SLBs) consist of a substrate, often glass or mica, on which a 10-20 Å thin water layer exists, see **Figure 49**. By the hydrophilic lipid heads, the lipid bilayer attaches to the water, and so the substrate. This method is excellent to investigate effects of cortical proteins or cortex-membrane organization.

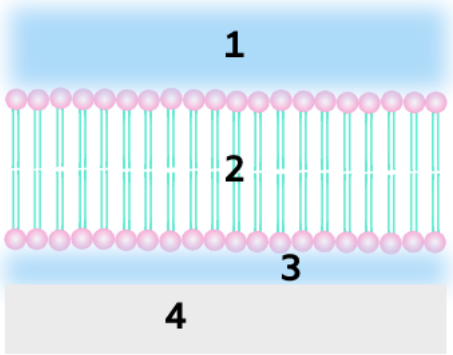

Figure 49: Supported lipid bilayer. 1) Buffer in the sample channel covering the lipid bilayer. **2)** Lipid bilayer. **3)** Buffer/water between substrate and lipid bilayer, adhering the lipid bilayer to the substrate. **4)** Glass or mica substrate.

The advantage of using SLBs is that they provide robust and stable bilayers. However, the bilayer will always be influenced by the attachment to the substrate. This can lead to limitations when studying membrane properties, such as an influence on dynamics of lipids and associating proteins, functionality loss, lipid composition or necessity of more complex imaging systems. Additionally, substrate compatibility is not always self-evident, leading to immobility of the lipids or adhering proteins [38, 71, 86]. To minimize this effect, the substrate can be improved by specific surface treatment.
The material for the substrate is preferably hydrophilic, smooth and clean, to maintain maximum mobility of the lipids, such as quartz, mica, soda-lime or borosilicate glass [98]. Furthermore, these materials are transparent which is preferable for imaging.
Formation of the lipid bilayer onto the substrate can be performed by three different categories of methods, depending on the required properties of the bilayer.
Vesicle based methods involve vesicle rupture and fusion, onto a substrate. Symmetrical membranes can be formed by small unilamellar vesicle (SUV) rupture on a substrate. Practically, this method is easiest and least time consuming. Unfortunately, asymmetric bilayers are technically challenging when using vesicles, made by for instance inverted emulsion [99]. Langmuir-Blodgett (LB) based methods involve transfer of the first lipid monolayer, or leaflet, from a water subphase by a vertical motion onto the substrate [41, 42]. The upper monolayer can be fashioned in a similar manner or by the Langmuir-Schaeffer technique. In the latter technique the upper monolayer is obtained by horizontal deposition onto the subphase [41, 42]. An advantage of these techniques is the ability to create asymmetric lipid bilayers. On the other hand the techniques are time consuming and have many factors, such as position of cover slip and surface pressure on the subphase, that can influence the quality of the lipid bilayer [41, 42].
LB methods can be combined with the vesicle fusion method to make asymmetric bilayers [41, 42]. Here, a LB monolayer is created, followed by vesicle fusion that forms an upper leaflet.
Lastly, droplet interface bilayers (DIBs) can be made that can produce asymmetric bilayers. However, bilayer area is limited and lipid composition has to be soluble in oil. Incorporation of transmembrane proteins, such as ion channels, is possible with this technique. Assembly of the DIB can combine two droplets or a planar

monolayer with droplets.
Supported lipid bilayers can also be indirectly linked to their substrate. Spacer molecules provide a type of anchor, resulting in a so-called hybrid LBM, which makes the membrane more robust than SLBs. Due to the strong interaction between the spacer molecule and membrane [98]. Another option is polymer-cushioned LBM, which is used when transmembrane proteins needed to be incorporated into the membrane [86]. Lastly, tethering of lipids via polymer strands can ensure a more mobile system than any other type of indirect linking [86].

topography Deviations from a perfectly planar flat surface. Usually artificially manufactured to significantly affect surface material properties, in this case, to enhance implant adhesion properties.

transition temperature Specific temperature for a lipid at which it changes its state (gel vs fluid).

vesicles Biomimetic membranes can also be modeled spherically as vesicles. Vesicles are deformable structures and have a large free standing membrane area. Experimentally, vesicles are more difficult to investigate compared to SLBs, due to free movement within a fluid environment.